FORSCHUNGSZENTRUM ROSSENDORF
Mitglied der Wissenschaftsgemeinschaft Gottfried Wilhelm Leibniz

WISSENSCHAFTLICH-TECHNISCHE BERICHTE
FZR-375
April 2003
ISSN 1437-322X

Radiation Source ELBE

Annual Report 2002

Cover Picture

View of the ELBE control room during the first user experiments done at the nuclear spectroscopy beamline.

Herausgeber:

Forschungszentrum Rossendorf e.V.

Postfach 51 01 19
D-01314 Dresden
Bundesrepublik Deutschland

Telefon +49 (3 51) 2 60 21 01
Telefax +49 (3 51) 2 60 36 90
E-Mail P.Michel@fz-rossendorf.de
Internet www.fz-rossendorf.de/fwl/

Als Manuskript gedruckt.

FORSCHUNGSZENTRUM ROSSENDORF
Mitglied der Wissenschaftsgemeinschaft Gottfried Wilhelm Leibniz

WISSENSCHAFTLICH-TECHNISCHE BERICHTE
FZR - 375
April 2003

Radiation Source ELBE

Annual Report 2002

Editor: U. Lehnert

Contents

Accelerator Development

The year 2002 of the ELBE accelerator was characterized by a lot of construction work. The niches for the beamdumps od the radiation physics and nuclear physucs beamlines were finished and, finally, all the holes for the beamlines connecting the different caves were drilled.

However, during this shut-down period many improvements of the accelerator instrumentation were established. First to mention here are improvements in the operation of the liquid helium cryogenic system which now allow a much more stable accelerator RF operation due to an improved pressure stability. The machine protection interlock has undergone a complete redesign. Now, two independent systems monitor beam loss to prevent accidents like the one in August 2001. Long ionization chambers made of RF power cables are placed along all beamlines to detect radiation produced by lost electrons and a sophisticated system measures current differences.

From September 2002 the acclerator was in operation again with clear advances in stability and reliability of operation. After completion and commisioning of the beamline, since December the bremsstrahlung facility is in full user operation.

The transition from comissioning to user operation at ELBE

P. Michel

It is pretty difficult to define the starting point of the Elbe project. One could choose the decision to build the facility by the management of the Research Centre Rossendorf in September 1996 or the beginning of the construction work at the Elbe building in June 1998. However for the future users of the radiation source ELBE only one date is really important: When the first beam with the desired characteristics is available. In order to accomplish it as fast as practical, the commissioning is to be arranged step by step. Upon completion and initial commissioning of the electron accelerator the first beam for Physics will follow. It means that setting up of the machine, commissioning, optimization and achieving the required beam parameters will overlap with the first experiments during the next months and years. The safe and reliable operation of the accelerator is essential for a user.
The most important milestones in the life of the machine were:

- start-up and the optimization of the thermionic injector in December 2000
- successful first acceleration in the superconducting RF accelerator module in May 2001 (5 mA, 6 MeV)
- reaching the full beam energy of 20 MeV in July 2001
- acceleration of the maximum bunch charge of 77 pC in August 2001
- reaching 850 μA at 12 MeV in CW-mode in the December 2001

The final beamline for the production of MeV-Bremstrahlung was assembled and commissioned during a shut-down period from January to September 2002. All of the technical changes and extensions for the final completion of the machine were implemented at this time such as the drilled holes between the separate caves of the accelerator building. In September 2002 the beam operation began again with various improvements of machine protection system [1,2] and the cryogenic system [3]. After few days the beam parameters could be reproduced. In particular due to the mentioned improvements of the liquid helium supply a very stable machine operation was obtained. Due to the clear improvements of beam loss monitoring the machine can be now operated safely and reliably without damage by energy deposited in beam line components.

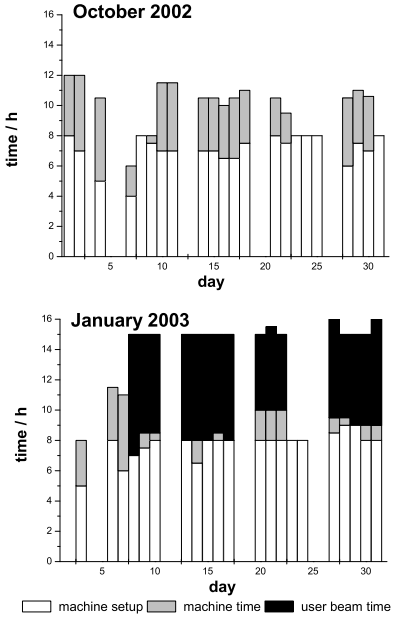

Fig. 1: *ELBE setup and beam time statistic from October 2002 and January 2003*

The first user operation with Bremstrahlung started in January 2003. Typical beam parameters were 12 MeV and 300-600 μA in CW or macro pulsed mode [4]. Primarily a 4 μm thick Nb radiator was used. Fig. 1 shows the daily time statistics from October 2002 and January 2003. The day shifts were used to complete the beam lines in the accelerator cave and the night shifts were devoted to accelerator development for optimisation of machine or beam parameters and to deliver beam for users.

References:
[1] this report, p. 9
[2] this report, p. 11
[3] this report, p. 7
[4] this report, p. 23

ELBE-Cryomodule Hardware Test and Design Changes

J. Stephan

Until the end of 2002 the cryomodule CM1 went trough twelve cool-down warm-up cycles. In addition, the module had to survive two breaks of warm RF-windows, causing collapses of the insulating vacuum and also a sudden break of the beam line vacuum caused by an errant electron beam. All but the latest event did not have any bad effect on properties and behavior. The cryomodule CM1 worked well until its last warm-up in February 2003.

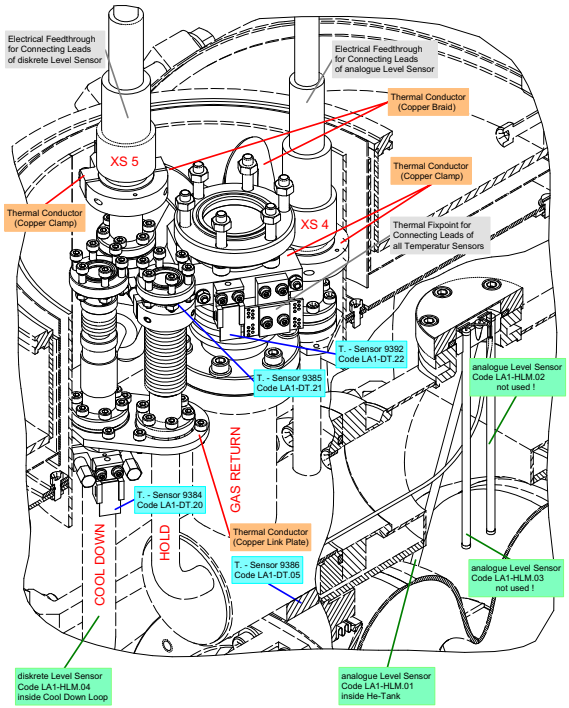

Fig. 1: *Additional sensors at the helium port CM1.*

A big time-lag during the module test was caused by helium pressure oscillations inside the bath cryostats. Therefore, the tuning systems were in continuous use as pressure deviations above ±0.2 mbar drive the RF-phase loop controller out of its range. Initially, the reason of these oscillations were completely unknown. A lot of assumptions were established, e.g. "standing waves at the helium bath surface" or "thermodynamic oscillations inside the cool down loop". To find their origin the test arrangement showed a lack of temperature sensors at the helium port of the module. Therefore, some design changes were done without opening the vessel. Only the port below helium transfer line was accessible for detecting pipe temperatures by means of four additional sensors shown in Fig. 1. A bypass between the cool down loop and the gas return line was added for pressure compensation. Copper braids were needed for compensating heat transfer from both electrical feedthroughs to the helium pipes. After all things mentioned above were built in no improvement beyond the possibility of measuring pipe temperatures during tests of the helium refrigerator. Finally, the pressure oscillations were found out to be caused only by refrigerator components as there is a hard misfit of the cold compressors to the helium mass flow and some misadjustments between the filling valve controller and level meter. After compensating all these mismatches the refrigerator and the cryomodule work together fine.

Unfortunately, the former assumptions led to a redesign of the helium supply system for ELBE-Cryomodule CM2 (shown in Figure 2) before the origin of the pressure oscillations was found. Still, the changes may be usefull to supply more modules at the same time with liquid helium without oscillations inside gas return pipe.

Notable design changes to the helium supply are:

- A stilling pot for helium feed and gas return with integrated phase separator and electrical heater.
- An invisible cool down loop that lies inside the helium collector and will have the same temperature.
- A funnel for the helium feed that goes through the stilling pot behind a barrier inside collector tube.
- Some additional helium temperature sensors composed vertically on a ladder inside stilling pot for better level detection and controlling the heater.

Little design changes are made to the thermal and magnetic shielding, and to the central holder for the stilling pot at the helium port. Last but not least more thermal insulating was wound around the bath tanks and a simple multi-turn position indicator for tuning systems was added.

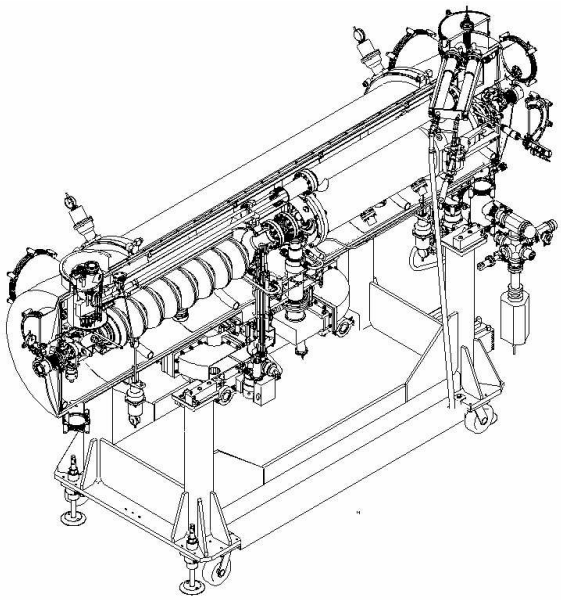

Fig. 2: *ELBE cryomodule.*

Operation experience and status of the Helium plant

Ch. Schneider

In the years 2001 and 2002 two major problems for operating the liquid helium plant together with the Elbe cryostat had been encountered. The first was to guaranty a pressure stability in the cryostat of around ±0.1 mbar. The second one relates to gas purity within the helium plant and its effects on the helium filling of the cryostat.

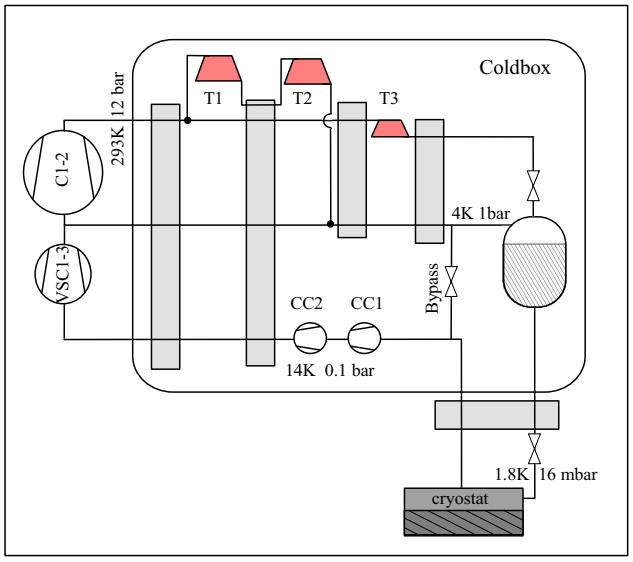

Fig. 1: *Flow chart of the liquid helium plant. C1 and C2 are the cycle compressors, T1 – T3 the expansion turbines, CC1 and CC2 the cold compressors and VSR1 – VSR3 the vacuum screw compressors.*

In Fig. 1 a basic scheme of the helium plant is shown. The plant was designed for a maximum cooling power of 200 W and a maximum mass flow of around 12 g/s. The main difference to conventional designs used for accelerator cooling are the two cold compressors (CC1, CC2). Besides recompression of the helium gas at the 4 K level they are mainly used for stabilizing the pressure level for the cavity operation. From the beginning of the accelerator operation pressure fluctuations in the cavities with frequencies in the Hz region and amplitudes in the mbar range were observed. At last we found that they are related to operation of the cold compressors outside the surge margin, whenever the mass flow is below 7 to 8 g/s. At ELBE finally two cryostats will be used to accelerate the electron beam up to 40 MeV. They will produce a helium mass flow around 2 to 4 g/s, only!
Foresightedly, the design of the helium plant has a bypass line running from the helium recycling line at the 1 bar level to the entry of the cold compressors. This bypass line can be used to artificially increase the mass flow above the stability threshold of 7 g/s. This leads to an overall pressure stable cryostat operation, shown in Fig. 2.

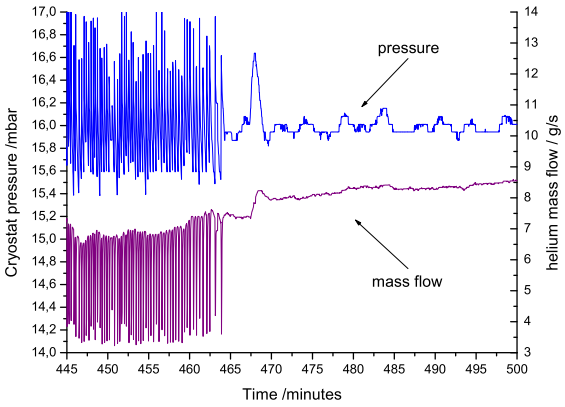

Fig. 2: *Pressure in the cryostat in relation to the helium mass flow. For a mass flow greater than approx. 7 to 8 g/s the pressure stabilizes around 16±0.1 mbar*

The liquid helium from the helium plant is transported via a transfer line to the accelerator hall. There the helium is cooled down finally to the 2 K level by expansion valves and is than distributed to the different cryostat modules. This is the place where problems with the long time continuous operations of the helium plant have been observed first. The expansion or fill valve for the cryostat had to be opened more to keep the fill level constant. Furthermore this mean value shifts accidentally over time. A second indicator was a steadily droping pressure at the entry of the expansion turbines T1 and T3. This leads to increasingly difficult operation conditions of the helium plant, beginning with an overall power reduction up to a failure of the helium plant due to unstable operation of turbine T1.
During the maintenance period in summer 2002 massive impurities (mainly water) have been found in different sections of the plant, which could give a reasonable explanation for the reported effects. Up to now, the source of the impurities is not quite clear. Under discussion and further investigation are particular leaks (one was found in the compressor section), the constant leakage rate of the complete plant over time or possibly operational problems with the purifier section of the plant. After the maintenance in summer 2002 the cleaned plant was operated unchanged and stably over a period of 3 month with pressure stability like shown in the second half of Fig. 2. However, at the end of year 2002 the purity problem arose again and is still under investigation.

Beamline Installation to the Nuclear Physics Cave

J. Claussner, M. Freitag, R. Schlenk, B. Wustmann

After dismantling the test beamline, which was used to establish and characterize the beam from the first linac, during 2002 the first beamline section after linac 1 including the nuclear physics beamline were installed. It's main components are :

- the vacuum system (pumps, valves, tubes ...)
- the beam optical elements (dipoles, quadrupoles, steerer)
- the beam diagnostics (position and current monitors, viewscreens)
- the magnetic chicane
- the beam dump (vacuum chamber with the graphite dump, beryllium window, the coolant circuit and the radiation shielding)
- the bremsstrahlung radiator, beam shutter and hardener

With the available experience setting up the beamline is now routine work. However, installing a "particle-free" UHV system requires carefull cleaning and mounting procedures in laminar-flow chambers. Main cmponents like the magnetic chicane the bremsstrahlung radiator and the 50 kW beam dump were new to the ELBE crew.

The magnetic chicane for bunch compression consists of four dipole magnets and a large flat vacuum chamber manufactured by DANFYSIK. In order to retain the width of the chamber against the athmospheric pressure it was necessary to attach some reenforcement ribs what had to be done after the magnet alignment was established.

In the central section of the chicane a moveable viewscreen for optical transition radiation was installed. An aluminum foil stretched on an oval frame can be moved with wires over the whole width of the chamber. The drive system, position sensor and stop position switches are installed easily accessible outside the vacuum chamber. The camera is mounted in a fixed position viewing the foil via a prism that is moved along with the screen, thus, yielding a constant viewing distance and constant magnification.

The bremsstrahlung radiator consists of a ladder with 3 different thin foils that can be inserted into the beam path. The foils are mounted on a water cooled copper frame that can be moved by a DC drive. The drive, position sensor and end switches are mounted outside the vacuum chamber so that abrasion cannot produce dust particles.

The safe operation of the bremsstrahlung radiator requires a considerable diagnostic effort. To tune the beam position and spot size a radiator foil for optical transition radiation can be inserted at the target position. Also the radiator itself emits optical transition radiation which is used to monitor the beam position on the radiator through a mirror mounted in the backward direction. For low-melting target materials a pyrometer allows an observation of the foil temprature at the beam spot. Besides vacuum gauges several thermocouples are installed to monitor the beamline towards the dump which is heated by scattered electrons.

The beam dump is made of an isolated graphite block mounted inside a water cooled vacuum chamber. The heat transfer from the dump to the cooling media works by thermal radiation, only. The chamber is separated from the beamline UHV by a beryllium window that is water cooled as well. For radiation shielding the whole setup is surrounded by 10 cm of iron except for the backward direction where especially shaped lead blocks are used.

For the beam dump cooling a separate closed cooling circuit was set up which is thermally coupled to the main cooling system by a heat exchanger. The amount of water in the primary loop is sufficient to accept the considerable residual heat of the hot graphite block in case of a power failure. For this case, the redundant water pumps of the primary coolant loop are powered by a backup supply.

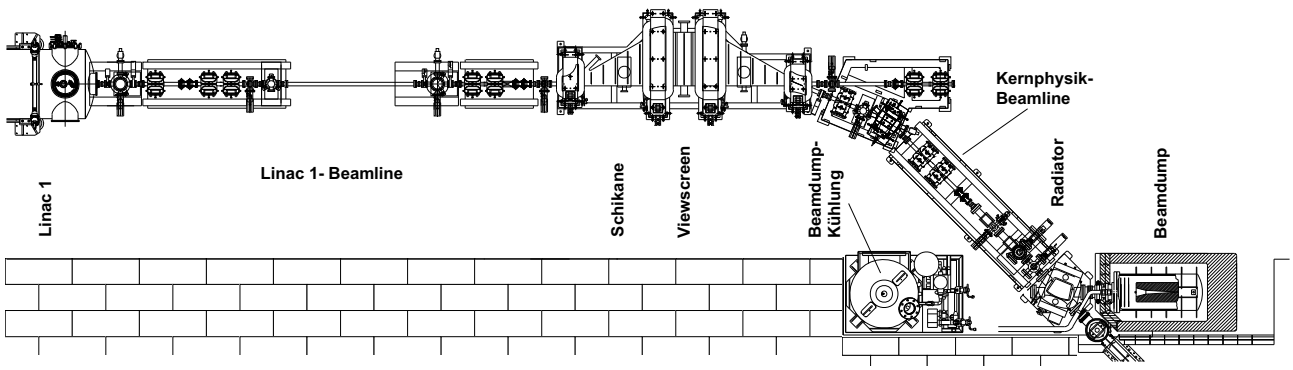

Fig. 1: *The beamline from the first accelerator module to the bremsstrahlung radiator and beam dump.*

Beam Loss Monitoring with Long Ionization Chambers at ELBE

P. Michel, R. Schurig, J. Teichert

The safe and reliable operation of the accelerator is essential for a user facility like the ELBE radiation source. The machine should run over many shifts and for long periods with constant and reproducible parameters. The facility must be able to be operated by a minimum number of trained operators. Because of the extremely high beam power (max. 40 kW) and the electron energy range of 15–40 MeV the prevention of beam losses in the beam line plays a special role. Due to the average electron penetration depth at these energies approximately the full beam power can be deposited into the vacuum pipes. Apart from the production of ionizing radiation and activation, the vacuum pipes can be melted. It is inevitable that the vacuum system, and in particular the superconducting accelerator cavities, would be contaminated. The result would be long down-times and substantial costs for repairs.

Multiple systems for the measurement of the beam loss were tested at the ELBE beam line. These were photomultipliers (PM), Compton diodes (CD) [1] and long ionization chambers (LIC) [2] constructed from air-filled high frequency cables.

PM: Photomultipliers (Electron tubes P30P) were installed approximately 3 m away from the beam line. Due to the nonlinear behaviour of the PM signals saturation effects in the PM problems appear at very high dose rates. At very fast increasing and extremely high beam losses the PM's saturate before the necessary signal level for the accelerator shut-off is reached. In addition, the continuous monitoring of the beam pipe can be guaranteed only when using a large number of detectors ($\approx$1 PM per meter) due to the strong dependence of the monitor signal on the distance between PM and the location of the beam loss.

CD: Compton diodes were installed similar to the PM's. They showed a very good linear behaviour up to extremely high beam loss levels. The Compton diodes exhibit an angle dependent signal and thus a directional characteristic based on the geometry of the detector. This can be used in order to supervise certain segments of the beam line with increased sensitivity. Nevertheless, the crucial disadvantage remains the same as for the PM. A complete beam line monitoring with approximately constant sensitivity is attainable only with a very large number of detectors.

LIC: Air-filled high frequency cables of the type Andrew HJ5-50 (diameter 22.2 mm) were mounted approx. 20 cm away parallel to the beam pipe. The cables were operated as ionization chambers applying a high voltage to the inner conductor and measuring the ionization current. The detector showed a very good linear behaviour up to the maximum possible beam loss (0.85 mA with 12 MeV). Due to the ideal geometrical constellation, the BLM signal varied approximately only $\pm$50% along the beamline, which is caused by the inhomogenous distribution of attenuating material (magnets, flanges...).

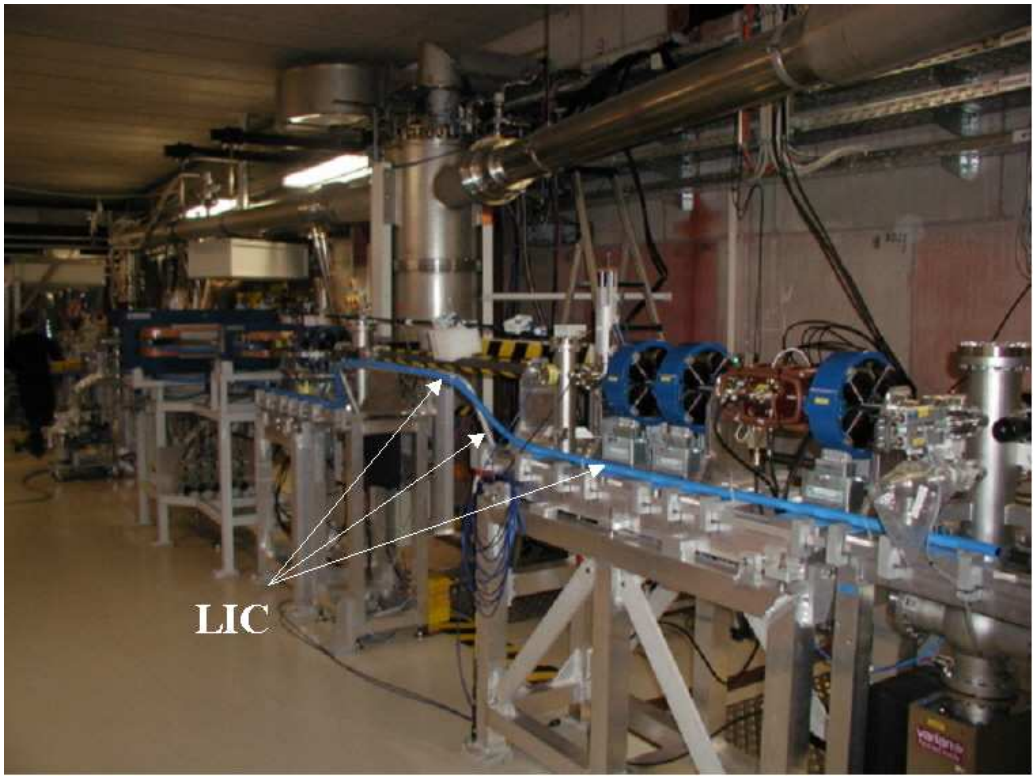

Fig. 1: *Installation of LIC at the ELBE beamline*

The response time of all three detectors is sufficient for fast shut-off system (<1ms). The LIC was chosen because of the ability to monitor the entire beamline with the same shut down level and the small number of electronics that is required for such a system. The Andrew HJ4-50 (diameter 12.7 mm) Heliax cable was selected for the ionization chamber [3]. The system was segmented corresponding to the logical sectioning of the ELBE beamlines, adding some segments with special shielding conditions (e.g. large chicane vacuum chamber). Fig. 1 shows the installed LIC in a beamline section behind the cryomodule. The cable is covered with a plastic tube to prevent damage and to provide high voltage insulation. It was mounted as closely as possible (approx. 200 mm) to the beamline. The cable was installed within the iron yoke of the dipole magnets to avoid their shielding effect. Fig. 2 shows the BLM signal of two detector sections with artificially produced beam loss at different locations along the ELBE beam line.

The shut-off threshold of the system was set on 0.85 μC loss charge integrated over 100 ms. In consideration of all fluctuations of the signal a maximum beam loss current of 8.5 μA in CW operation at 12 MeV beam energy is tolerated. In the worst case 100 W of thermal power are deposited into any beam line components. Thus, a safe operation of the accelerator is ensured.

Since the system very sensitively measures beam loss currents of few μA, we plan to develop a second system for on-line monitoring the beam transmission during accelerator operation. This system is divided into sections with a length of 0.5 m and a special serial read out electronics is under development [4]. Thus a position resolved measurement of the beam loss becomes possible. The operator will be able to judge and correct the quality of beam transmission while running the machine in high beam power mode.

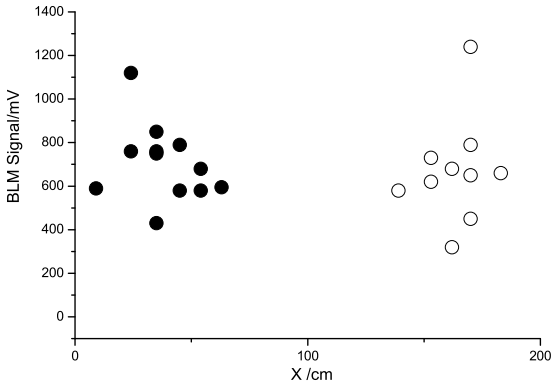

Fig. 2: *BLM signal from the same beam loss current at different locations along the beam line. Full and open circles are measured with different cable sections. The open circle section belongs to the chicane vacuum chamber.*

[1] M.Brunken et al. Latest Developments from the S-DALINAC, FEL Conference, Hamburg, (1999)
[2] J.Rölfe et al. SLAC-PUB-4925, 3/1989
[3] this report, p. 11
[4] this report, p. 13

Machine Interlock System Improvements by new Beam Loss Monitors

A. Büchner, J. Voigtländer, F. Gabriel, H. Langenhagen

The high continuous beam power up to 40 kW at ELBE requires a reliable beam loss detection system to prevent damage of the beam line. Experiences made so far have shown that two independent, redundant systems of beam loss monitors are needed.
The first system uses long ionization chambers along the beam line. Any beam loss in the beam line produces bremsstrahlung which generates a current in an ionization chamber. The current is measured. If the beam loss exceeds a certain level, the beam is switched off.
The second system measures the beam current at different positions along the beam line. The difference between adjacent measurement positions is monitored. If the difference exceeds a certain level, the beam is also switched off.
At ELBE several beam paths to the different experiments can be choosen. Therefore, and also because of local layout complexities the beam loss monitor system is segmented. The ELBE beam loss monitor scheme is shown in Fig. 1.
Andrew HJ4-50 type RF cable is used as an ionization chamber. The inner conductor is only centered by a helical plastic spacer. So the cable forms an air filled ionization chamber which is operated with a high voltage of 1 kV.
The electronics is designed to switch off the beam at a beam loss of 8.5 μA which corresponds to 1% of the full 850 μA beam current. Another design criteria was to switch off the beam in 1 ms when 850 μA (100%) beam loss occures. These criteria gave a time constant of 100 ms for signal integration (see [1]). Tests made at the accelerator showed that a sensitivity of approximately 3 V per μA ionization current is needed. By clever cabling of the detector it was possible to reduce the noise and other errors to insignificant levels. A block diagram is shown in Fig. 2.
The whole beam loss detection system is divided into several segments to match the physical layout of the accelerator. Up to 28 chambers with their electronic moduls are now planned. To compensate sensitivity tolerances the treshold of every module is adjustable with jumpers in 12 equal steps of 28% over a range of 1:15 and is shown on a LED display. Also the module state is signaled by LED's.
In order to prevent damage to the system, all the electronics was installed outside the accelerator enclosure. Special care is taken to make the system intrinsically safe. Any cable errors or high voltage failures are detected. A module function check can be initiated from the accelerator control and should be done before every beam time run.
Practical experience was gained with 3 detectors during 6 months of beam operation. The system worked very reliably and no damage occured.

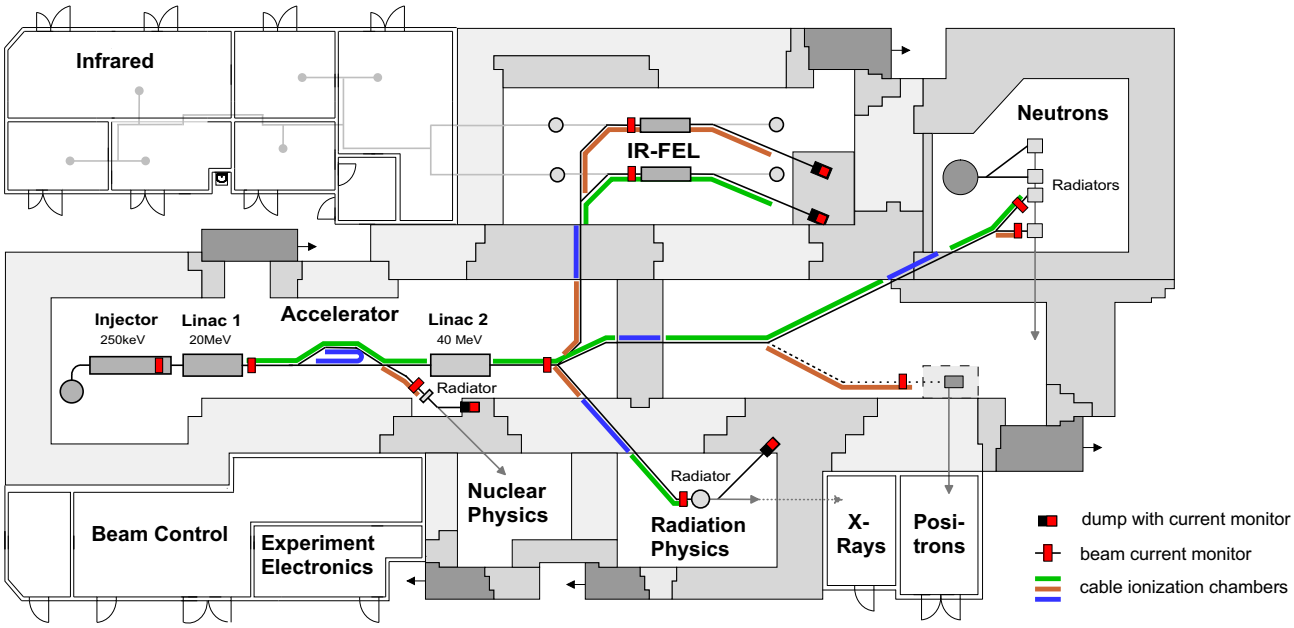

Fig. 1: *Beam loss monitor system for ELBE.*

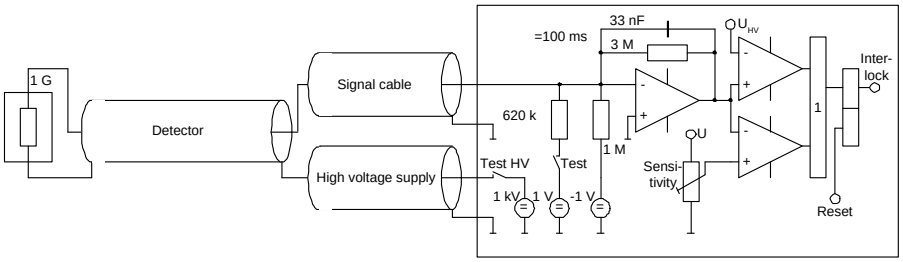

Fig. 2: *Block diagram for the cable ionization chamber electronics.*

A second, completely independent system of monitoring beam loss is based on current difference measurements. Fig. 3 shows the design taking the difference between a $\lambda/4$ stripline monitor (see [2]) and the beam dump as an example.

Each channel comprizes an RF amplitude detector for the $\lambda/4$ stripline monitors and a LF current measurement for use with a beam dump. The selection is done by jumpers. The amplitude controllers for the current calibration have to be changed accordingly. A module function check is possible using test signals from the accelerator control. The signals Test 1 and 2 simulate an error (failed cable or connector) in channel 1 or 2.

Lab tests of the RF part showed an uniformity of both channels of 0.45% at 1.3 GHz over a dynamic range of 31 dB. The temperature coefficient is $\pm 0.02\%/°C$.

Tests at the accelerator with two $\lambda/4$ stripline monitors showed an integral nonlinearity of $\pm 3.5\%$ per channel and $\pm 0.5\%$ difference between the two channels over a beam current range of $100 \ldots 600$ μA. It should be noted that the measurement accuracy is 0.5% for these measurements. The signal dependency on the micro pulse rate is $\pm 3.0\%$ for one channel and $\pm 0.5\%$ for the difference between the two channels.

The electron bunch in the injector is much longer than in the accelerator and influences the measurements with the $\lambda/4$ stripline monitor in the injector. When the subharmonic buncher voltage is varied within 25 ± 5 kV the signal changes less than 1.5% at 400 μA beam current. In comparison the signals of the detectors after the first accelerator stage change by less than 0.5%.

The accuracy of the beam current measurement allows a minimum switch-off treshold of 2.5% (21 μA) for the difference between the stripline monitor in the injector and the stripline monitor in the nuclear physics beam path.

A minimum treshold of 5% (42 μA) could be used for the difference between the stripline monitor in the nuclear physics beam path and the beam dump in this path. This is possible because the individual errors don't add in this case. Even for an inserted target it is possible to use this treshold.

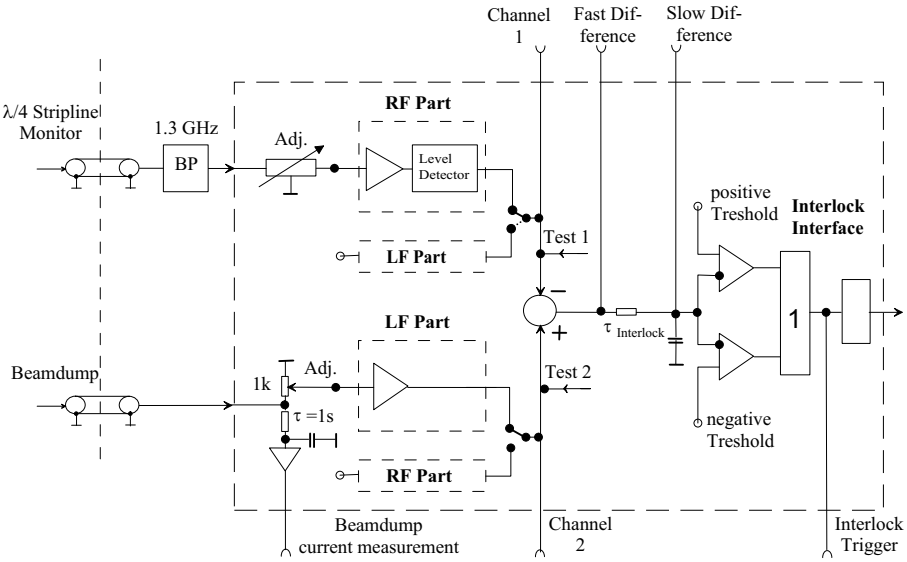

Fig. 3: *Block diagram of the beam current difference measurement.*

[1] this report, p. 9
[2] this report, p. 17 f.

A Beam Loss Monitor with Longitudinal Resolution

R. Schurig, P. Michel

At ELBE, beam loss is measured in two different ways. Long ionization chambers (LIC) made from coaxial cable with air dielectric are used to detect beam loss at critical sites along the machine. In the second system, beam current is measured at three different locations. The sum signals from two stripline beam position monitors and the nuclear physics beam dump currents are compared. A difference in current at these points indicates that portions of the electron beam are lost somewhere. Above a certain level the interlock is triggered and the beam is switched off. Both kinds of measurement are described in detail elsewhere in this annual report.

A new system of beam loss measurement has been built and is currently tested at ELBE. In difference to the other systems it has a longitudinal resolution of the location where the beam loss occurs. Like for the LIC, ionization chambers made from Andrew Heliax [1] coaxial cable are used as detectors. The principle of the detectors is sketched in Fig. 1.

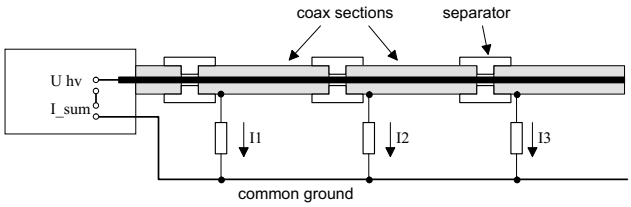

Fig. 1: *Principle of the sectioned beam loss monitor (BLM).*

The outer conductor of the coaxial cable is cut every 500 mm leaving a 5 mm gap between each section, the inner conductor remains untouched. Plastic separators are used to fix the system mechanically. A high voltage is applied between the inner conductor and a common ground line. Each section is connected to the ground line through a resistor. Thus, ionisation current can be measured for every cable section separately as a voltage across the according resistor.

The data acquisition electronics consists of one master and multiple slave modules. The modules are connected via standard RS485 serial bus. A block diagram of the electronics is shown in Fig. 2. The core device of each module is an ATMEL [2] 8-bit RISC controller with integrated 10-bit ADC, 512 byte EEPROM and SDRAM and 8 kbyte of in-system programmable FLASH memory. Each module has an unique device address. This addressing is used to automatically detect devices that are connected to the bus. Thus, no changes in soft- or hardware are required if the system is extended by connecting further modules in the future.

The front end of the slave module is a differential operational amplifier (op-amp). A shielded twisted pair cable connects the op-amp input terminals to the sensor resistor. Amplification can be varied between 10 and 100. The output of the amplifier is connected to the ADC. The maximum ADC sampling rate is 15000 samples per second at full resolution, the test modules are running at 100 Hz. In the basic mode, the slave-controller perform a floating averaging. Minimum and maximum peak hold functions can be activated. A line transceiver device translates the TTL signals from the controller to differential RS485 bus level. RS485 bus standard was chosen because of its ruggedness in noisy environment. At the data rate of 115 kBaud, the length of the bus cable is limited to about 1500 m which is more then sufficient for the use at ELBE. All slave modules are installed on the ground below the beam line in the accelerator cave. They are covered with lead blocks to be protected against radiation. Standard RJ45 patch cable is used for bus interconnection.

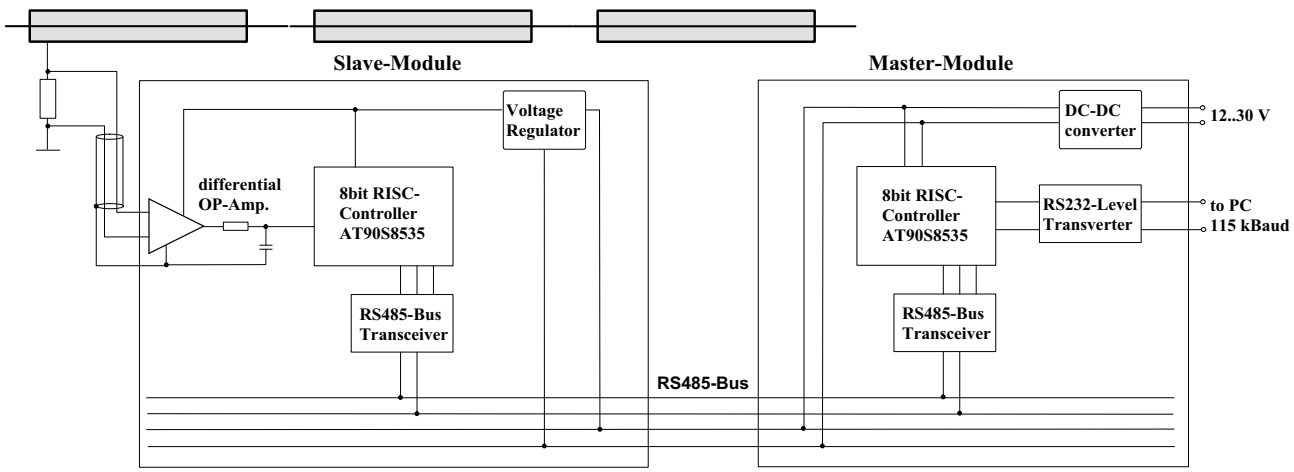

Fig. 2: *Acquisition electronics, block diagram.*

The master module handles the data transfer protocol with the slave modules, checksum calculations for data validity verification and connects to a monitoring PC via an optical isolated RS232 bus. The galvanic isolated power supply is also hosted on the master board. The isolation is necessary to make the high voltage ground return the only ground line for the whole system.

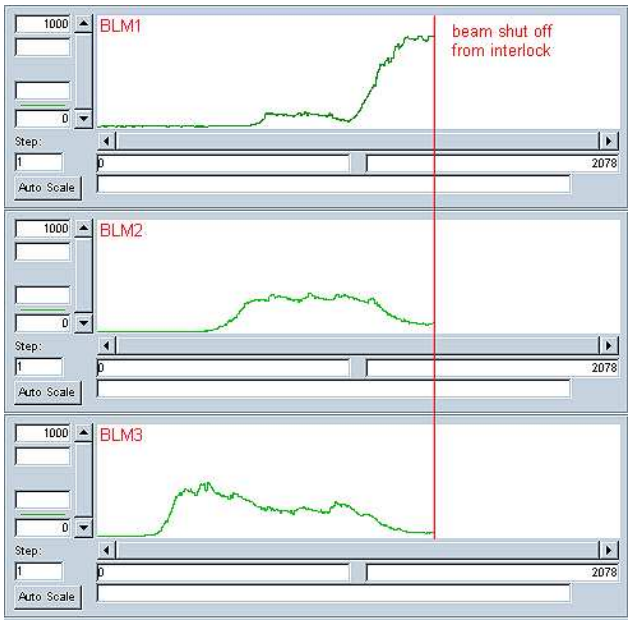

Fig. 3: *Screenshot of the time domain recorder.*

[1] www.andrew.com
[2] www.atmel.com

The software used for the first test was created with HPVee. When the software is started it scans the bus for devices. This is repeated periodically. The main task of the software is to read data from the master module and make them visible to the machine operator. The amplitude of beam loss at each position is displayed in bargraph columns. In addition to that, the lapse of amplitude change can be traced in time domain recorders. A screenshot of tree time domain recorders during an typical electronics test procedure is shown in Fig. 3.

For this test, a detector string of three sections was mounted parallel to the beam line at a distance of about 150 mm. A steerer, about 2 m upstream of the detector was used to generate loss of 3 μA cw electron beam at different positions. The steerer current was increased, thus the beam loss moved from downstream to more upstream positions. As shown in Fig. 3, the most downstream detector, BLM3, detects beam loss first. Later amplitude in BLM2 rises while amplitude in BLM3 is dropping. Finally the signal in BLM1 rises until a LIC detector fired the interlock for excessive beam loss.

It is planned to install as many detectors and slave modules as required to cover the whole beam line. It will then be possible for the machine operator to see where beam is lost with a resolution of better than one meter.

Revision of the Pulse Generation for ELBE

F. Gabriel

Due to more precise defined, higher requirements and from the gathered experience with the ELBE accelerator the pulse generation was revisited. Improvements were needed for bunch to bunch jitter and for phase stability between gun and accelerator cavities for all the quite different operating modes of ELBE. They were possible by significant hardware progress and a new, common interface standard for fast pulse transmission. Ultimately bunch to bunch jitter could be reduced by a factor of 4 and the phase stability could be improved in the same order. The block diagram is shown in Fig. 1.

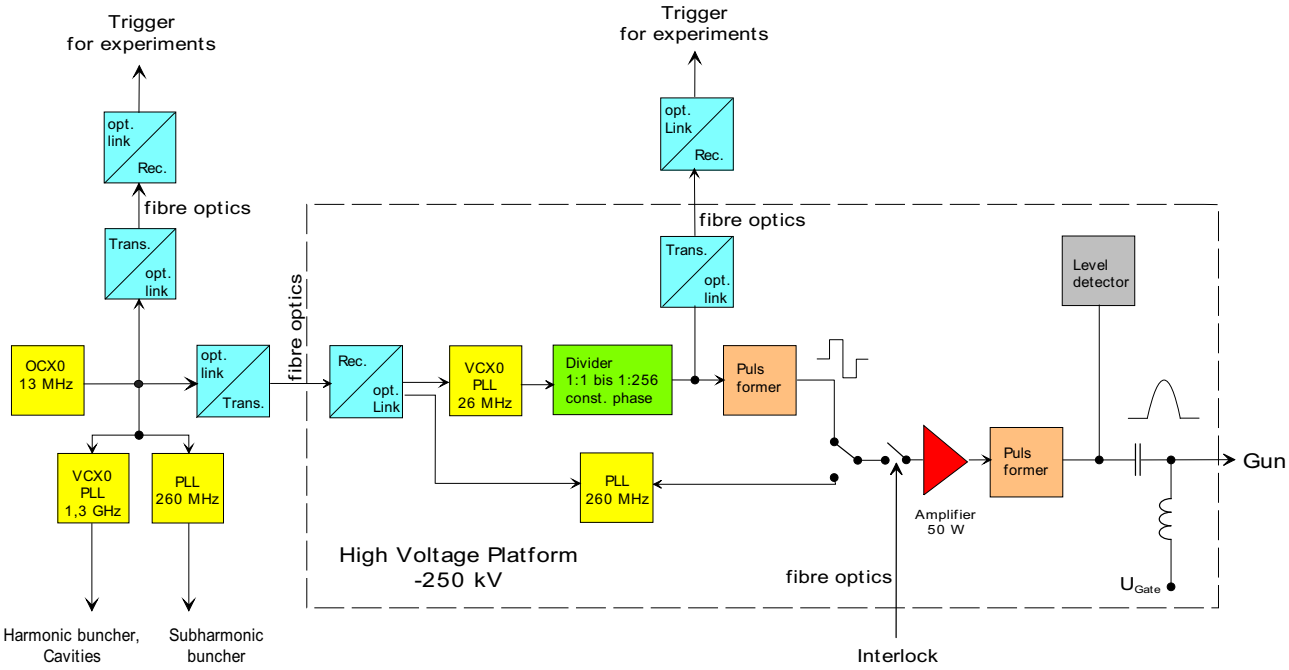

Fig. 1: *Block diagram of the pulse generation for the ELBE accelerator.*

26 MHz Generation

For later planned 2 colour experiments a micro pulse rate of 26 MHz is needed to operate 2 FELs at 13 MHz micro pulse rate simultaneously.

The micro pulse rate of 26 MHz is generated by a PLL with a voltage controlled 26 MHz quartz oscillator. The 26 MHz PLL has the following jitter data for the following cut-off frequencies of the noise spectrum (Allan Variance):

f_c=1 kHz :	0.33 ps
f_c=10 kHz :	0.38 ps
f_c=100 kHz :	0.42 ps

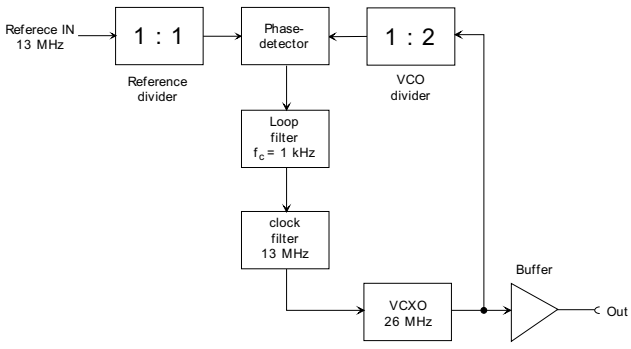

Fig. 2: *Block diagram of the 26 MHz PLL.*

Micro pulse rate divider

A synchronous counter allows a reduction of the micro pulse rate from 13 MHz (later 26 MHz) in binary steps till 1:256. Experience shows that by switching the divider ratio the propagation time should change by less than ±15 ps.

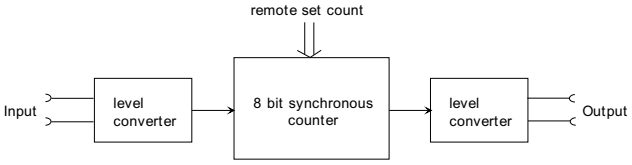

Fig. 3: *Block diagram of the synchronous counter.*

The following results were measured:

- propagation time approximately 2 ns
- change from 1:1 to 1:256 for 13 MHz ≤10 ps
- temperature drift approximately 2.5 ps/deg
- maximum input frequency ≥900 MHz
- jitter for 1:1 ratio for the following cut-off frequencies of the noise spectrum:

f_c=1 kHz :	0.17 ps
f_c=10 kHz :	0.32 ps
f_c=100 kHz :	0.55 ps

Pulse shaper

The pulse shaper generates a special formed signal at the micro pulse rate which is used to build the spike pulses for the gun grid. The pulse shape is made by delay time differences between different coaxial cables and logical processing.

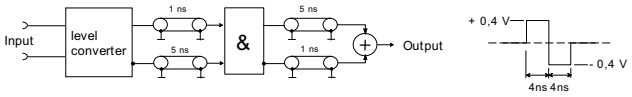

Fig. 4: *Block diagram of the pulse former.*

Optical link

An optical link uses an optical transmitter and an optical receiver. The transmission operates with light of 820 nm wavelength and uses a multimode glas fibre with a size of 62.5/125 μm. An optical connector according to the FSMA standard for screw joints is used which gives a connection reproducibility of approximately 10 ps.

Optical Transmitter

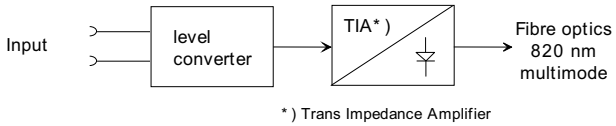

Optical Receiver

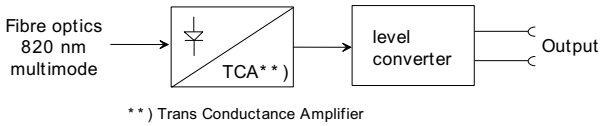

Fig. 5: *Block diagram of the optical links.*

An experiment may be triggered by the micro pulse rate or the macro pulser. The transmission of such arbitrary pulse duty factors requires a DC coupling. Because commercial optical receivers for DC are not available a quasi DC coupling was realized by evaluation of the leading and the trailing edge of the signal. The following results were measured:

- propagation time approximately 10 ns at 1 m fibre length
- change from 1:1 to 1:256 for 13 MHz ≤10 ps
- temperature drift approximately 2.5 ps/deg
- maximum operating frequency ≥150 MHz
- jitter at 1:1 ratio for the following cut-off frequencies of the noise spectrum:

f_c=1 kHz :	0.11 ps
f_c=10 kHz :	0.29 ps
f_c=100 kHz :	0.82 ps

System jitter

The 26 MHz PLL in Fig. 1 acts as an filter for the jitter from the optical link and adds his own jitter. The following results were measured at the PLL output:

f_c=1 kHz :	0.45 ps
f_c=10 kHz :	0.52 ps
f_c=100 kHz :	0.55 ps

This jitter is changed by the micro pulse rate divider. For a dividing ratio of 2:1 (13 MHz output) the final result is for the different cut-off frequencies of the noise spectrum:

f_c=1 kHz :	0.38 ps
f_c=10 kHz :	0.49 ps
f_c=100 kHz :	0.67 ps

Performance of the BPM electronics

P. Evtushenko, R. Schurig

It was already reported about prototyping work on the BPM electronics [1,2]. It was decided to run the accelerator not only with earlier planed repetition rates 13 MHz and 260 MHz but also with reduced repetition rate. The rate must always be a sub-harmonic of the fundamental frequency 1.3 GHz. Now it is possible to operate at repetition rate $13/n$ MHz, where n can be 2,4,8,16,32,64 and 128. It is required that the BPM system supports any of these operation modes.

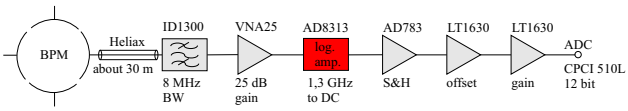

Fig. 1: *The BPM electronics scheme.*

A core element of the BPM electronics is a logarithmic detector AD8313 made by Analog Devices Inc. [3]. The logarithmic detector is a direct RF to DC converter rated up to 2.5 GHz. Bandwidth of the AD8313 is about 10 MHz. That means if the micropulse frequency is less than 13 MHz output voltage of the logarithmic detector follows the micropulse time structure of the beam. To enable the ADC to sample at the proper time some changes in the BPM electronic were done. Actual layout of the BPM electronic is shown on the Fig. 1. First of all the ADC is synchronized to an external clock. Additionally a sample and hold amplifier is built in to provide enough time for the ADC to make measurements. The sample and hold amplifier is synchronized with the micropulse frequency as well. Each BPM electronics board has an individual delay line to compensate for the different arriving time of an electron bunch to the BPM. Changing the electronics layout can lead to a change in the signal to noise ratio and hence can affect resolution of the beam position measurements. For that reason after making the changes in the BPM electronics it had to be tested again.

First of all we characterized the resolution of the BPM. Dependence of the BPM signal at 1.3 GHz on the beam current is known. To make the characterization, an RF cable which delivers the BPM signal from the accelerator cave to the electronics is connected on the BPM side to an RF generator via a 4-way splitter. Attenuation of the splitter and connecting cables is measured with accuracy of about 0.1 dBm. Thus, the RF generator substitutes an "ideal" beam. Since the generator is very stable in the sense of RF power level one can measure accuracy of the position measurements, which is defined only by the electronics noise and ADC digit size. It is almost not possible to measure the resolution of the electronics itself with beam since the beam always has position jitter, which now at ELBE is at least one order of magnitude higher than the BPM accuracy. The beam position is measured over several milliseconds and the standard deviation of such measurements is defined as the BPM accuracy. The equivalent beam current is calculated from the power level of the RF generator using a calibration, which was done before with the electron beam. Results of such measurements for both vertical and horizontal plane of one of the BPM boards are shown on the Fig. 2. As one can see the accuracy is better than 100 μm if the beam current is more than 30 μA. Note that resolution of the position measurements is better than the accuracy and the required resolution is about 100 μm. Since every BPM electrode has own electrical chain it is important to make the difference between the chains as small as possible for accurate beam measurements. The deviation of different channels on one BPM board is typically less than 5%. Every channel performance is measured and the BPM software takes the difference in to account.

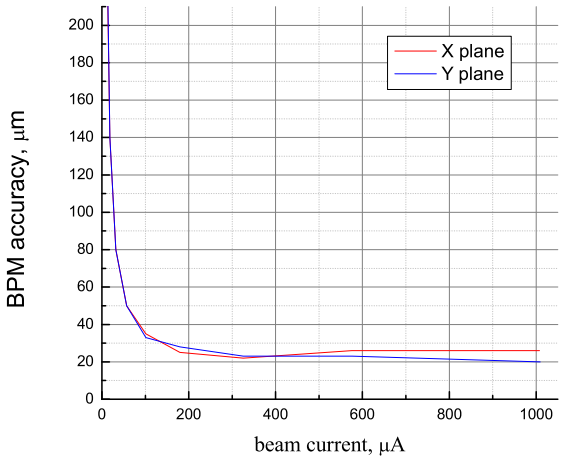

Fig. 2: *Accuracy of the position measurements.*

All tests have shown that the modified BPM electronics provide beam position measurements with resolution much better than required. Twenty units of the BPM electronics were manufactured. A part of the electronics is already installed at ELBE and operating 100% of the beam time. New boards of the electronic are installed as soon as required.

[1] P. Evtushenko et al., Proceedings of DIPAC 2001, Grenoble, 2001
[2] P. Evtushenko et al., Proceedings of BIW 2002, Upton, New York, 2002
[3] www.analog.com

Design and architecture of the BPM system software

P. Evtushenko

A system of stripline beam position monitors (BPM) is installed at ELBE [1]. In this note the software is described which provides the operator with the information obtained from the BPM.

One can split the software into two main parts. The first one is the data acquisition (DAQ) part, the second is the user interface. The software schematic is depicted on Fig. 1. The BPM software is realized in LabVIEW, which is an object oriented graphic programming language [2]. Every BPM delivers four broadband RF signals. To treat them, the BPM electronics has a single electrical chain for every channel. Thus, there are four DC signals fed to analog to digital converters (ADCs). The DAQ consists of six DATEL CPCI-510L boards in Compact PCI standard with 16 12-bit ADCs each. So the total number of ACD channels in the BPM acquisition data system is 96. To reduce the RF cable length from the BPM the electronics is placed in two different 19" chassis near accelerator but outside the accelerator cave. Next to the electronics PXI chassis with the ADCs are located. Both PXI chassis are connected to a DAQ computer via optical fiber using a so called PCI bridge. The distance between the DAQ computer and PXI module can be very high without introducing extra noise in the measurement data. In fact all ADC boards work like sitting on one single PCI bus of the DAQ computer. Advantages of the PCI bus are high possible data transfer rate, which can be up to ~130 MB/s and relatively low cost. An ADC samples BPM signals with frequency 101.5625 kHz, which is the smallest used subdivision of the 13 MHz standard repetition rate. Thus the ADC sampling is always synchronized with the micropulse of the accelerator. The LabVIEW programs accomplish the following DAQ functions:

- configure the ADCs,
- monitor the proper operation of all ADCs,
- combine the data from all ADCs after accquisition,
- share the measurement data.

The program obtains information about the macropulse length and about the beam mode (CW or pulsed) from the main ELBE control system to configure the ADCs. The total data rate is about 20 MB/s with maximum acquisition time of about 40 ms. In Fig. 1 the program is represented by the element "BPM DAQ".

As mentioned above, another part of the BPM software is the user interface. This is a set of programs, which provide the user with the information obtained from the BPM measurements. Basically, the data are transferred from the DAQ computer to any client computer via network using the DataSocket technology [3]. This fact makes the system very flexible. The number of computers using the BPM measurements is unlimited. It is also possible to share the data and to monitor the machine status via Internet. Once the format of the data published by the DAQ is known everyone can write his own application and use the data. A set of such applications was written in LabVIEW for routine beam observation during machine operation. First of them shows the beam position and intensity for all BPM simultaneously, averaged over a macropulse or ~20 ms in the case of CW operation. A second one provide more detailed information for any single BPM showing the beam position and the beam current as a function of time within a data acquisition. One more program is used to display the raw output voltage of the BPM electronics. This application is very useful for setting up, tuning and debugging the BPM electronics. The applications use the LabVIEW option to communicate with Excel. When the BPM electronics is calibrated the calibration results are saved in one Excel file. This Excel file is read by the BPM applications during their initialization.

As mentioned, the applications can be installed on any computer including the WinCC client stations. To prevent any interference between the WinCC and a BPM application, every application is tested for CPU usage on a standard WinCC client computer. The usage depends on the acquisition time but never exceeds 30%.

[1] P. Evtushenko et al., Proceedings of DIPAC 2001 Grenoble, 2001
[2] www.ni.com/labview/
[3] www.ni.com/datasocket/

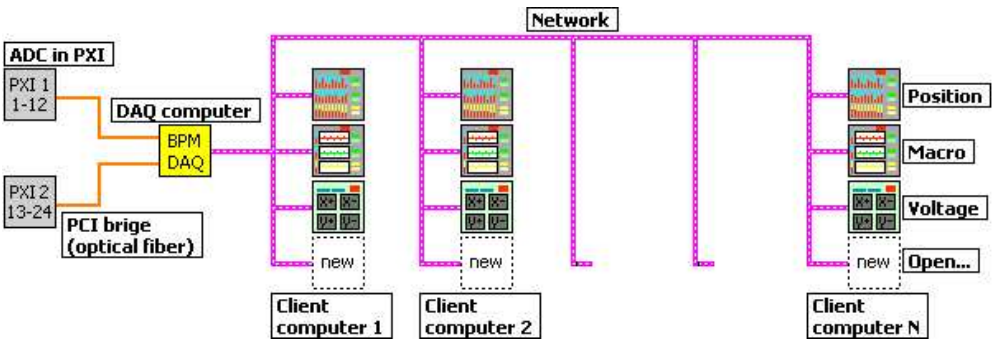

Fig. 1: *The BPM system software structure.*

Longitudinal Phase Space Analysis at ELBE

U. Lehnert, P. Michel, J. Teichert

Due to the acceleration principle the longitudinal phase space of an electron beam at the exit of an RF accelerator shows a strong correlation which depends on the actual accelerator tuning. Therefore, measurements of single parameters as energy spread and bunch length do not deliver enough information to judge the quality of the beam for applications like free-electron lasers or for bunch compression using a magnetic chicane. Here, we describe a scanning method used to gain the complete phase space information of the ELBE beam.

The main longitudinal beam parameters as energy spread, bunch length and emittance are determined by the quality of the injected beam and the capture process of the beam into the the RF field of the first cavity. At its exit the beam already has relativistic energy (to date 8 MeV) and its longitudinal emittance is essentially fixed. Now, one ELBE cryomodule comprises two completely independent accelerator cavities. This opens the opportunity, to use the second cavity as an analyzer to determine the beam properties at the exit of the first one.

In the normal mode of operation the phase of the second cavity is adjusted so that the beam sits on the crest of the accelerating field. However, it is possible to detune the phase which yields two effects. First, the average beam energy is accordingly reduced. But in addition to that, an energy slope is imposed to the beam changing the energy of those electrons which deviate from the mean phase of the bunch. As Fig. 1 illustrates, measured energy spectra contain different projections of the longitudinal phase space effectively yielding different "viewing angles" of the distribution.

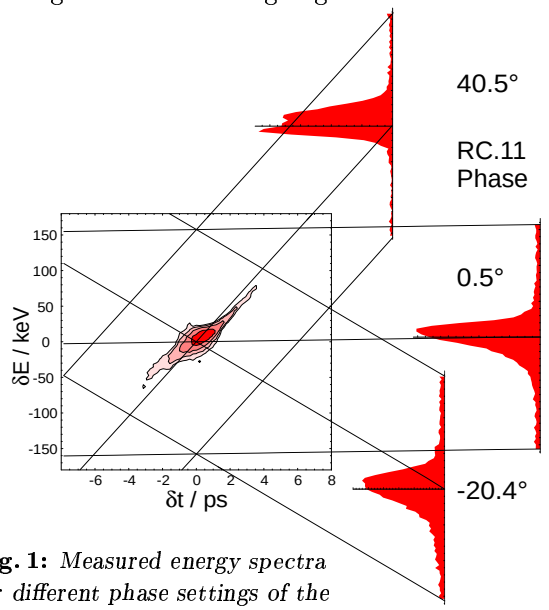

Fig. 1: *Measured energy spectra for different phase settings of the second accelerator cavity together with the reconstructed phase-space density of the electron beam.*

We have measured a set of 15 energy spectra covering a phase span of 60 degrees. The beam energy at the exit of the first cavity was 8 MeV with the second cavity accelerating by 3...4 MeV depending on its phase setting. The bunch charge was C=3 pC for all measurements. Using an image reconstruction algorithm like the ones used in X-ray tomography, we have obtained a complete mapping of the longitudinal phase space from the measured energy spectra.

From the reconstructed phase space distribution it is now possible to obtain several parameters which are commonly used to characterize such distributions. However, due to noise and background in the measured energy spectra, the phase space reconstruction shows spurious densities far off the main beam. To reduce the influence of those artifacts the lowest densities in the distribution were chopped, retaining 95% of the distribution integral. For this chopped distribution a longitudinal emittance ε_{RMS}=50 keV ps was computed. It has to be considered, however, that the chopping itself reduces the computed emittance. Assuming gaussian distributions the amount of this reduction can be estimated and the computed emittance can be corrected for this error. If one does that, one arrives at the so-called core emittance (see Fig. 2).

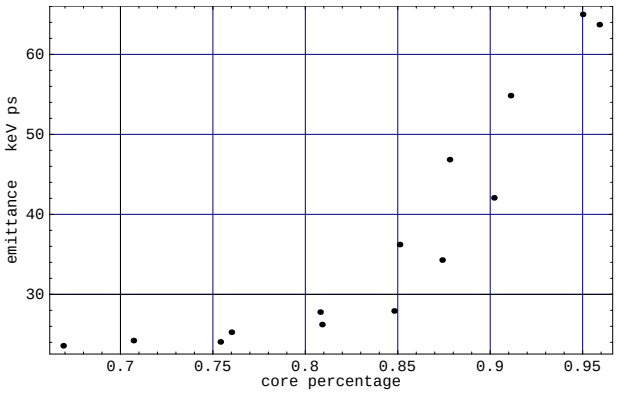

Fig. 2: *Core emittance computed with only considering a certain core fraction of the phase space distribution.*

This core emittance is stable for low fractions of the beam showing that the main part of the beam behaves approximately gaussian. However, if one consideres more than 80% of the reconstructed phase space distribution the emittance grows substantially. This is exactly the behaviour one would expect for a beam with large tails. For all practical purposses the long tails are irrelevant and mainly caused by the measurement method. So, one can conclude that an emittance of ε_{RMS}=25 keV ps is best fit to describe the measured values. The bunch length was estimated to τ = 1.9 ps but can be reduced to $\tau \approx 1$ ps using a magnetic chicane.

Experimental Work at ELBE

As the ELBE accelerator is operational and the electron beam is available, the main focus of the work at ELBE is shifting from the accelerator buildup to the setup of the different experimental areas and beamlines. Major contributions to this task come from the FZR institutes that will be users of the ELBE facility as well as from outside users. While most of the scientific aspects of this work are published elsewhere, this chapter shall give a representative overview of the user activities at ELBE.

Naturally, the highlight of this year are the first experiments at the Bremsstrahlung facility. Set up by the Institute of Nuclear and Hadron Physics of the FZR, this beamline has been the first one to become operational at the end of year 2002. But also the installation of the Radiation Physics beamline and the mid-infrared FEL were continued. Both facilities are expected to deliver first beams in year 2003. In the neutron laboratory a neutron generator was successfully put into operation. The electron beamline to the neutron laboratory and a neutron generator target are designed in collaboration with the Dresden Technical University. Newly added to the account of ELBE are plans to install a pulsed positron source in collaboration with the University Halle-Wittenberg.

First Experiments with the Bremsstrahlung Facility

R. Schwengner, F. Dönau, E. Grosse, L. Käubler, S. Mallion, G. Rusev,
K. D. Schilling, W. Schulze, A. Wagner, A. Wagner II

The facility for the production of bremsstrahlung at ELBE has been designed for nuclear-structure experiments using photon-induced reactions such as (γ, γ') (nuclear resonance fluorescence), (γ, n), (γ, p) (nuclear photoeffect) and photon-induced fission. In 2002, the beam line in the accelerator hall was assembled by the department for experimental facilities and by the department of the radiation source ELBE. The main components such as the beam-diagnostic elements, the water-cooled radiator holder with three radiator positions [1], the beam shutter/hardener [2], the electron beam dump and the conical collimator for the bremsstrahlung made of pure aluminium [3] were installed.

In the experimental area, the beam line behind the collimator was completed. The polarisation monitor [4], the tube for transporting the photon beam in vacuum, the photon beam dump [5] and a NaI(Tl) detector for monitoring the Compton-scattered incident photons [6] were installed.

For the measurement of the characteristic γ radiation of the nuclides to be studied a setup of high-purity germanium (HPGe) detectors [7] was mounted. Four HPGe detectors are designed for experiments with polarised bremsstrahlung and are placed at 90° relative to the beam direction and at 90° to each other. Each of these four detectors with an efficiency of 100 % relative to a 3" × 3" NaI detector is surrounded by an escape-suppression shield consisting of eight bismuth germanate scintillation detectors. A fifth HPGe detector is positioned at 130° with respect to the beam direction in order to enable the measurement of angular distributions of the γ rays. The detector setup in the experimental area is shown in Fig. 1.

Fig. 1: *Setup of high-purity Ge detectors surrounded by escape-suppression shields. The photon beam enters the experimental area from the right.*

The first nuclear-resonance-fluorescence experiment was carried out on the nuclide ^{88}Sr at an electron energy of 12 MeV. A γ-ray spectrum measured in this experiment is shown in Fig. 2. We observed transitions known from previous studies [8] as well as several additional transitions in the range from 7 to 11 MeV. The experiments are carried on with the investigation of molybdenum isotopes with various neutron numbers. These investigations aim to identify excitation modes at higher energies than reached in previous studies [9] and thus, to get new information about the proton-neutron interaction and its influence on the properties of the nuclear many-body system. Special emphasis is laid on the search for electric and magnetic dipole strength in and above the range of the particle-separation thresholds, which may also have implications for reaction rates important for the element production in the universe.

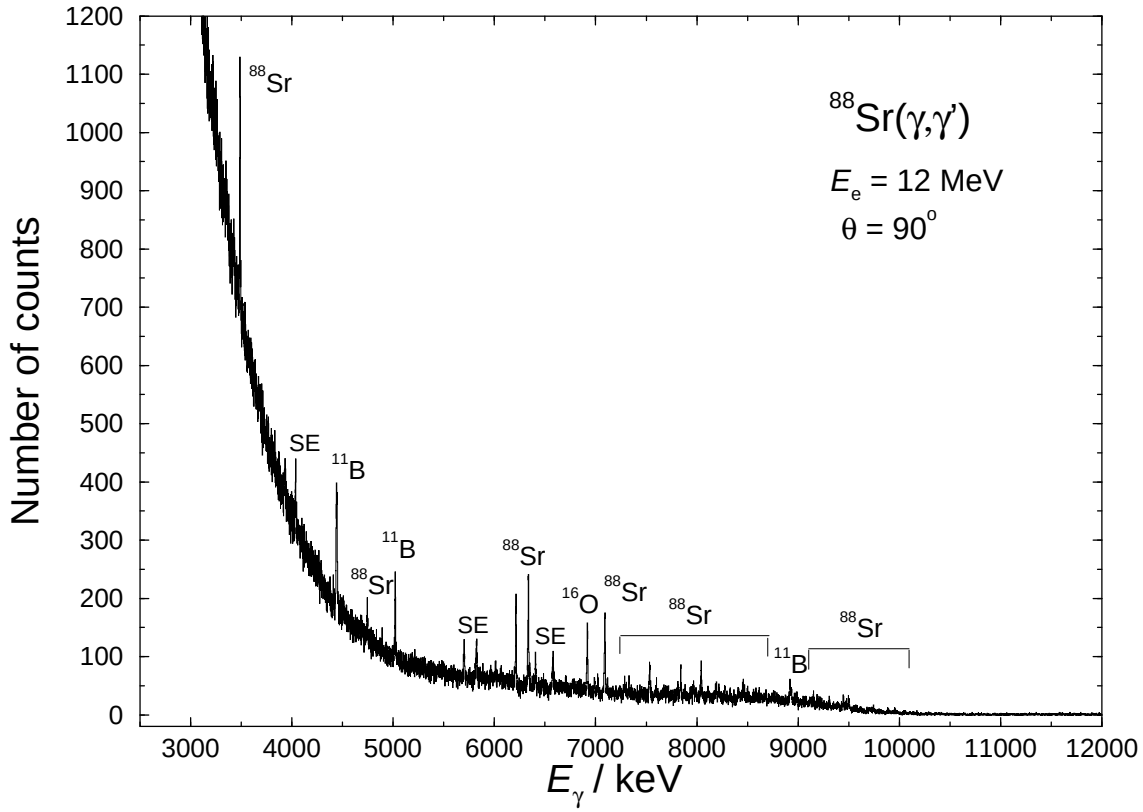

Fig. 2: *Spectrum of photons scattered from ^{88}Sr and measured at 90° relative to the beam direction. Transitions labelled ^{88}Sr are assigned to this nuclide. Transitions labelled ^{11}B and ^{16}O arise from H_3BO_3 combined with the target and used as a calibration standard. Peaks labelled SE are single-escape peaks.*

[1] K.D. Schilling et al., IKH Annual Report 2002, in preparation
[2] K.D. Schilling et al., IKH Annual Report 2001, FZR-341 (2002), p. 41
[3] K.D. Schilling et al., IKH Annual Report 2001, FZR-341 (2002), p. 37
[4] R. Schwengner et al., IKH Annual Report 2001, FZR-341 (2002), p. 39
[5] A. Wagner et al., IKH Annual Report 2000, FZR-319 (2001), p. 40
[6] A. Wagner et al., IKH Annual Report 2001, FZR-341 (2002), p. 38
[7] R. Schwengner et al., IKH Annual Report 2002, in preparation
[8] L. Käubler et al., Eur. Phys. J. A 7 (2000) 15
[9] G. Rusev et al., IKH Annual Report 2001, FZR-341 (2002), p. 77
and IKH Annual Report 2002, in preparation

Dose-Rate Measurements around the Bremsstrahlung Facility at ELBE

K.D. Schilling, P. Michel, R. Schurig, H. Taubert

Our goal was to study the radiation problems that arise around the nuclear physics beam line during the production of nuclear bremsstrahlung. This beam line will be used - in the first place - for nuclear resonance fluorescence (NRF) experiments and - at a later stage - for the study of exotic nuclei via bremsstrahlung-induced photofission.

In order to assess all aspects realistically, we have to take into account a variety of possible beam losses inherent in the accelerator layout and operation together with the physics of the production of secondary radiation. All this together makes it extremly difficult to quantify radiation in an absolute way.

The most important aspect was to get a scale for the radiation fields that were generated under measuring conditions and that may lead to damages of the electronic equipment for the beam diagnostics along the beam line.

Electrons interact primarily by way of bremsstrahlung photons (γ-rays) they emit when slowing down in an absorber. These γ-rays may go on to produce high-energy electron-positron pairs and hence propagate an electromagnetic shower in the absorber. Above a certain threshold energy (usually 6 to 13 MeV), high-energy photons may undergo photonuclear reactions and produce neutrons, protons and heavier particles. The radiation level around an electron accelerator will be entirely dominated by bremsstrahlung photons produced in all kinds of target material. The local dose rate will be dependent on emission angle, target thickness and the presence of surrounding material.

The dose rates summarized in Table 1 were measured with the universal dosemeter UNIDOS (PTW Freiburg) at different positions around the nuclear physics beam line as indicated in Fig. 1. They are mainly due to the interaction of electrons of the beam envelope with beam-line components. Thereby, the main source of bremsstrahlung background seems to originate from beam-line elements downstream of the radiator - the latter being the converter of kinetic electron energy into bremsstrahlung for the nuclear-physics experiments. Those parts of the beam line are hit by electrons of the beam envelope (halo) that is produced by small-angle scattering of the electrons during their passage through the radiator foil. This observed radiation level can be influenced by the beam parameters (e.g. beam energy, intensity, alignment) as well as by the radiator thickness and composition, as can be seen in Table 1.

We have to conclude that careful beam and radiator optimization as well as shielding of the relevant beam-line elements are needed to minimize the radiation losses and, thus, to reduce the risk of radiation damages of the electronic devices along the nuclear physics beam line.

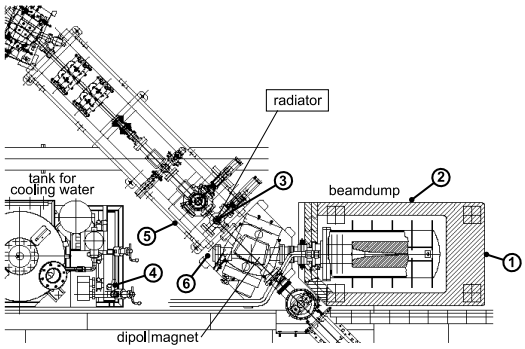

Fig. 1: *Site map of dosemeter positions given in Table 1 (col. 1) around the nuclear physics beam line.*

[1] W.P. Swanson, IAEA Technical Report No. 188, Vienna, 1979

[2] A.H. Sullivan, A Guide to Radiation and Radioactivity Levels near High Energy Particle Accelerators, Nuclear Technology Publishing, Ashford, Kent, UK, 1992

Position	$\dot{D}$ [Gy/h]	I(e-) [mA]	E(e-) [MeV]	P [kW]	Estimate [Gy/h]	Remarks
1	2,7	0,6	12	7,2	80 (R) 7 - 10 (S)	Pb wall (5 cm) behind BD
2	6,6	0,6	12	7,2	70 (R) 15 - 20 (S)	do.
3	2,2	0,6	12	7,2		10 cm Pb behind BD & around bellows
4	12	0,6	12	7,2	8 (R) 1,2 (S)	do.
5	3,6	0,6	12	7,2		do. measurement at pyrometer site
5	3	0,6	12	7,2		do. do. & Pb & Pb plate (2 cm) in front
5	0,2	0,6	12	7,2		do. do. & 15 cm Pb in front
5	1,8	0,6	12	7,2		do. do. + pyr. hole: no Pb, but Pb around
6	36	0,2	8,5	1,7	25 - 50 (R) 6 - 10 (S)	do. behind DM/ at videocam site
6	60	0,6	12	7,2	50 - 100 (R) 14 - 24 (S)	do. do.
6	2,1	0,6	12	7,2		do. do. /without radiator

Tab. 1: *Dose rates $\dot{D}$ at positions marked in fig.1 and associated beam parameters (I = intensity, E = energy, P = power). Estimates of $\dot{D}$ labelled with (R) resp. (S) have been calculated according to fomulae given in [1] and [2], respectively. They and their intercorrelations may be considered as approximate guideline values rather than exact ones. BD = Beam Dump, DM = Dipole Magnet.*

The influence of electron scattering in the target on the beam transmission

H. Müller, W. Neubert, U. Lehnert

The interaction of the electron beam with targets increases the divergence and leads to collisions with the beamline materials producing bremsstrahlung and, to a lower extend, neutrons. According to the demands of radiation protection in the radiation physics cave such beam loss must be less than 5 μA supposed that the current delivered by the accelerator is 1 mA. The intended irradiation of cell cultures with quasi-monochromatic channeling radiation requires also a very low background level. These requirements can be fulfilled only by an optimized beam transport to the beam dump. Since beam transport codes usually do not take into account interactions with target materials specific simulations with other transport codes like GEANT become necessary. In our calculations we defined the transmission as the ratio of the number of electrons at the exit of the bending magnet or at the entry of the beam dump, respectively, to the number of electrons started in front of the target.

Earlier simulations carried out with GEANT 3.21 [1] have shown that the original beamline design [2] had to be upgrated with an increased beam tube 66 mm in diameter connecting goniometer chamber and bending magnet. Further, an increase of the gap of the original 45^o bending magnet to 90 mm was necesssary. Simulations carried out with targets of carbon (35 and 100 μm thick, with the density of diamond) showed that the above requirements can be fulfilled for this new design for beam energies above 15 MeV only. But the limited power of the dipole magnet allows at 90 mm gap and higher electron energies only deflections less than 45^o. Therefore, the new vacuum chamber was designed for the bending angle of 35^o.

The complete upgraded beamline with the 35^o bending magnet and the beam tubes to the beam dump [3] with additional quadrupol lenses has been implemented into a geometry file for GEANT 4. Instead of the constant magnetic field in the GEANT 3.21 simulations the complete magnetic field cards [2] have been used in the GEANT 4 version. Fig. 1 shows the results of these simulations with incident energies from 5 MeV to 40 MeV.

In Table 1 we summarize and compare the results obtained by GEANT 3.21 and GEANT 4 behind the beam bending magnet. Both code versions show a reasonable agreement at the reference energy of 20 MeV. Slight differences in Table 1 are due to different bending angles and the treatment of the magnetic field. There are considerable differences at lower energies but both simulations show that the requirements of about 98 % transmission rate cannot be fulfilled at energies lower than 20 MeV.

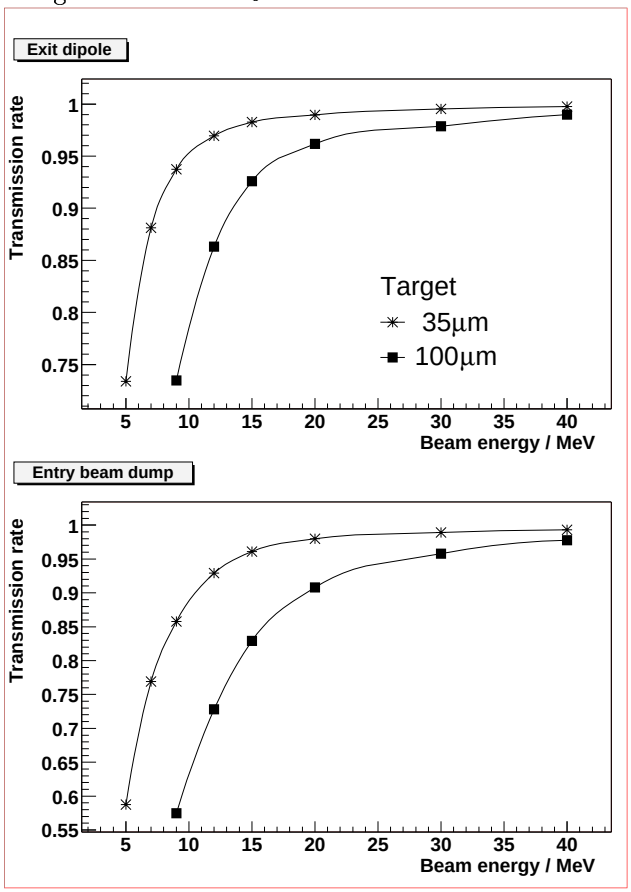

Fig. 1: *Transmission rate for the exit of the dipole (upper panel) and the entry of the beam dump (lower panel) as function of the electron energy obtained from GEANT 4 simulations.*

GEANT version	g4	g3	g4	g3
cryst. thickness	35μ	35μ	100μ	100μ
E_e=7 MeV	0.88	0.76	0.60	0.55
E_e=9 MeV	0.94	0.86	0.73	0.70
E_e=12 MeV	0.97	0.94	0.87	0.86
E_e=15 MeV	0.98	0.97	0.93	0.92
E_e=20 MeV	0.99	0.99	0.96	0.97
E_e=40 MeV	1.00	-	0.99	-

Tab. 1: *Transmission rates for the exit of the dipole magnet calculated by GEANT 4 (g4) and GEANT 321 (g3). 35 deg bending in g 4 ; 45 deg. bending in g 3.*

[1] W.Neubert, W.Enghardt, U.Lehnert, E.Müller, B.Naumann, A.Panteleeva, J.Pawelke:, "Optimization of a Tunable Quasi-Monochromatic X-ray Source for Cell Irradiations" Proceedings Monte Carlo 2000 Conference, Lisbon, 23-26 Oct. 2000, p.123

[2] U.Lehnert: Annual Report 2000, WTB FZR-319, April 2001, p.18-19

[3] B.Naumann:"Berechnung des Strahlungsuntergrundes in der Umgebung der Strahlfänger an der Strahlungsquelle ELBE",WTB FZR-345, März 2001.

Radiation Shielding of the Beam Dump of the Radiation Physics Beamline

W. Enghardt, W. Neubert, J. Pawelke, W. Wagner

A channeling radiation (CR) source is being developed at ELBE in order to perform measurements of RBE values of quasi-monochromatic photons in the energy range of $10 \div 100$ keV [1]. Reliable studies of radiobiological effects on living cells need irradiation dose rates of $0.1 \div 1$ Gy/min where a sufficiently low level of background radiation (polychromatic bremsstrahlung and neutrons) in the experimental area is required. The background equivalent dose rate should contribute less than 5% to the biological effect, i.e. 300 mSv/h in the worst case scenario at a CR dose rate of 0.1 Gy/min. The beam dump of the electron beam situated inside the wall of the Radiation Physics cave is a rather strong source of photon as well as neutron radiation which, therefore, has to be efficiently shielded to enable such investigations (see Fig. 1).

Principally the design of a radiation shielding has to be carried out conservatively considering the most critical conditions. Equivalent dose rates at the surface of the beam dump vessel have been calculated my means of Monte Carlo simulations using the FLUKA code [2] and assuming a maximum average beam current of 250 μA at a maximum electron energy of 50 MeV. The resulting values amount to 500 Sv/h for photons and 40 Sv/h for neutrons. Hence, the necessary radiation shielding of the electron beam dump has to simultaneously reduce the influence of these background components by factors of the order of $10^{-3} \div 10^{-4}$. Assuming a tenth value attenuation length (TVL) of 30 cm for concrete [3] this would require a wall thickness of about 1.2 m which would reduce the space for experiments considerably.

Layer	Material	Thickness/cm	AL/TVL
1	Pb	10	0.47
2	Pb	6	0.28
3	PE [1]	15	1.00
	PE [1]	12	1.20
4	Pb	6	0.12
5	PE [1]	3	0.30
Sum			3.37

Tab. 1: *Attenuation lengths for neutrons [4,5]*

The more compact shield designed consists of an optimized sandwich structure of the shielding wall containing several layers of different materials where high-Z elements absorb the photons and layers containing hydrogene effectively thermalize the neutron spectrum to reach a large rate of neutron capture. Successively, the γ-rays being emitted during neutron capture reaction (e.g. 2.22 MeV at ^{1}H) have to be absorbed by the outer shielding materials.

The sandwich structure chosen is given in Tab. 1. Calculating the macroscopic attenuation cross sections for the layers one obtaines the partial attenuation lengths (AL) for neutron removal in units of TVL (Tab. 1).

Layer	Material	Thickness/cm	AL/TVL
1	Pb	22	3.65
2	PE [1]	27	0.17
Sum			3.82

Tab. 2: *Attenuation lengths for photons [3]*

The corresponding integral AL for photon attenuation are given in Tab. 2. By summing up of the partial AL values one can evaluate the attenuation factors for the components of background radiation which amount to 1.5×10^{-4} and 4.3×10^{-4} for photons and neutrons, respectively. In result equivalent dose rates of 75 mSv/h and 17 mSv/h are obtained behind the radiation shield of the beam dump what eventually provides a total background equivalent dose rate of 92 mSv/h and meets the above determined requirement. It should, however, been noted that additional background radiation components emerging from unavoidable beam losses along the electron transfer line from the X-ray source to the beam dump have to be expected [6]. The dose rate due to neutron capture γ-quanta can be neglected.

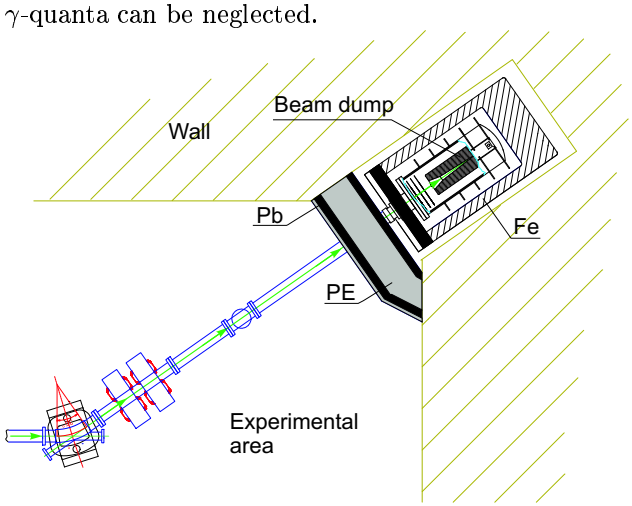

Fig. 1: *Layout of the radiation shield near the beam dump*

[1] A.Panteleeva et al., FZ Rossendorf, Wiss.-Tech. Ber. FZR-271 (1999) 95
[2] B.Naumann: Berechnung des Strahlungsuntergrundes in der Umgebung der Strahlfänger an der Strahlungsquelle ELBE, Wiss.-Techn. Berichte, FZR-345 (2002)
[3] J.H.Hubbell, S.M.Selzer, http://www.physics.nist.gov/PhysRefData/XrayMassCoef
[4] K.Shure et al., Nucl. Sci. Eng 35 (1969) 371
[5] Medizinische Elektronenbeschleuniger-Anlagen, DIN 6847, T. 2, S. 197
[6] W.Neubert et al., FZ Rossendorf, Wiss.-Tech. Ber. FZR-319 (2001) 41

[1] polyethylene

A Magnetic Chicane for Phase Matching of Two Separate Undulator Units

P. Gippner, R. Wünsch

If the undulator of a free-electron laser consists of separate units the phases of the electron-wave interaction in the various units have to be matched. The corresponding matching condition depends on parameters of both the electron and the electromagnetic beam.
The undulator U27 consists of two separate sections with a drift space d between them. Varying the undulator gap g the optical wavelength is changed and consequently the phasing between the undulator sections has to be changed as well. This can be done by properly choosing the length of the electron flight path between the sections by varying their distance d in dependence on undulator gap and electron energy. This method was extensively described in ref. [1].
To avoid moving the second section it was proposed to install a magnetic chicane [2-5], which can continuously increase the electron path with respect to a copropagating light ray and hence ensure the phase matching for a constant separation d at any undulator gap and electron energy.
Such a chicane may consist of three [2-4] or four dipoles [5] deflecting the electrons to only one side or to both sides. The design of a suitable chicane consisting of 3 dipoles is shown in fig. 1. The outer magnets have the same field strength B and iron yokes of the same lengths l_m, whereas twice the dipole strength is required for the central magnet most easily realized by twice the iron length l_m. The corresponding fields have been calculated using the code RADIA [6].

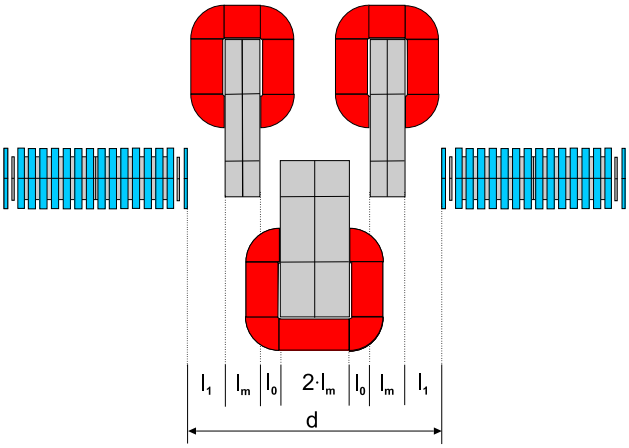

Fig. 1: *The dipoles of the 3-pole chicane between the undulator segments.*
(l_m=40 mm, l_0=25 mm, l_1=45 mm and d=300 mm.)

It is the aim of this investigations to study the influence of the superimposing fringe fields on the matching conditions. The necessary stability of the currents exciting the magnetic fields in the dipoles is a second point of interest.
Fig. 2 shows three typical field distributions and the resulting electron paths when the chicane is adjusted along the z-axis. Further calculations have shown that the dipole strength $B = 3.3\,\mathrm{T\,mm}$ is sufficient for matching the beam in the electron energy range $E = 12 - 40\,\mathrm{MeV}$. This strength can be generated by excitation currents $I * n = 0.8\,\mathrm{kA}$ turns in the dipole coils, far from nonlinearities of the hysteresis curve of ARMCO iron. The stability of the power supply should be 10^{-4}.

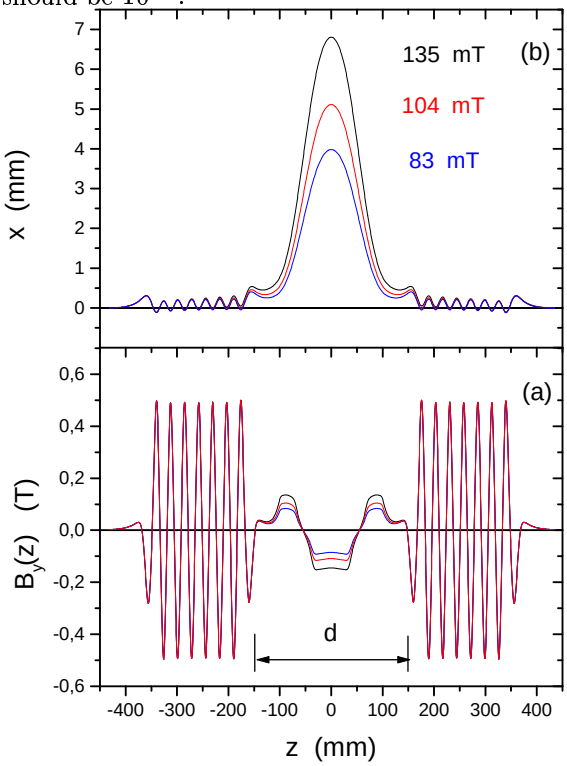

Fig. 2: *Field distributions (a) and corresponding electron trajectories calculated for a 3-pole chicane (b) for 3 different field strengths. The two undulator units are indicated by a few periods only.*

The design of a possible chicane consisting of 4 dipoles is shown in Fig. 3. Fig. 4(a) indicates three typical field distributions when this chicane is adjusted along the z-axis. The outer and inner magnets exhibit the same absolute field strengths $|B|$ since the coils of the dipoles (D1,D4) and (D2,D3) operate in series supplied with the currents I1 and I2, respectively. The trajectories of electrons with a kinetic energy of E = 20 MeV are shown in Fig. 4(c) for three values of the field strength. In a 4-pole chicane electrons cross the optical axis at the same intersection point nearly independent of the strength of the magnetic field (center of Fig. 4a, Table 1). This can be used for Compton back-scattering of infrared light quanta stored in the resonator. Fig. 4(b) indicates the angle of the electron velocity vector with respect to the axis. The intersection angle changes by varying the magnetic field strength.

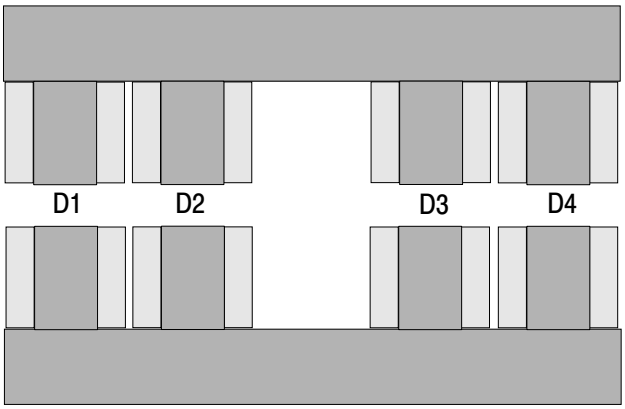

Fig. 3: *Cross section of the projected 4-pole chicane. The dipoles D1 ... D4 have the same dimensions. The wide interval between the dipoles D2 and D3 forms a space for the flange of the vacuum chamber.*

$\frac{I_1 * n}{\text{A turns}}$	$\frac{I_2 * n}{\text{A turns}}$	$\frac{\alpha}{\text{mrad}}$	$\frac{x_s}{\mu\text{m}}$	$\frac{L}{\text{mm}}$	$\frac{\tau}{10^{-9}\text{s}}$
-600	+963	35	5.6	320.057	1.0679
-800	+1338	49	0.3	320.108	1.0681
-1000	+1720	62	2.9	320.177	1.0683

Table 1: *Parameters of the electron path (E=20 MeV) within the 4-pole chicane;*
α, x_s: angle and displacement in the center;
L, τ: path length and time of flight.

Fig. 5 shows the normalized single-pass gain as a function of field strength B in a 3-pole chicane calculated for a monoenergetic 20 MeV beam in the U27 undulator. The peaks correspond to the points of optimum phase matching. The Figure illustrates that the gain can be considerably increased by a magnetic chicane with a sufficiently high field. However, due to its rapid variation the gain is highly sensitive to the field strength and to the electron energy as well. In particular for fields above 100-150 mT the energy spread of the ELBE beam turns out to be too large for such a chicane. A remarkable increase of the gain can only be achieved with a beam energy spread smaller than 0.05% [3]. The calculations have been performed by means of the code GPT [7].
It is the main purpose of future investigations experimentally to confirm the correct phase matching.

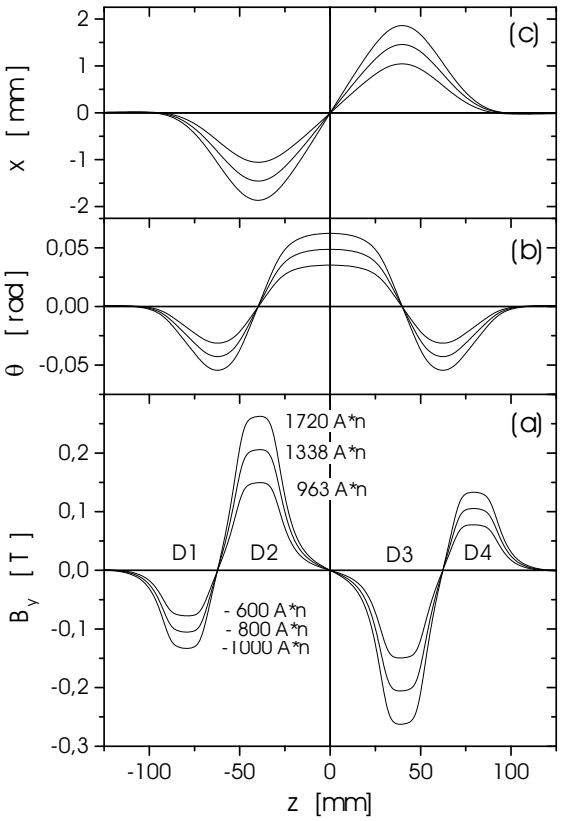

Fig. 4: *Field distributions within the 4-pole chicane (a) for three dedicated values Ampere*turns and the corresponding trajectories for an electron with the kinetic energy of E = 20 MeV (c). The symbol θ indicates the angle of the electron velocity vector relative to the z-axis (b).*

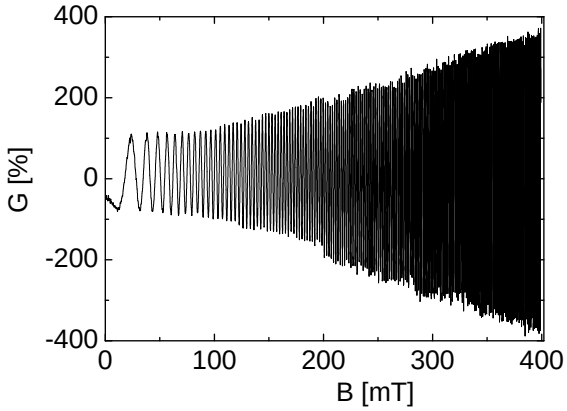

Fig. 5: *Single-pass gain of the U27 undulator calculated as a function of the field strength in a 3-pole chicane. The first peak has been normalized to 100%.*

[1] P. Gippner and J. Pflüger, FZ Rossendorf, Annual Report, FZR-319 (2000) 26
[2] J. Pflüger and M. Tischer, TESLA-FEL 2000-08, December 2000
[3] R. Wünsch et al., Proc. 23rd Int. Free Electron Laser Conf., Darmstadt 2001; Elsevier Science, Amsterdam 2002, p. II-61
[4] P. Gippner, FZ Rossendorf, Annual Report, FZR 341(2002)28
[5] S. Benson, G. Biallas, T. Hiatt, J. Karn, JLAB-ACC-97
[6] P. Elleaume, O. Chubar and J. Chavanne, J. Syn. Rad 5 (1998) 481
[7] S.B. van der Geer and M.J. de Loos, The General Particle Tracer, http://www.pulsar.nl

Temperature Stabilization of the Out-Coupling Mirror Wheel

W. Seidel, M. Sobiella, D. Wohlfarth, U. Wolf

For the U27 Free-Electron Laser (FEL) the so-called hole coupling method, using broad-band metal mirrors with an on-axis aperture in one of the mirrors was selected. It is important to know the extraction ratio, i.e. the fraction of intracavity power that is coupled out of the cavity per roundtrip of the optical wave. We have optimized the extraction ratio for the wavelength range of U27 by using different holes in different mirrors [1]. The optical resonator will be equipped with Au coated Cu-mirrors on a revolvable holder (wheel). To bring one of the mirrors in the right position for lasing, we use a high-precision rotating stage on which the 5 out-coupling mirrors are mounted. Although only a small absorption (about 1 %) is expected in the mirror, the entire construction will be heated up to a definite temperature during the normal laser operation without any additional precautions. This will lead to a change in the resonator adjustment (length and angle) by thermal expansion and to an unacceptable heat load of the precession mechanics. For an intracavity power of up to about 1 kW we estimate a permanent heating power of about 10 W at the mirror. By heating the mirror in vacuum with this power, we measured a saturation temperature of the wheel of around 100^{o}C after 20 hours. This temperature is to high for the mechanical layout of the high-precision rotation stage of the construction. A temperature-stabilized system based on water cooling at a movable precession construction in ultra high vacuum is difficult to realize. Therefore we introduced a special heat isolation between the high-precision rotation stage and the wheel. The wheel was also made from Cu to reduce mechanical tension between the mirrors and the surrounding material. Furthermore, the heat exchange is now realized by a more flexible heat dissipation to the outside of the vacuum chamber (peltier element or air cooling) rather than by thermal radiation only. The most important change was the installation of a heater in the center of the wheel, which stabilizes the mirror wheel temperature at a level slightly above the laser heating temperature. In this way, we achieve that all components are stabilized at the same low temperature undependently whether the laser is working (heating) or not. Fig. 1 shows the measured temperature dependence on time of the working mirror and the wheel by using a permanent heating power of 15 Watt (instead of 10 W for safety reasons). The temperature sensor for the wheel was located at the opposed site of the heated mirror. After 22 hours the saturation temperature of about 50^{o}C was achieved by using the peltier cooler outside. We observed a temperature difference between mirror and wheel of about 4^{o}C, which originates from the temperature gradient inside the wheel by the heat dissipation system. By using air cooling we get a temperature of about 54^{o}C at the mirror. The stabilization of the mirror temperature around 57^{o}C, i.e. slightly above laser saturation temperature of 54^{o}C, is demonstrated in fig. 2. By switching the laser (external heating at one mirror with 15 W) on (▲) and of (▼), we simulated a working regime of an FEL. The black circle indicates that moment when the heating system for the wheel is switched on. The maximum temperature difference of 3.5^{o}C over 20 minutes in the mirror leads to a change in the cavity length of about 1 μm. This effect has a small influence on the FEL operation. Thus, we are satisfied with the presented solution.

[1] W.Seidel, E. Grosse, D. Oepts, B. Rimarzig, U. Wolf, Wiss.-Tech. Ber. FZR-341 (2002) 26

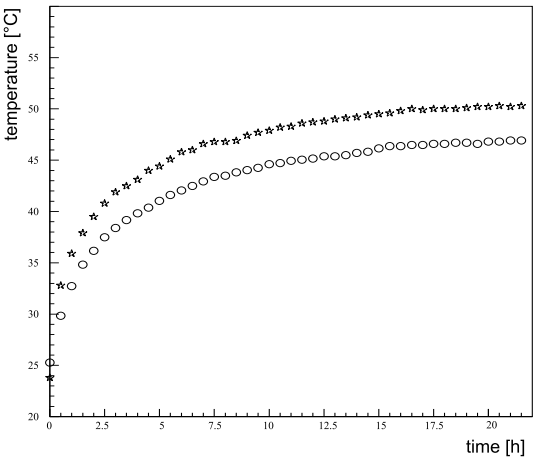

Fig. 1 *Temperature dependence of the working mirror (stars) and the wheel (open circle) with a permanent heating power of 15 Watt at this mirror by using a peltier element for additional cooling (see text).*

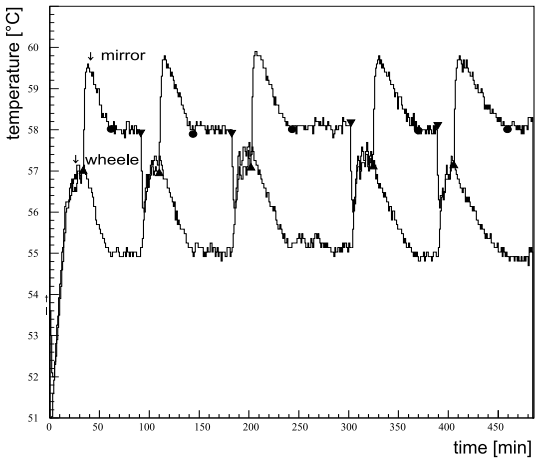

Fig. 2 *Temperature behaviour of the mirror and the wheel during a simulation of a working regime of a FEL (see text; ▲ laser switched on, ▼ laser switched of, • heating for the mirror wheel switched on).*

An Intense Photoneutron Source at ELBE

H. Freiesleben[1], M. Greschner[1], D. Richter[1], K. Seidel[1]

The neutron laboratory of the Institute for Nuclear and Particle Physics, TU Dresden, installed at the ELBE facility will provide researchers with various sources of energetic neutrons.

1. Mono-energetic neutrons of 14.1 MeV kinetic energy will be produced by the DT-reaction – an accelerator providing 300 eV deuterons with a current of up to 10 mA is presently being installed. The beam can be delivered to two tritium targets in dc mode as well as in pulsed mode (slow mode: repetition frequency 1, 10, 100, 1000 Hz, adjustable pulse width between 10 and 100 μs; fast mode: repetition frequency 1, 2, 5 MHz, pulse width 1–1.5 ns).

2. Neutrons with continuous energy spectra will be provided by two photoneutron sources, a massive one (W-PNS) for continuous, an other one [1] (Pb-PNS) for pulsed mode operation; both are driven by the ELBE beam.

A cross section of the neutron hall is shown in Fig. 1 with the position of the neutron sources indicated.

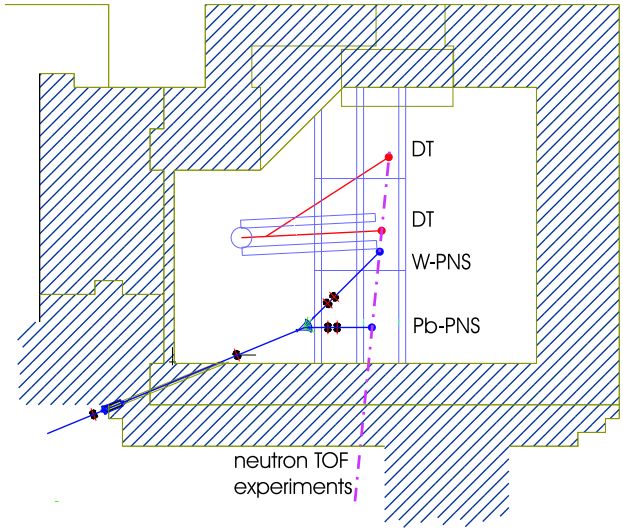

Fig. 1: *Cross section of the neutron hall with the position of the DT-neutron sources and the photoneutron sources.*

Intensive fields of fast neutrons are needed particularly for applied nuclear physics research in the field of thermonuclear fusion technology, where the investigation of neutron interactions in reactor components is a main issue. DT fusion neutrons of 14.1 MeV energy are moderated in the reactor blanket up to thermal energy. As shown in Fig. 2 for the flux spectrum of the shielding blanket of the International Thermonuclear Experimental Reactor (ITER), the neutron spectrum typically consists of a peak at 14 MeV and a broad continuous part extending to low energy. The primary neutron flux has decreased by almost five orders of magnitude at this penetration depth of about one meter.

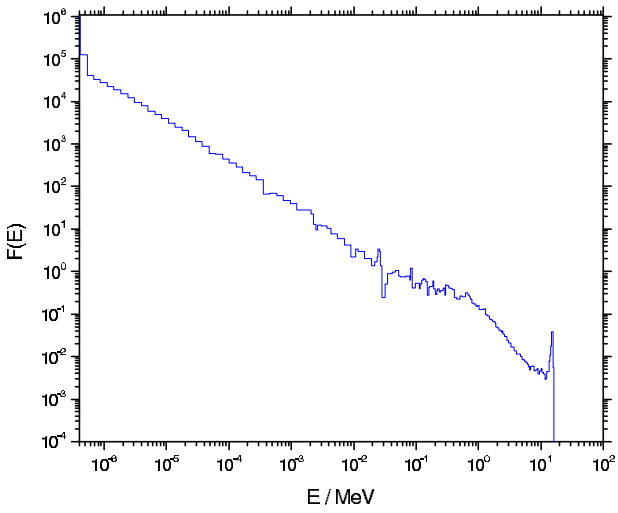

Fig. 2: *Neutron flux spectrum in the ITER Bulk Shield Experiment normalised to a fluence of 1 cm^{-2}.*

As the source strength of the DT neutron generator is limited to 10^{12} s^{-1}, experiments under "deep penetration" conditions can hardly be performed. However, the continuous part of this spectrum can be produced by the massive photoneutron source presently under construction at TUD. With the electron beam of ELBE (1 mA, 40 MeV) which is stopped in a massive radiator about $8{\cdot}10^{13}$ neutrons/s can be expected [2].

The following is a brief description of the various considerations and calculations performed which led to the design of an intense photoneutron source. In order to determine the flux density of electrons and photons as well as the production of photoneutrons in various radiator materials, detailed studies using the Monte Carlo code MCNP3 were carried out to find the most suitable radiator material, in which the bremsstrahlung of electrons is most effectively converted into "photoneutrons" via (γ,xn)-reactions. In these calculations the electrons impinge along the axis of a 10 cm long cylinder, the diameter of which was 10 cm for pure material. In case of composites, a 2 cm cylinder of tantalum was surrounded by a shell of 10 cm outer diameter. The results of these calculations for various radiator materials are summarised in Table 1.

[1]Institute for Nuclear and Particle Physics, TU Dresden

Target material	Neutron Production per 1 electron	Leakage (Backscattering)	
		Photons	Electrons
W	0.0076	0.804 (0.752)	0.0427 (0.0421)
Ta	0.0065	0.842 (0.751)	0.0425 (0.0415)
Ta + Be	0.0042+0.0004	3.007 (1.241)	0.0725 (0.0490)
Ta + D_2O	0.0044+0.00035	3.059 (1.226)	0.0749 (0.0499)

Tab. 1: *Effectiveness of various radiator materials.*

These calculations also showed that the energy deposition of electrons and photons from bremsstrahlung is well concentrated within a cylinder of 5 cm length and 4 cm diameter as can be inferred from Fig. 3. However, the deposition of the beam power of 40 kW in such a small volume would result in the immediate melting of the radiator. Hence, the heat must be distributed over a larger volume for which sufficient cooling must be provided as well. This can be achieved by a rotating massive disk which is cooled by helium; this system is similar to the one at GELINA [4]. The He coolant enables the production of a fast flux spectrum which can be externally moderated according to the requested experimental conditions. The basic layout of the radiator is sketched in Fig. 4.

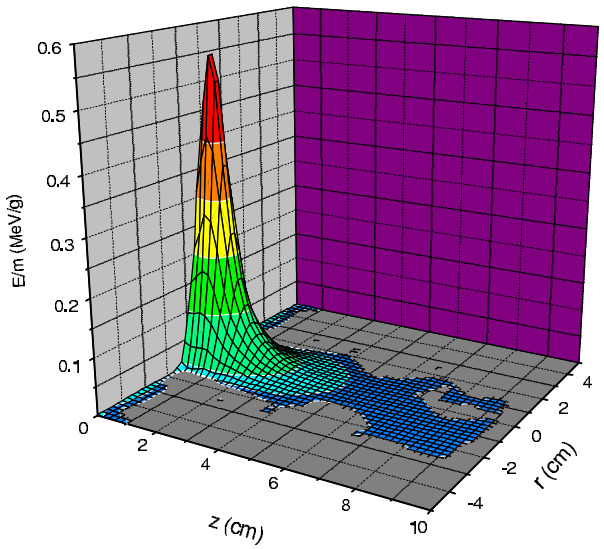

Fig. 3: *Deposition of beam power.*

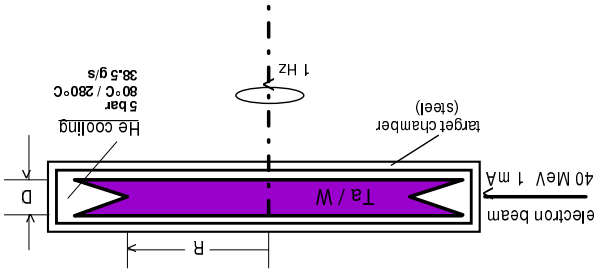

Fig. 4: *Layout of the radiator.*

The radius of the disk and the parameters of the He cooling were derived from calculations of the temperature profile. Examples of radial temperature profiles in the disk for different radii and cooling conditions are shown in Fig. 5. A disk radius of 20 cm and cooling with He gas flowing at 5 bar pressure is found to reduce the radiator temperature sufficiently. As the disk also acts as beam dump its thickness was optimised with respect to photon and electron shielding.

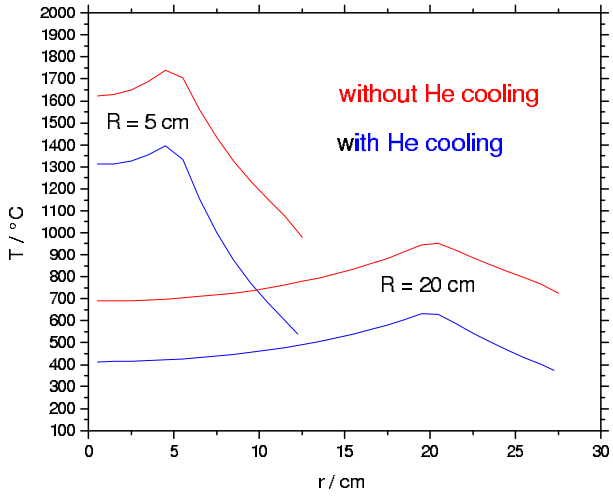

Fig. 5: *Examples of radial profiles of the temperature in the disk for different radii R and cooling conditions.*

The results shown in Fig. 6 led us to design the radiator as a disk of 6 cm thickness; the dove tailed groove serves to maximise the surface hit by the electron beam (cf. Fig. 4). The disk material, heavy met D180 (W-95wt%, Ni-3.8, Fe-1.2), of density ρ=18.0 g/cm^3 was preferred over pure tantalum (ρ=16.6 g/cm^3) because of the higher density, machinability and slightly higher neutron production rate. In addition, the specific radioactivity induced is lower for D180 than for tantalum. This radiator is capable of producing 7.5*10^{13} neutrons/s with 95% escaping the disk if an electron beam of 40 MeV and 1 mA is used.

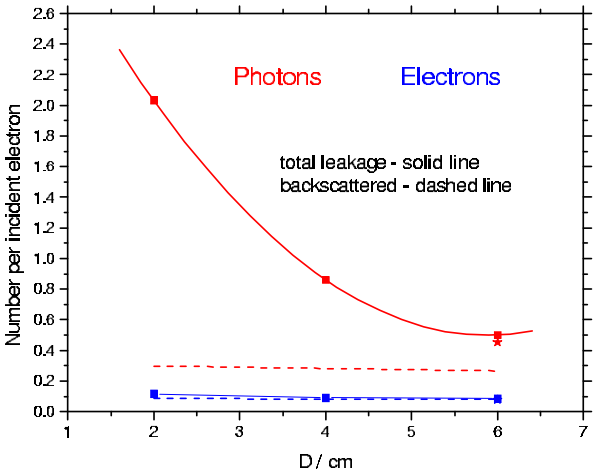

Fig. 6: *Electron and photon leakage as a function of the disc thickness for two different radii, R=5 cm and R=20 cm.*

Fig. 7 displays the neutron spectrum originating from the radiator (D=0 cm) and its modification due to a CH_2 moderator of thickness D=3 and 6 cm placed above and below the radiator. The moderated spectra are very similar to those expected inside an ITER shielding mock-up, thus furnishing fast neutrons of high fluence for studies of e.g. the ITER shield properties well inside the shield.

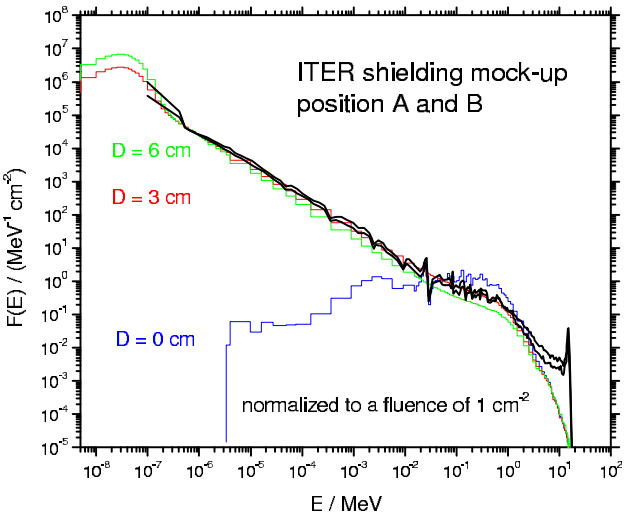

Fig. 7: *CH_2 moderated neutron flux spectrum in comparison with spectral shapes of neutron flux in the ITER blanket.*

The engineering design of the massive tungsten photoneutron source was done by FRAMATOME ANP, Erlangen; it is displayed in Fig. 8.

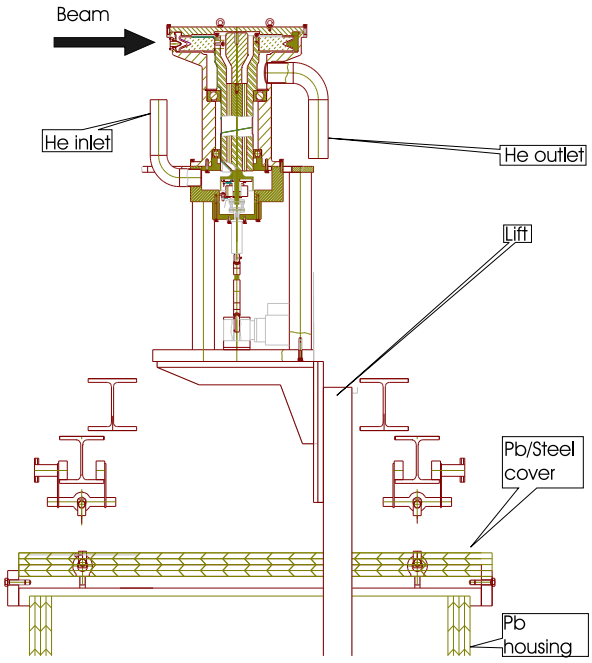

Fig. 8: *Engineering design of the massive tungsten photoneutron source.*

The whole assembly can be raised out of a lead housing (normally covered by a 10 cm thick steel/lead plate) on the ground floor of the neutron hall to a height fo 4.50 m at which the ELBE beam enters the hall. The production of the whole radiator set-up is close to completion; the He cooling system is available and the assembly of the photoneutron source is about to begin.
A source of fast neutrons of such an intensity may also be useful for other applications.

[1] E. Altstadt et al: Design of a Pulsed Photoneutron Source at ELBE, this report
[2] S. Cierjacks, Neutron sources for basic physics and applications, Pergamon Press,Oxford, 1983
[3] J. F. Briesmeister (Ed.), MCNP – A general Monte Carlo n-particle transport code
Los Alamos National Laboratory, Report LA-13709, 2000
[4] J. M. Salome and R. Cools, Neutron producing targets at GELINA, Nucl. Instr. Meth. 179(1981)13

Design of a Pulsed Photoneutron Source at ELBE

E. Altstadt[1], C. Beckert[1], S. Eckert[1], H. Freiesleben[2], V. Galindo[1], E. Grosse[3], B. Naumann[2], F.-P. Weiss[1]

Neutron time-of-flight (TOF) experiments are foreseen at the ELBE facility for energy dispersive studies of the interaction of fast neutrons with matter [1]. The development of a technologically feasible photoneutron source incorporates the design of the radiator and the beam dump. A principle sketch of the photoneutron source driven by the ps-pulsed electron beam of ELBE is shown in Fig. 1.

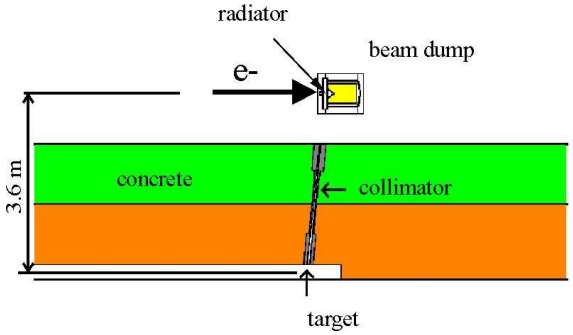

Fig. 1: *Sketch of the TOF-experiment.*

For effective neutron production a radiator material with a high atomic number has to be used. The localized deposition of energy due to the focussed electron beam requires the application of a heavy liquid metal target. Liquid lead was chosen as target material which circulates inside a closed loop. The time resolution of the TOF-experiment depends on the spread of the time the neutrons spend inside the radiator volume. Therefore short neutron path lengths inside the active volume have to be realised. The material depth and width were chosen in the order of one radiation length ($X_0(Pb) = 5.6\,mm$). The liquid metal is exposed to the electron beam if it passes a target section with a cross sectional area of $5.6\,mm \times 5.6\,mm$. The walls of the target section are considered to be manufactured from beryllium or molybdenum with a thickness of 0.5 mm. Energy deposition and particle flux calculations were carried out with the Monte Carlo codes FLUKA [2] and MCNP [3]. The results of detailed calculations of energy angle distribution of the neutrons, photons and electrons leaving the lead radiator showed, that photons and electrons are preferentially scattered in beam direction and the neutrons are scattered isotropically. To reduce the photon and electron background at the target the neutrons are decoupled at about 90 degrees and are directed through a collimator to the target. For an incident electron energy of $E_{e-} = 30\,MeV$ the particle spectra on the radiator surface in front of the collimator were calculated using MCNP and are shown in Fig. 2. Electrons and photons falling below 100 keV have not been tracked further.

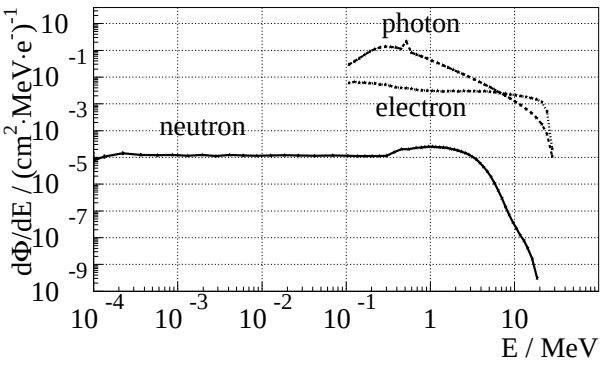

Fig. 2: *Particle spectra for neutrons (full line), photons (dashed line) and secondary electrons (dotted line) on the radiator surface in front of the collimator for* $E_{e-} = 30\,MeV$.

A flight path of about 3.6 meters allows to separate neutrons from bremsstrahlung and secondary electrons simply by their time of arrival. A first calculation of the neutron flux at a distance of 3.6 m only with the lead beryllium radiator neglecting all other constructional components yields a neutron fluence of $7.94 \cdot 10^{-10}\,n/(cm^2 \cdot e^-)$ at $E_{e-} = 30\,MeV$. Assuming an electron current of 1 mA yields a total flux of about $5 \cdot 10^6\,n/(cm^2\,s)$ at the target position. For further reduction of background and increase of flux at the target two concepts were exploited, first: move material, especially near the radiator, out of sight of the collimator and second: reduce the background of thermal neutrons from the collimator by boric polyethylene as cladding material of the collimator. The resulting neutron fluence spectra at the target position show that almost all neutrons come directly from the lead and the radiator wall without further collisions. The background is low and is due to materials close to the radiator which are in sight of the collimator and from the collimator itself. In Fig. 3 the neutron flux due to a δ-shaped electron pulse is shown at the target position as function of time of arrival. At $t = 0$ the electron pulse hits the radiator and at 12 ns the prompt photons reach the target position. The energy range of the measurement determines the maximum number of usable electron pulses. For example if only each fourth electron pulse is taken, the next bunch of photons arrives at $2^2 \cdot 77\,ns + 12\,ns = 320\,ns$. This determines the lowest usable neutron energy of 660 keV ($t < 320\,ns$ corresponds to $E_n > 660\,keV$). However, the neutron flux is reduced by a factor of four.

[1] *FZR, Institute of Safety Research*
[2] *TU Dresden, Institute for Nuclear and Particle Physics*
[3] *FZR, Institute of Nuclear and Hadron Physics; also TU Dresden*

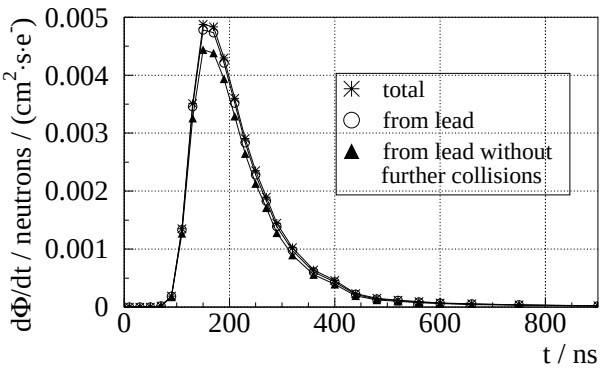

Fig. 3: *Neutron flux per incident electron at the target position as function of time of arrival due to a δ-shaped electron pulse on the radiator with $E_{e^-} = 30\,MeV$.*

The calculated neutron intensity at the target shows that there is a usable energy range from about 660 keV up to 6 MeV. To increase the neutron intensity a bigger radiator is under discussion.
A rough estimation of the energy resolution at the target position for an assumed detector time resolution of 300 ps provides values of about $\Delta E/E \approx 0.4\%$ for $E_n \approx 3$ MeV for a radiator depth of $X_0 = 5.6$ mm.
Numerical calculations of the temperature distribution in the radiator section predict maximum temperatures of 900 °C at the molybdenum wall assuming a mean velocity of about 5 m/s and temperature of 400 °C of the lead flow at the inlet of the radiator section. A mean temperature of 470 °C is obtained in the lead at the outlet of the radiator section.
A test loop (Fig. 4) was designed to validate the numerical calculations and to gain experience with respect to the behaviour of the materials as well as the handling and instrumentation of the loop. The facility was manufactured by the Institute of Physics in Riga. The main components of the loop are an electromagnetic (EM) induction pump, a heat exchanger, an expansion tank and a storage tank with a volume of 10 l. The pipes and the target test section were manufactured from stainless steel SS316L. A traditional EM induction pump is based on a configuration of 3-phase windings to generate a travelling magnetic field which drives the flow. The EM induction pump realised here uses a rotating system of permanent magnets to induce the alternating magnetic field. Advantages of this pump concept are the absence of windings, the compactness, the robust and proper construction. The loop is designed to operate at a pressure up to 6 bar and a maximum flow rate of 0.2 l/s. This corresponds to a maximum velocity of 6.4 m/s in the radiator section. The heat exchanger transfers the heat from the liquid metal through an intermediate fluid - stagnant oil column - to a water circulation system. The quantity of the transferred heat can be controlled by the oil level in the heat exchanger. The maximum power of the heat exchanger is about 30 kW. 16 Thermocouples are used to monitor the temperature of the loop. The flow rate is measured by means of an electromagnetic flowmeter. The principle of the flowmeter is the counterpart to the EM induction pump. The liquid metal flow inside the channel induces a torque on a system of permanent magnets mounted on a freely rotating disk. The angular velocity of the disk is proportional to the flow rate in the channel.

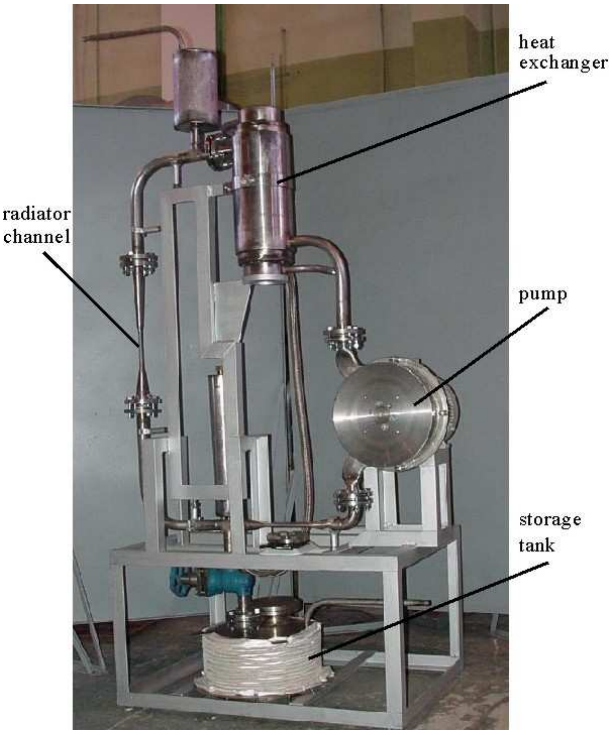

Fig. 4: *The lead loop.*

Because of the large energy loss of the electron beam it emerges as well as the produced photons with sizeable emittance. Hence, a beam dump with large acceptance was designed. It consists of a water cooled cylindrical aluminum body (length 50 cm, diameter 50 cm) with a lead cover (thickness 10 cm at the circumference and 15 cm at the circular bottom). In Fig. 5 the radiator and the beam dump are shown represented in xz-cross section. The electron beam hits the radiator in x-direction, the lead flow is in z-direction.

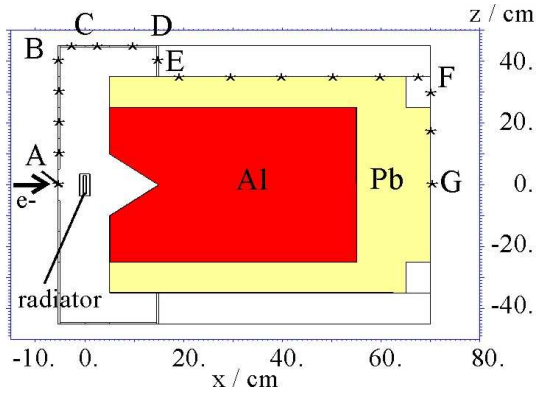

Fig. 5: *The photoneutron source represented in xz-cross section. Capital letters stand for the position points remarked in Fig. 6 and Fig. 7.*

The lead cover is required for reasons of radiation protection. Using the particle transport code FLUKA [2] the dose equivalent rate for neutrons and photons were calculated around the photoneutron source and the beam dump i) without and ii) with the lead cover. The results for an electron beam of $E_{e-} = 50\,\mathrm{MeV}$ are shown in Fig. 6 and Fig. 7, respectively. In forward direction (between the points F and G, Fig. 5) lead reduces $\dot{H}_\gamma$ about three orders of magnitude and the limits of the dose equivalent rate in the neighbouring room are observed.

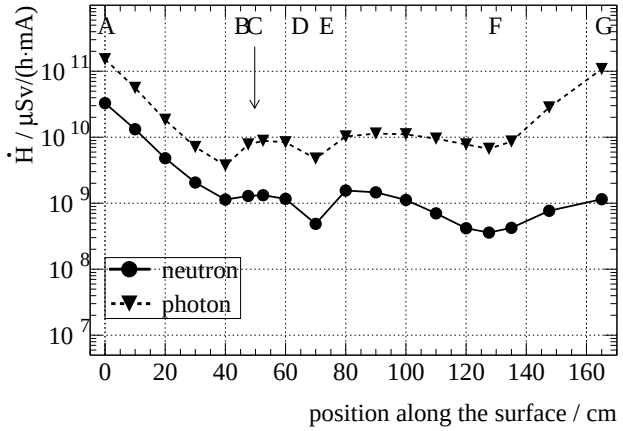

Fig. 6: *Dose equivalent rate for neutrons (full line) and photons (dashed line) around the photoneutron source and the aluminum body at $E_{e-} = 50\,MeV$.*

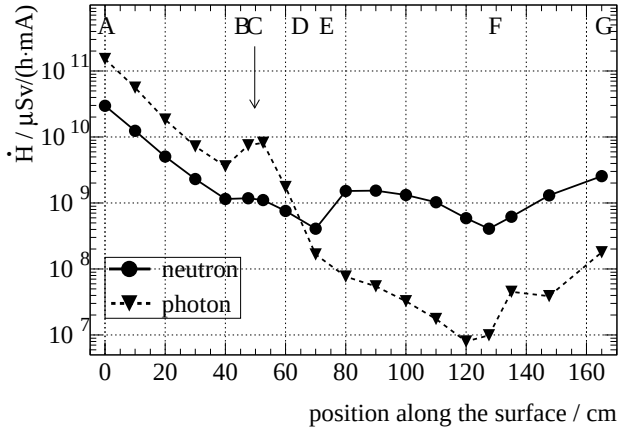

Fig. 7: *Dose equivalent rate for neutrons (full line) and photons (dashed line) around the photoneutron source and the lead shielded aluminum body at $E_{e-} = 50\,MeV$.*

Direct water cooling is realized by a water flow of about 1 l/s through a coil inside the aluminum body (pipe diameter 3 cm, coil diameter 40 cm). Assuming a beam current of 1 mA the total heating power to be removed is about 35 kW. This corresponds to an electron beam of 50 MeV. The radiator itself is housed in an evacuated steel shell which is flanged onto the front side of the beam dump. The temperature distribution to be expected in the beam dump was calculated in a thermal finite element analysis (ANSYS [4],[5]) and is shown in Fig. 8. The maximum temperature of 179 °C found at the cone tip is far below the melting temperature of 670 °C. The maximum lead temperature is about 62 °C. Hence, an additional cooling of the lead cover is not necessary.

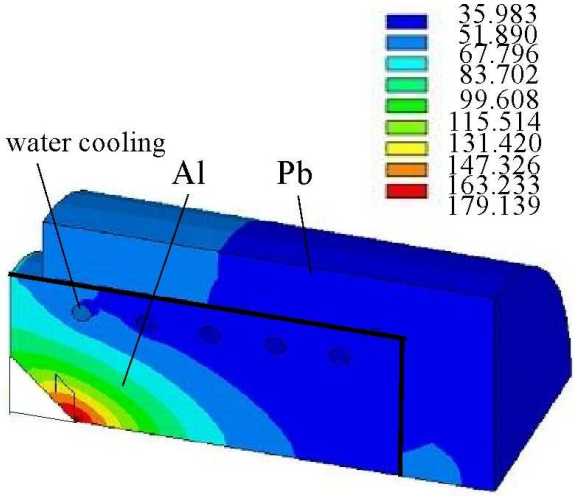

Fig. 8: *Temperature distribution to be expected in the beam dump at $E_{e-} = 50\,MeV$ and $I = 1\,mA$ [5].*

The distribution of the energy deposited in the components of the photoneutron source was calculated using the Monte-Carlo Code FLUKA [2]. For electron beams of 30 MeV and 50 MeV and a beam radius of 1.5 mm the results are shown in Tab. 1.

	beam energy E_{e-}	
	30 MeV	50 MeV
ΔE wall (Mo)	1.581	1.804
ΔE liquid lead	10.458	11.063
ΔE steel	0.765	0.570
ΔE dump	16.128	35.560
Al	14.264	32.265
Pb front end	0.574	1.738
Pb cover	1.290	1.557
E emitted	1.022	0.887
sum	29.954	49.884

Tab. 1: *Energy balance per incident electron in MeV.*

We conclude from these studies that the realisation of a pulsed photoneutron source is feasible.

[1] E. Altstadt et al., Annual Report 2001, FZR-341, 2002, 42-43.
[2] A. Fasso, A. Ferrari and P.R. Sala, Proc. of the Monte Carlo 2000 Conference, Lisbon (2000).
[3] Briesmeister J.F., Editor, *MCNP a General Monte Carlo N-Particle Transport Code*, Version 4A, LA 12625 M,1993.
[4] ANSYS User's Manual for Rev. 5.6., Swansons Analysis.
[5] Bergander, H.: FEM-Thermalberechnung des Beam Dump eines Neutronenproduktions-Target. Ergebnisbericht HTS-T-065-02 vom 23.11.2002.

The set-up of a laboratory for optical spectroscopic investigations of radioactive samples at the ELBE-FEL facility

H. Foerstenbdorf, K.H. Heise

The main goal of the scientific research of the Institute of Radiochemistry (IRC) at the FZR is the quantification of the interaction and mobility of radionuclides in the geo- and biosphere. Because of their high radiotoxicity and long half-life the actinides are of special interest. Among the actinides uranium and its manifold interactions with mineral surfaces, biological materials (bacteria, plants and natural organic matter) plays a major role in the institute's research activities.
The IRC is installing a laboratory for optical spectroscopy at the ELBE-FEL facility. The special feature of this laboratory will be its classification as control zone for radionuclides which will allow investigations of radioactive samples showing an activity 10^5 times of the admissible limit under consideration of all aspects of radiation protection (Fig. 1). Furthermore, the installation of a glove box is planned which will make it possible to carry out experiments on sensitive samples which have to be kept in an inert gas atmosphere.

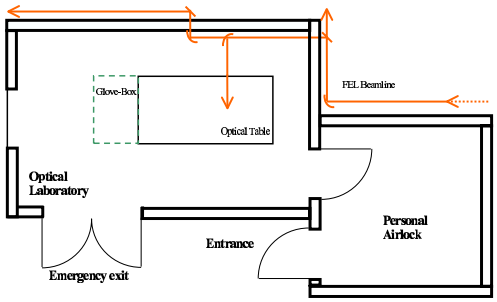

Fig. 1: *Floor plan of the control zone at the ELBE-FEL facility. Arrows indicate the FEL beamline.*

The study of interaction of sorbed molecules at a molecular level requires spectroscopic techniques which are sensitive to surfaces or interfaces. One promising technique is photo-thermal spectroscopy using pulsed FEL radiation. It is able to detect low concentrations of substances on a surface /1/. This method is based on thermo-elastic deformation bump generated by intermittent laser heating and thermal expansion. A solid sample is irradiated by a modulated beam of monochromatic light produced by a tuneable free electron laser (FEL) and a probe beam (e.g. HeNe laser) which is reflected from the sample. Depending on the modulated intensity of the pump beam the photoinduced displacement of the probe beam changes periodically and thus a different reflection angle is observed (Fig. 2). At first order the thermal beam deflection (TBD) is proportional to the absorption coefficient of the material under investigation, thus providing direct access to acquisition of absorption spectra /2/.

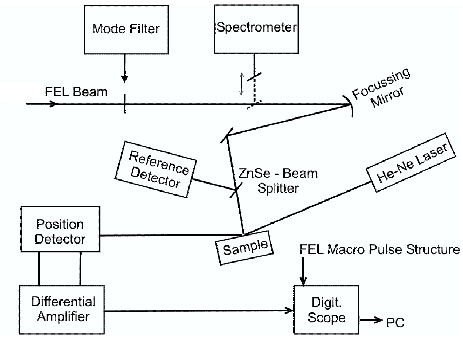

Fig. 2: *Scheme of a thermal deflection experiment set-up.*

Thermal expansion in the bulk is a very fast phenomenon, its time constant being of the order of the lifetime of the excited level (ps to ns), although the heating of the surrounding atmosphere is much slower. The incident energy is deposited in a short time, so that the heat generation will exhibit a corresponding time dependence. Therefore, it can potentially provide spatial information, e.g. on the distribution of a metal species in the sample.

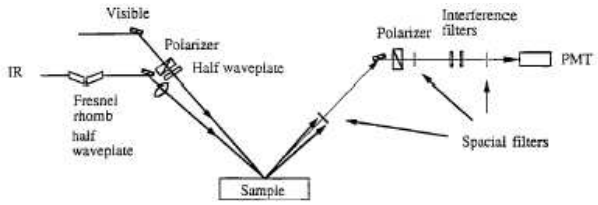

Fig. 3: *Typical set-up of an SFG experiment.*

The combination of high brilliance and pulse rate of the coherent light source allows the application of nonlinear second-order techniques such as sum frequency generation (SFG). Since this application is restricted to media lacking inversion symmetry, it is of special interest for interface studies where such symmetries are broken (Fig. 3). Because of its inherent surface sensitivity this technique directly measures the vibrational spectrum of molecules at an interface /3/. Contributions of the bulk are not present in the spectra. Binding studies of metal complexes at mineral surfaces will be feasible under natural conditions in an aqueous medium. A special challenge will be the application of SFG to biological interfaces e.g. lipid monolayers serving as model systems for the deduction of processes occurring on cell surfaces.

[1] Seidel, W. et al. (submitted).
[2] Olmstead, M.A. et al., Appl. Phys. A32, 141 (1983).
[3] Richmond, G.L., Annu. Rev. Phys. Chem. 52, 357-389 (2001).

EPOS Intense Positron Source at ELBE

R. Krause-Rehberg[1], G. Brauer[2]

Positron Annihilation is a powerful method for the characterization of nano-sized defects in many fields of materials science. The method has been established over the last three decades [1]. Usually, isotopic positron sources, such as ^{22}Na are used in most labs worldwide. The disadvantage of laboratory isotope sources is the relatively small number of positrons resulting in rather long spectra accumulation times.
A new alternative is the planned intense positron source EPOS (ELBE POsitron Source) which is based on pair production from the bremsstrahlung of the primary ELBE electron beam. This electron LINAC (40 MeV, up to 40 kW) has a worldwide unique time structure which is well suited for all techniques of the positron annihilation spectroscopy. While most other LINACs have repetition rates in the order of 10^3 s^{-1}, the time structure of ELBE can be adopted to the user demands in a wide range. The individual electron bunches have a length of only a few picoseconds, and the repetition time is in the nanosecond range. Fig. 1 illustrates the preferred time structure which is also used for infrared free-electron laser experiments at ELBE.

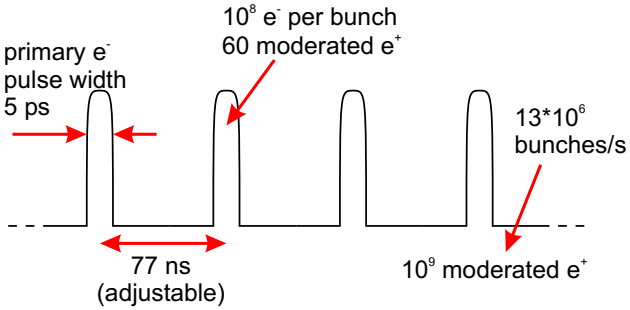

Fig. 1: *Time structure of the primary ELBE electron beam for the operation as EPOS. The intensities correspond to a primary beam power of 10 kW.*

Due to this unique time structure, the generated positrons can directly be used for positron lifetime spectroscopy. The low repetition rate at other LINACs requires there the use of a Penning trap to form first of all a continuous beam which then must be choppered and bunched to obtain a pulsed positron beam with adequate time structure. Thus, direct use of the ELBE time structure is an important advantage and will further improve the time resolution and the intensity of the positron source.
The positron converter is planned to be made from a stack of W plates which are directly water cooled. This ensures that the electron beam of a power of 10 kW can be focused to a spot smaller than 10 mm in diameter. The electron beam dump will be a large, water-cooled Al block. There will be an inner and an outer water cooling circle. The γ-positron converter and the moderator is made from Pt or W foils, and the slow positrons are extracted perpendicular to the electron beam. The beam will be extracted from cave 111b to the positron lab which will be situated outside of the control area but inside the ELBE hall. The extraction tube realizes a magnetic guidance through an already existing cable tunnel.
An innovative detector system is planned which is completely digital, i.e. the anode pulse of the photomultiplier and the output pulse of the Ge detector preamplifier will be directly digitized by appropriate digitizer PC cards. There are a lot of advantages of the digital detector system:

- no more adjustable electronic componenets (such as CF discriminators and TACs)
- easy remote control via internet
- extremely easy realization of a coincident registration of both annihilation γ quanta without any additional electronic components
- thus, extreme background reduction and improvement of time/energy resolution

The lifetime system will be constructed as an multidetector array of 16 detectors. Fig. 2 shows one of 8 coincidence channels which consist of two detectors.

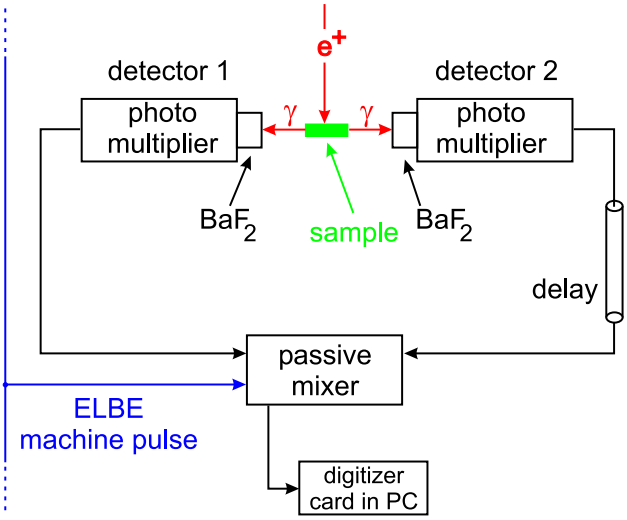

Fig. 2: *Setup of two detectors forming one coincidence channel of the digital lifetime system. The pulses of the γ quanta are mixed with the machine pulse to be measured in one sweep of the digitizer (Fig. 3).*

[1]Univ. Halle, FB Physik (mail@KrauseRehberg.de)
[2]FZ Rossendorf (G.Brauer@fz-rossendorf.de)

The lifetime is then measured as time difference between the ELBE machine pulse and one of the two γ quanta (high-rate) or both γ quanta (coincidence lifetime spectrum). This is schematically shown in Fig. 3.

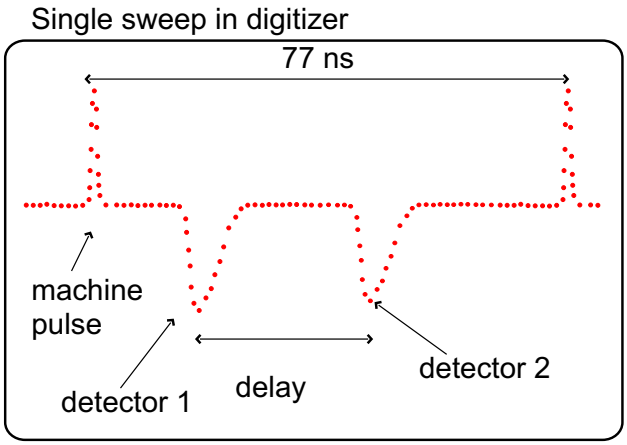

Fig. 3: *Schematic view of a single sweep of the digitizer card. The sweep is triggered by the negative multiplier pulses, so that the large number of empty events will not contribute to the pile-up of the digitizer system. The lifetime spectrum is then obtained by collecting a histogram of all individual registered lifetime events.*

Beside the lifetime system, EPOS will make use of the momentum techniques, i.e. the Doppler broadening coincidence spectroscopy and AMOC (age-momentum correlation) [1]. Since the required count rate of the Ge detectors used for these techniques is much smaller compared to the lifetime spectrometer, an additional conventional ^{22}Na source will be included so that the Doppler measurements can be done during the beam breaks, i.e. during the periods when the ELBE electron beam serves other experiments.
The EPOS system will be constructed and maintained by the CMAT of the University Halle (CMAT = Interdisciplinary Scientific Center of Materials Scince). The system will be organised as a user-dedicated facility. Thus, it will be open for any interested user in research or industry. In September 2002 the first annual user meeting EPOS-02 was organized. More than 20 scientists from 10 European countries discussed the construction and the operation of the system showing the vital interest of the positron community in this new positron source.

[1] R. Krause-Rehberg, H.S. Leipner, "Positron Annihilation in Semiconductors", Springer-Verlag, Berlin 1999

Femtosecond lasers synchronized to the repetition rate of the ELBE accelerator

T. Dekorsy, S. Winnerl, W. Seidel, F. Gabriel, A. Poppe[1], A. Stingl[1]

One of the key parameters of the superconducting ELBE accelerator is its quasi-cw operation at a repetition rate of 13 MHz. This is a great advantage in comparison to former generations of accelerators operating in a macro/micro-bunch regime. Especially when driving a free-electron laser (FEL) with such a quasi-cw stream of electron-bunches, the optical output of the laser emission is expected to provide a stable coherent light source with large benefits for the signal-to-noise ratio achievable in optical experiments. The two FELs under construction at ELBE are expected to emit coherent radiation in the frequency range from 5 to 100 μm, with pulse widths in the range of several hundered femtoseconds to some picoseconds and energies in the range of μJ per pulse. This is the wavelength range of interest for the study of biomolecules and elementary excitations in semiconductors and semiconductor quantum structures.

Due to the short pulselength of the FELs, one important class of optical experiments will be pump-probe experiments, where a sample is excited with an intense pump beam, while the changes of the optical properties of the sample are monitored with a time-delayed probe beam. A common distinction is made between single-colour or degenerate pump-probe experiments, where both pump and probe wavelengths are the same and two-colour or non-degenerate pump-probe experiments, where they are different. The latter experiments require two synchronyzed pulse sources. Therefore the synchronization of pulsed lasers operating in the visible or the IR has been established at several FEL facilities in the last years. The first demonstration of synchronizing a fs laser to an superconducting accelerator driven FEL was performed at Stanford, with a timing jitter of 3 ps [1]. The first sub-picosecond timing-jitter of such a synchronization was achieved at FELIX [2].

An independent tuning of the wavelength of the two laser sources would be highly desireable, since this allows the highest flexibility in the system under investigation, e.g., for semiconductor spectroscopy, a pump wavelength in the FIR could be chosen to pump intersubband transitions in a quantum structure, while the probe wavelength is tuned to an interband transition which has a common state with the intersubband transition. Thus the relaxation dynamics of excited carriers can be determined which is of great interest for the development of intersubband light emitters, so called quantum cascade lasers. Beside this spectroscopic application, a synchronized femtosecond laser can be used to determine the electron bunch length itself [3,4] as well as to characterize the FEL pulses [5].

In 2003, two fs laser systems have been equipped with synchronization electronics in order to synchronize them to the repetition rate of the ELBE accelerator. Both lasers are Kerr-lense modelocked Ti:sapphire lasers pumped by frequency-doubled, diode pumped cw Nd lasers. The repetition rate of these lasers is set to 78 MHz, which corresponds to 6 times the repetition rate of the electron bunches, thus allowing cross-correlation experiments with a duty cycle of 6. For the synchronization, 13 MHz are derived from the ELBE RF electronics which acts as the master oscillator. This frequency is distributed via optical fiber links into the optical laboratories, where the laser systems are installed. The 13 MHz frequency is multiplied by 30 to generate a 390 MHz signal. This frequency is the reference signal for the 5th harmonics of the fs laser. The advantage of synchronizing at higher harmonics of the laser frequency is the coupling of pulse energy noise and timing jitter in a passively modelocked fs laser [6]. The former noise contribution is reduced when working on a higher harmonics. The synchronization is achieved by a phase-locked loop, which provides an error signal based on the phase difference of the two 390 MHz frequencies. This error signal drives a piezo-stage on which one cavity mirror of the lasers is mounted thus changing the length of the optical caivity and in turn the repetition rate.

One synchronized laser is a Titanium sapphire laser (Spectra Physics Inc.), which delivers pulses tunable in the range from 730 nm to 880 nm with pulse widths of 45 fs and pulse energies of 20 nJ. The pulse width corresponds to a transfrom-limited spectral width of 50 meV. The pulse width can be switched to ps operation, thus delivering a much narrower spectrum of a few meV. The other laser system is a 12 fs Ti:sapphire laser (Femtolasers GmbH) delievering pulses of 12 nJ energy at a center wavelength of 790 nm. The oscillator pulses are temporally stretched and used to seed a multi-pass Ti:sapphire amplifier (Femtolasers GmbH). The amplifier is pumped by a flash-lamp pumped, frequency doubled Nd YLF laser operating at 1 kHz. After amplification the pulses of the Ti:sapphire oscillator are recompressed to 25 fs pulse duration and have an energy of 1 mJ per pulse. These pulses are used to pump a parametric generator/amplifier (Light Conversion Ltd.), which produces sub-100 fs signal and idler pulses at wavelengths between 1.1 μm and 2.6 μm. Signal and idler pulses are used to generate pulses in the range of 2.4 μm to 18 μm via difference frequency mixing in two different nonlinear crystals. Synchronization of the oscillator will allow to use all of these wavelengths in two colour experiments with the FELs.

[1] Femtolasers GmbH, Vienna

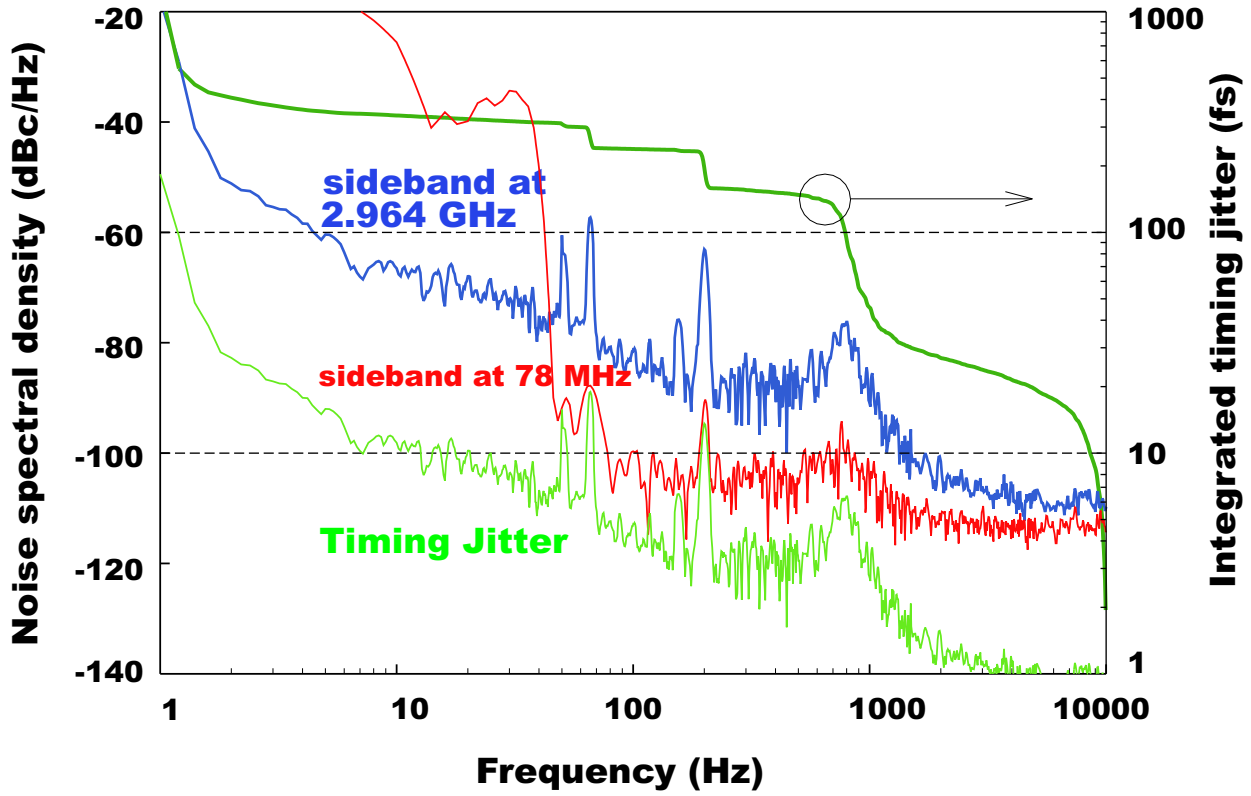

Fig. 1: *Noise spectral density detected at the fundamental (78 MHz), the 38th harmonics (2.964 GHz) of the laser repetition rate and calculated timing jitter and integrated timing jitter.*

We tested the synchronization electronics with a GHz bandwidth photodiode and a spectrum analyzer (FSP Rhode&Schwarz) by measuring the side band at the 38th harmonics of the 12 fs Ti:sapphire oscillator at 2.964 GHz. At this frequency, the pulse energy noise can be neglected versus the timing jitter, which is not the case for the fundamental sideband. The noise spectral density is obtained by measuring the noise band at 2.964 GHz in different steps of the resolution bandwidth. From this the timing jitter is calculated. By integrating the timing jitter starting at 10 kHz the integrated timing jitter is obtained. Fig. 1 depicts the noise spectral density and the integrated timing jitter in the frequency range of 1 Hz to 10 kHz. For a frequency of 10 Hz an integrated timing jitter below 400 fs is obtained. If the same timing jitter is obtained with in an all-optical cross-correlation experiment between FEL pulses and the fs oscillator, this synchronization allows a two-colour pump-probe experiments with high temporal resolution.

[1] R.J. Stanley, R.L. Swent, and T.I. Smith, "Synchronization of a femtosecond modelocked Ti:sapphire laser to the Stanford SCA/FEL", Opt. Comm. **115**, 87 (1995).

[2] G.M.H. Knippels,M.J. van de Pol,H.P.M. Pellemans, P.C.M. Planken,A.F.G. van der Meer, "Two-color facility based on a broadly tunable infrared free-electron laser and a subpicosecond-synchronized 10-fs-Ti sapphire laser", Opt. Lett., **23**, 1754 (1998).

[3] I. Wilke, A.M. MacLeod, W.A. Gillespie, G. Berden, G.M.H. Knippels, and A.F.G. van der Meer, "Single-shot electron-beam bunch length measurements", Phys. Rev. Lett. **88**, 124801 (2002).

[4] X.Yan, A.M. MacLeod, W.A. Gillespie, G.M.H. Knippels, D.Oepts, A.F.G. van der Meer, and W. Seidel, "Subpicosecond electro-optic measurement of relativistic electron pulses", Phys. Rev. Lett. **85**, 3404-3407 (2000).

[5] G.M.H. Knippels, X.Yan, A.M. MacLeod, W.A. Gillespie, M. Yasumoto, D. Oepts, and A.F.G. van der Meer, "Generation and complete electric-field characterization of intense ultrashort tunable far-infrared laser pulses" Phys. Rev. Lett. **83**, 1578-1581 (1999).

[6] A. Poppe, L. Xu, F. Krausz, and C. Spielmann, "Noise characterizetion of sub-10-fs Ti:sapphire oscillators", IEEE J. Quantum Electr. **4**, 179 (1998).

Dynamics of matrix–isolated molecules.

J.A. Piest

Gaining insight in the intra– and inter–molecular inter(re)actions is an important issue in order to understand physical, chemical, and biological reactions in micro– and macroscopic systems. Such reactions for instance determine the way molecules interact with their environment. In particular, recently verified in the field of astro–biology, formation of amino–acids takes place in interstellar ice–analogues[4, 5], which process can be studied in more detail with available time–resolved data in the IR[3].

Detection of time resolved optical parameters of molecules reveals the time–scales of energy re–distribution, which governs such processes. Therefore, it can be used as a powerful method to reveal the dynamics of molecular systems.

The advantage of doing experiments in the region slightly above zero Kelvin is clear: in this condition molecules have much lower internal energies than at room temperature. Generally, in the spectra of such cold molecules there are 1) less transitions present, and 2) the bandwidth per transition is smaller. Thus, spectra for these molecules are less complicated than those recorded for warm species and can be interpreted with less ambiguity.

In particular, time–resolved spectral data of cold molecules may lead to knowledge of the timescales on which intra– and inter–molecular energy re–distribution takes place, and inform us about the time–response of physical or chemical inter(re)actions in molecular systems. Due to lack of bright IR short–pulse light sources, time–resolved spectral data in the sub–nanosecond domain for matrix–isolated species are scarce, where spectra in the available μs region do not yield relevant information[1, 2, 3].

In room 113E of the ELBE–building a high–vacuum setup is under construction in order to do such experiments with cold molecules. In this setup isolated molecules are embedded in a molecular or inert gas ice. By mixing of gases more exotic ices, such as interstellar ice–analogues, can be generated easily.

The setup consists of two chambers *i.e.,* commercially available six–pieces, pumped by two Varian V301 Navigator turbo–molecular pumps, with a pump capacity of ~300 l/s each. Two Varian SH100 membrane pumps provide a sufficiently low roughing pressure to drive the Varian V301's.

A liquid helium cooled Janis ST-400 UHV cold–head, operating between temperatures of 1.5K and 300K, and with a cooling power of 3W at 5K, is to be mounted on one of the chambers. Thus, with an assumed FEL output of ~50W the summed column widths of molecular absorption lines, present under the IR spectral profile, can be as large as a few percent of the column–width of the FEL–pulse.

In situ sample generation takes place on a transparant surface mounted on the tip of this cold–head. Purified gases, *e.g.,* Ar 6.0/Ne 5.0/N_2 6.0, are mixed with sample species to well defined concentrations, before being deposited on the cryogenically cooled window. The deposition rate is controlled with a micro–flow meter. A liquid nitrogen trap prevents backflow of the sample species in the gas–lines towards the clean gas–buffers, additionally, in the opposite flow direction it dries the purified gases before mixing with the sample species.

In principle there is no limit to the nature of the species that can be studied. Any molecule that can be brought in the gas–phase at room or elevated temperature can be isolated in the cryogenic matrix.

Besides, samples can be prepared externally, *e.g.,* by preparing thin films of species in solid or liquid, and mount them on the tip of the cold–head before evacuating the vacuum chambers and cooling the sample.

Experiments to be done with this setup in order to yield time–resolved spectral information vary from simple one–color pump–probe experiments in direct absorption, to more sophisticated back–ground free detection methods such as: detection of the photon–echo, scattering of IR or UV light on a transient grating provided by the IR pulse, or laser induced fluorescence (LIF). The both latter experiments desire a resonant IR–UV excitation scheme.

For the experiments in direct absorption the variation of IR absorption of the probe pulse as a function of time–delay is the relevant parameter to be determined. Dependending on the line integrated absorption cross–section of the sample species this variation is usually not larger than a few percent of the total absorption strength. Considering the spectral width of the transition smaller than the IR spectral profile the change in the signal detected may be only a fraction of a percent. Thus, it is highly desirable to resolve the IR pulse spectrally, for instance by coupling it into a fourier transform infrared spectrometer (FTIR) after passing the sample. The IR pulse, with elongated duration either due to the absorption lines present under the IR spectral profile, or due to an artificial modulation, can then be analyzed.

In case of transient grating scattering and LIF a tunable laser in the UV is desirable. Background free detection of UV–photons then can be accomplished by a photo–multiplier tube (PMT). The transient grating scattering method may also yield detectable signal without application of a UV laser, when applying a single color three–photon scheme.

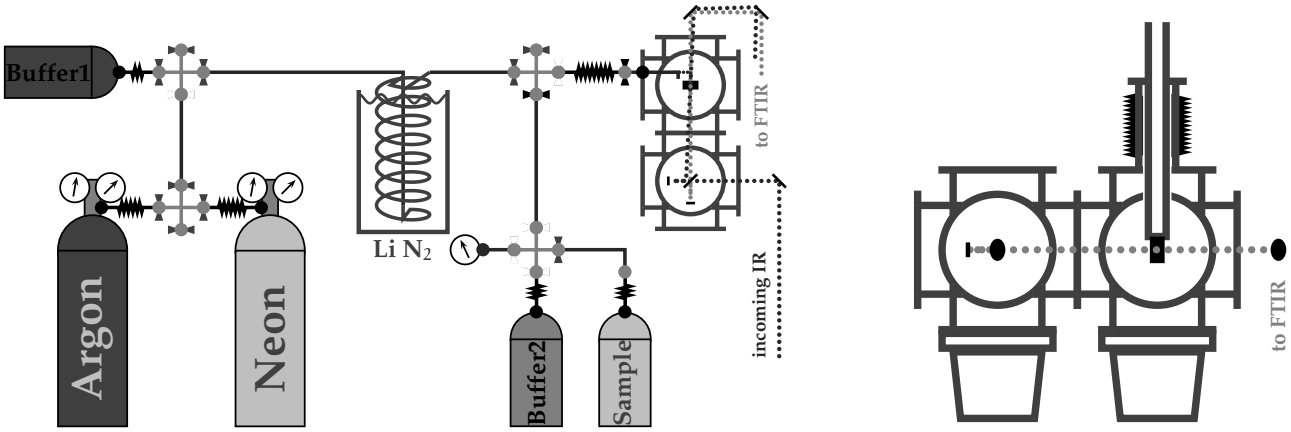

Fig. 1: *(l) Scheme of the gas–mixing setup. Left from the liquit nitrogen trap purified gases are fed into the gas–lines. After passing the trap they are mixed with sample molecules and deposited in the vacuum setup, here shown from the top viewpoint. The IR beamline in this setup is depicted. (r) The setup, with beamline and cryostat, is shown from the side viewpoint.*

The IR light has to be provided by either the FEL or the Topas, whith a strong preference for the FEL, because of its higher averaged output power as a result of a much higher repetition rate. Scattering of IR light on an IR induced grating may possibly only work with the FEL, due to the feeble signals expected, *i.e.,* some milli–Watts of scattered signal with some Watts of resonant input photons.

In future, besides the matrix–isolation experiments, the setup can be extended easily to do experiments on molecules or ions applying either effasive or supersonic, pulsed or continuous, jets, while exploiting high sensitive ion detection methods.

[1] Allamandola and Nibler, Chemical Physics Letters, 28, 335 — 340, 1974
[2] Allamandola *et al.*, Journal of Chemical Physics, 67, 99—109, 1977
[3] L.J. Allamandola, NASA/Ames Research Center, private communications, 2002
[4] Bernstein *et al.*, Nature, 416, 401, 2002
[5] Muñoz Caro *et al.*, Nature, 416, 403, 2002

Development of a Superconducting RF Photo Gun

For all electron accelerators the quality of the injected beam is of crucial importance for the operation of the whole facility. Driven by this need a worldwide research effort is directed towards the development and improvement of electron injectors. RF photoinjectors claim a central part in this field as they are able to produce very high quality electron beams.

Special requirements arise from the operation of high-average-power free-electron lasers and energy recovery linacs. To overcome the serious challenges which the huge RF power requirements and the coresponding cooling efforts present to a normal-conducting design an RF photoinjector with a superconducting cavity would be the natural choice for CW operation. Several approaches have been made, but for the first time a superconducting RF photo gun was successfully put into operation during the year 2002 in Rossendorf. This one is based on a half-cell resonator designed in collaboration with the Budker Institute of Nuclear Physics in Novosibirsk.

The ongoing effort in Rossendorf is now directed to develop a superconducting RF photoinjector for ELBE. In collaboration with the Max Born Institute, Berlin and BESSY, Berlin a 3-1/2 cell photoinjector is planned. This design is targeted to deliver a 77 pC, 1 mA$_{\mathrm{CW}}$ beam corresponding to the ELBE specifications but also to allow tests with up to 1 nC bunch charge.

First operation of a superconducting RF-gun

D. Janssen[1], H. Büttig[1], P. Evtushenko[1], M. Freitag[1], F. Gabriel[1], B. Hartmann[1], U. Lehnert[1], P. Michel[1], T. Quast[1], B. Reppe[1], A. Schamlott[1], Ch. Schneider[1], R. Schurig[1], J. Teichert[1], S. Konstantinov[2], S. Kruchkov[2], O. Myskin[2], V. Petrov[2], A. Tribendis[2], V. Volkov[2], W. Sandner[3], I. Will[3], A. Matheisen[4], W. Moeller[4], M. Pekeler[5], P.v. Stein[5], Ch. Haberstroh[6]

For the first time, a superconducting RF gun where a photo cathode is inside a superconducting cavity has been working stably over a period of seven weeks.
The cavity of the RF gun is a TESLA type [1] half cell closed by a shallow cone with a centred hole in which the cathode is situated. A detailed description of the cavity has been published in [2]. An overview of the gun is shown in Fig. 1. The gun cavity, together with the cathode support, the RF coupler and a part of the beam tube are installed in the He vessel of the cryostat.

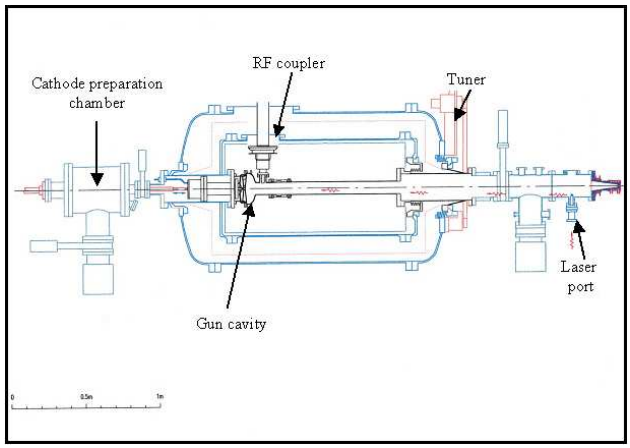

Fig. 1: *Cryostat of the SRF gun with preparation chamber.*

The cathode can be moved by means of a manipulator from the preparation chamber into the cavity. Through a port at the beginning of the beam line laser light is guided to the cathode.
In the preparation chamber Cs_2Te layers are deposited onto the cathodes. In the chamber the pressure was 10^{-10} mbar, but during the heating of evaporators it increased to 10^{-6} mbar. For that reason the quantum efficiency of the cathodes was not better than 0.25%.
The laser consists of an oscillator which works in the additive pulse modelocking (APM) mode. The oscillator supplies a pulse frequency of 26 MHz. After amplification and conversion UV laser pulses with 263 nm wave length and 5 ps (FWHM) length are obtained. A jitter σ=2 ps (peak-peak) was measured with a stable reference signal from the RF oscillator.
Beam line diagnostics include steerers, view screens, solenoids, a pepper pot mask for measuring the transverse emittance, and a dipole magnet for measuring energy and energy spread. The beam current can be measured by an insulated beam dump at the end of the line.
Fig. 2 shows the measurement of the quality factor of the cavity in dependence on the field strength. The values are from direct RF measurement and from a comparison of measured electron energy with simulation.
The maximum field strength of 22 MV/m near the cathode is limited by field emission. The insignificant difference of Q values with and without cathode shows the good performance of the four stage coaxial RF filter.

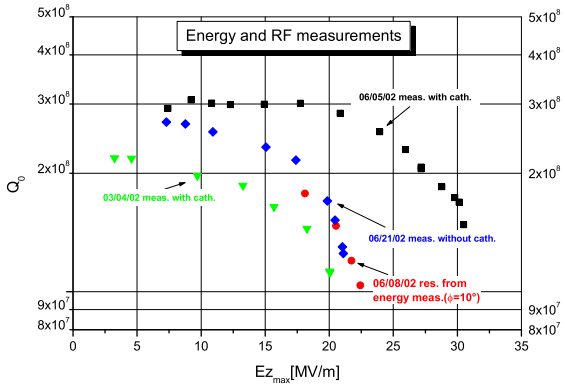

Fig. 2: *Determination of the maximum field strength from RF and energy measurements.*

Fig. 3 presents the cathode emission and accelerated (dump) current together with the corresponding electron energy as a function of the laser phase.
For a phase window of 60° we obtain complete transmission and the energy reaches its maximal value at ϕ=0°. These properties are determined by the geometry of the cavity and the field amplitude.

[1]FZ-Rossendorf, Postfach 510119, 01314 Dresden, Germany
[2]Budker Institute of Nuclear Physics, Novosibirsk, Russia
[3]Max Born Institut, Berlin, Germany
[4]DESY, Hamburg, Germany
[5]ACCEL Instruments, Bergisch Gladbach, Germany
[6]TU Dresden, Germany

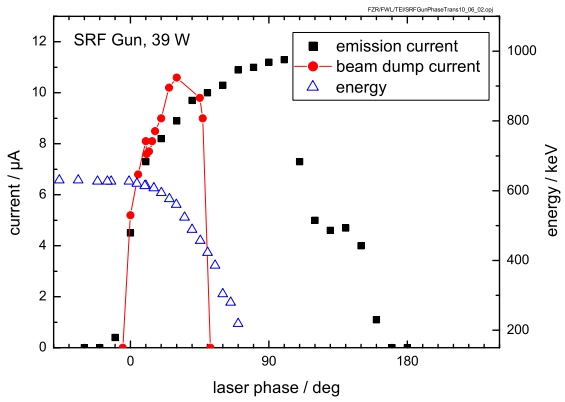

Fig. 3: *Transmission of the electron beam and the dependence of the energy from the laser phase.*

At a temperature of 4.2 K we could not see any changes of the quality factor $Q = 2.5*10^8$ of the cavity during the whole period of operation. The field emission of the cavity, which is the reason for the limitation of the field strength, is caused by the difficult clean room handling of the big intrinsic parts of the cryostat. But nevertheless a field strength of 22 MV/m and an electron energy of 900 keV have been obtained.

The maximum bunch charge was 20 pC, which corresponds to an average current of 520 μA in the cw-mode. It is limited by average power and repetition rate of the laser and by the small quantum efficiency of the photo cathode.

Due to the long drift space after the gun and the arrangement of optical elements, we could measure the transverse emittance for bunch charges between 1 and 4 pC only. In agreement with PARMELA calculation we have measured normalized rms-values between 1 and 2.5 mm mrad.

[1] A.Aune et al., DESY 00-031, Hamburg2000
[2] P.v.Stein, Internal report, FZR-227, Forschungszentrum Rossendorf 1998

RF System and Measurements at the Superconducting RF Gun

H. Büttig, R. Schurig, A. Tribendis[1]

The Superconducting RF Gun (SRF GUN) was put into operation successfully in 2002 [1]. During a seven week period several experiments had been done to study the performance of the system itself and to measure beam parameters. The RF system was designed to provide flexibility, e.g. to measure the cavity performance and to operate the gun with beam. A modified self exciting RF system was chosen in which the sc cavity determines the frequency because the built-in cavity tuner could not be used.

The general outline of the RF system is shown in Fig. 1. The generator operates in a phased locked loop (PLL) and its frequency is controlled by the eigenfrequency of the TM_{010}-mode of the cavity. A self exciting circuit oscillates under the condition that the total gain in the loop amounts to one and that the total phase shift along the loop is an integer multiple of 2π. In principle one doesn?t need a generator to operate a self exciting loop. In our case the error signal of the PLL drives the automatic frequency control (AFC) of the generator and closes the loop.

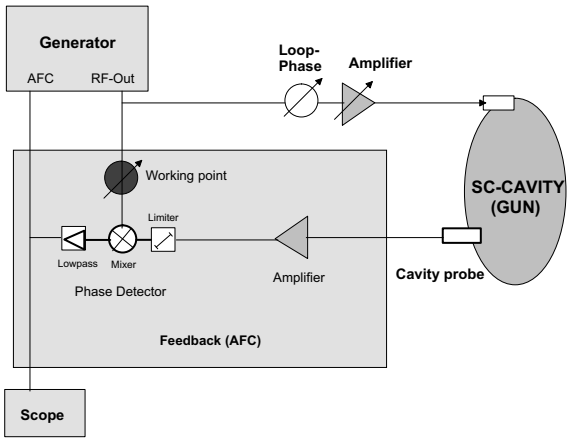

Fig. 1: *General Outline of a self-exciting (AFC) RF-system.*

In the phase detector (a high-level mixer was used) the phases of the cavity probe signal and the RF output signal of the generator are compared. If the amplitudes of the two input signals are kept constant the filtered dc output signal of a mixer depends only on the frequency- and phase difference of its two input signals. If the frequency and phase of the generator signal match the cavity TM_{010}-resonant frequency and zero phase, the system locks in, indicated by zero output voltage of the phase detector. The phase shifter in the LO-path of the mixer controls the working point of the system. Care must be taken when tuning this phase shifter because of two working points with opposite phase settings. Only one setting is stable and provides "lock-in" and tracking.

The block diagram of the RF-system used is shown in Fig. 2. Its "core" is the self exciting frequency loop described above. The output signal of the generator (SMT-Rohde & Schwarz) is distributed into three signals, one to synchronize the laser system, one to control the self exciting frequency loop (AFC) and one to drive the RF amplifier providing the cavity gradient and the beam power. Several tests had been done to ensure that the internal PLL system of the laser locks to the signal of the self exciting RF system, which is frequency- and phase modulated by microphonics. The PLL of the laser is remote controllable.

Gradient- and phase control of the SHF Gun are performed by individual control loops. The controller board used was designed for the ELBE RF-system and is described in [2]. Two RF-amplifiers were planned, a 150 W solid-state amplifier (SSB-Electronic GmbH) to study the cavity performance without beam and a 5 kW klystron amplifier to operate the cavity with beam. The VKL7811 klystron provides 10 kW RF-saturated power at 1300 MHz, its 3-dB bandwidth is 3.5 MHz. The TM_{010}-eigenfrequency of the GUN was lower. Detuning was possible by carefully adjusting the cavity-plungers of the klystron while increasing the power step by step. The body-current has to be monitored permanently during the procedure and was kept below 40 mA. Because the input cavity and the output cavity of the klystron are not tunable, the output power of the detuned klystron is limited to about 5 kW.

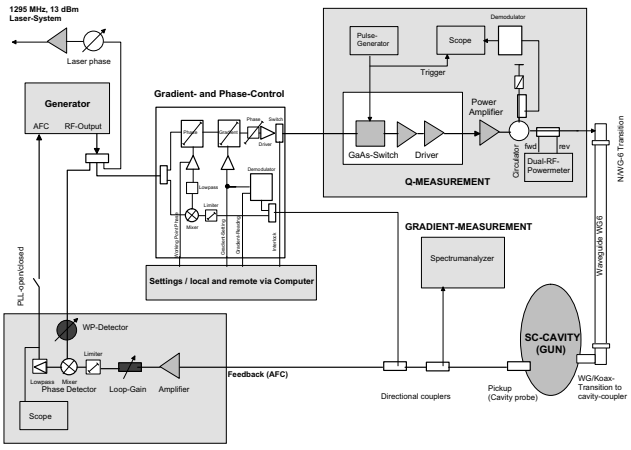

Fig. 2: *Block diagram of the RF-system.*

Measurements had been done to test the setup itself and to verify the measurements done at DESY using the vertical test stand [3]. The setup used is given in Fig. 2, the procedure used is described in [4] and [5].

[1] Budker Institute Novosibirsk

Cavity parameters:

- TM_{010}-eigenfrequency: 1297.234 MHz @ 4.2K
  1294.545 MHz @ 4.2K.
- Characteristic Impedance $R/Q = 120.5\ \Omega$
- Transit time factor TTF= 0.7525
- Coupling $\beta = 1$
- Length of the accelerating gap: 0.0738 m
- DESY: Q_0 @ 4.2 K = $2.3{\cdot}10^8$ [2]
- DESY: Q_0 @ 1.8 K = $1.5{\cdot}10^{10}$ [2]

Because of the manual helium filling using a dewar most of the experiments were performed at 4.2 K. Two tests had been done using pump-down technique to achieve a helium temperature of 2.5 K. The unloaded quality factor Q_0 is increased by a factor of three when changing the helium temperature from 4.2 K to 2.5 K.

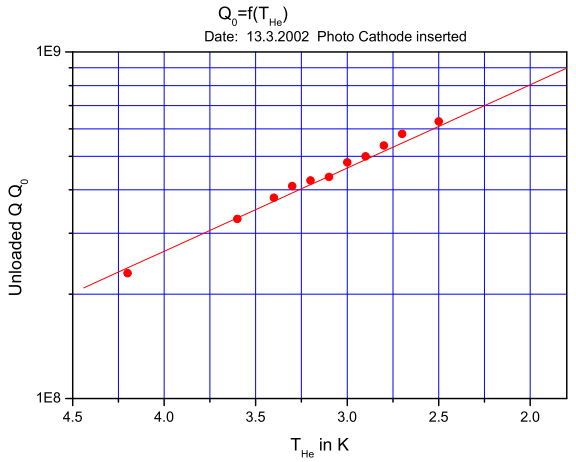

Fig. 3: *"Pump-down" curve of the lossless Q_0 versus the He temperature.*

Fig. 4 shows the Q/E curve measured at 4.2 K and verifies the Q_0 value measured at DESY before assembling the cryostate. All the procedures concerning transportation, assembling and adding the photo cathode did not change the performance of the superconducting resonator.

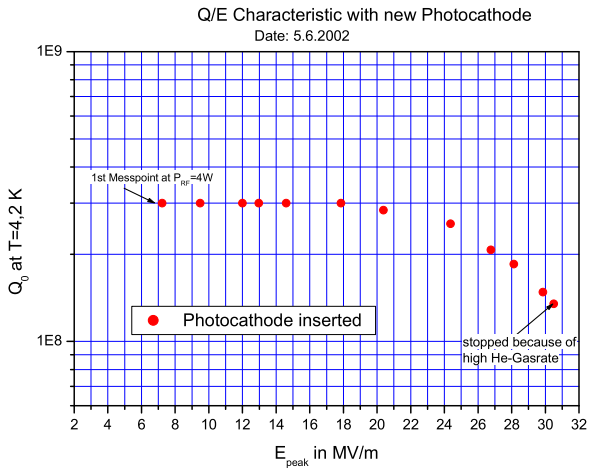

Fig. 4: *Q/E curve measured at 4.2 K in Rossendorf.*

The gradient against the incident RF power is shown in Fig. 5. The maximum incident RF power was limited by field emission without photo cathode as well as with photo cathode inserted. Because the photo cathode represents a certain load the maximum gradient is reached at higher RF power levels. In both cases field emission limits operation at the same gradient.

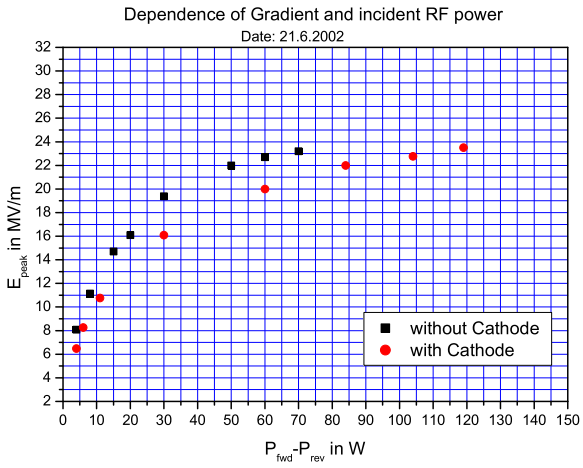

Fig. 5: *Gradient vers. incident RF-power(field emission limited).*

During all experiments the flow of the helium return gas was measured. In Fig. 6 the helium flow rate is plotted against the gradient E_{peak}. The helium flow represents the dissipated power ($P_{diss} \sim E^2$).

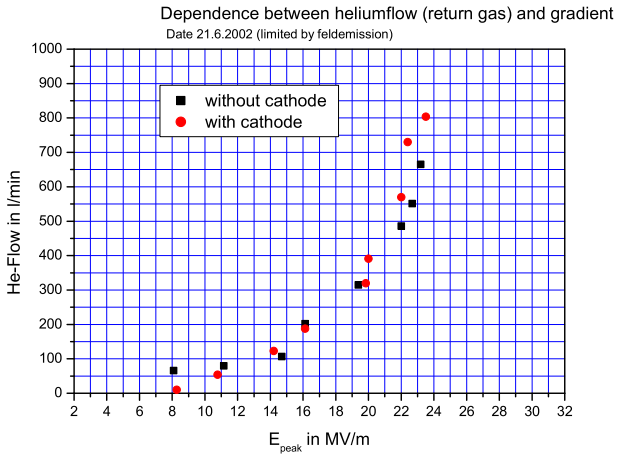

Fig. 6: *Helium gas flow vers. gradient, without beam.*

[1] D.Janssen et.al.: NIM A445(2000)408
[2] F.Gabriel et.al.: FZR-341 (2002) 7
[3] A.Tribendis, private communication
[4] J.Knobloch, Report SRF910927-07 (1991)
[5] M.Pekeler, ACCEL Report A-BP-0390-A(1999)

Beam Parameter Measurements for the superconducting RF photoelectron gun

J. Teichert, H. Büttig, P. Evtushenko, D. Janssen, P. Michel, T. Quast, C. Schneider, R. Schurig

In 2002 the project for a cw-mode photo injector with superconducting cavity has been continued. With the test-stand containing a half-cell cavity the operation of a superconducting rf gun was demonstrated successfully. In the following the results of the beam parameter measurements will be presented. These results were obtained during two operation period in March and June 2002. A description of the gun design is published elsewhere [1], and further information on the various subsystems are given in some other contributions of this annual report.

For the beam parameter measurements a diagnostic beam line was installed. Its layout is shown in Fig. 1. At the beam line the following elements were arranged: two solenoids for focussing, three steerer sets for adjustment, four movable Chromox view screens, a pepper-pot mask for transverse emittance measurement, a 30° spectrometer magnet, a kicker cavity planned for pulse length determination, and a beam dump with current measurement. The essential drawback of the measurement set-up was the position of the first solenoid. Although it was as close as possible to the cryostat vessel, the distance between it and the cavity was too long. Due to a strong increase of the beam divergence from the gun for higher bunch charges, the beam envelope at the solenoid was too large for a proper focusing and the beam was partly lost.

The UV laser delivered pulses up to 40 nJ with a micropulse frequency of 26 MHz. This corresponds to a bunch charge of 25 pC for a photo cathode with a quantum efficiency of 0.3%. Lower bunch charges were produced by reducing the laser power with a polarization filter. The macropulsing of the electron beam, necessary in the case of inserted view screens, was done by pulsing the pump diodes of the laser amplifiers. The Measurements were carried out with an rf input power between 40 and 100 W (without beam) corresponding to peak field strengths E_{zmax} between 18 and 22 MV/m.

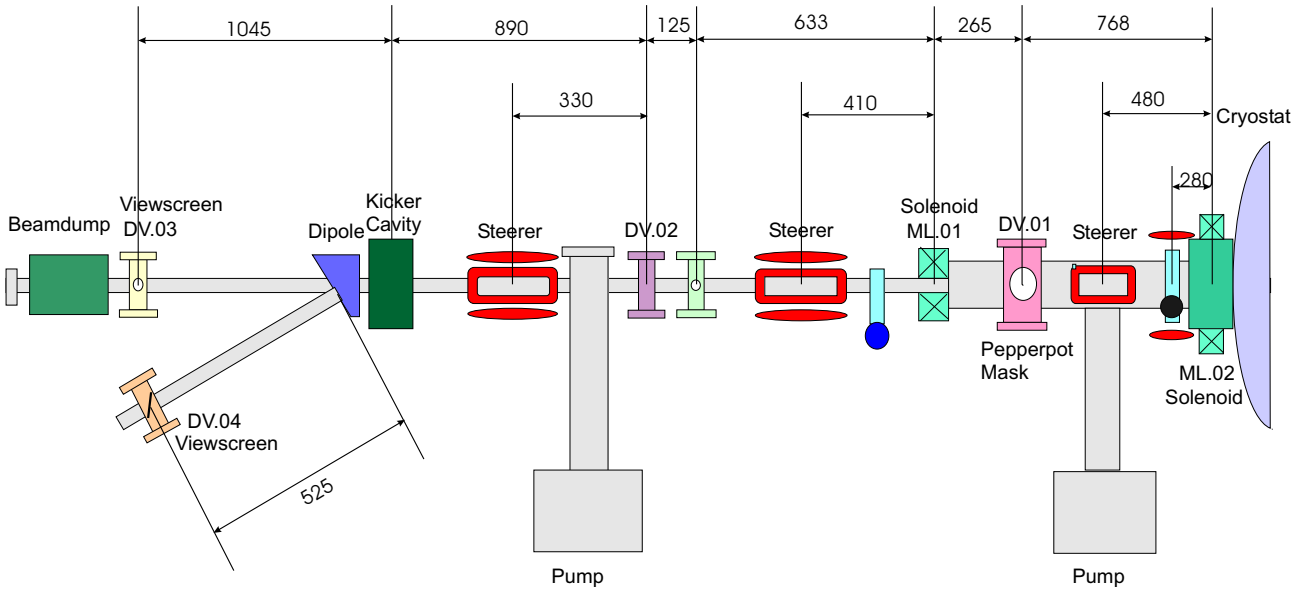

Fig. 1: *Schematic of the diagnostic beam line at the superconducting rf photoelectron gun.*

Fig. 2 presents the variation of the laser pulse. The emission current at the cathode, the accelerated beam current (dump current) and the beam energy are shown. The cathode current could be measured since the photo cathode is electrically insulated with respect to the cavity. The measurement was done at 39 W rf power (18 MV/m peak field strength) and approximately 2 pC. An operation window was found between about 0° and 50° where the rf field extracts the electrons and their energies are high enough that they can pass through the beam line.

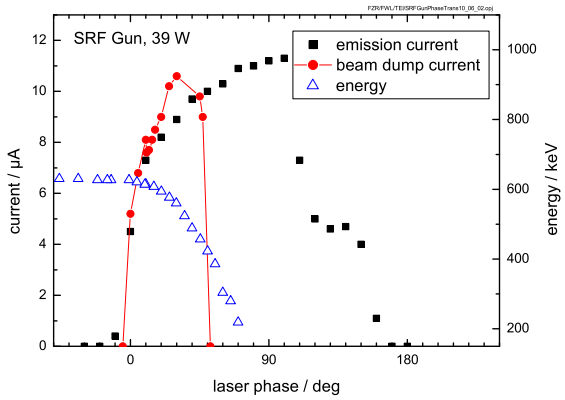

Fig. 2: *Cathode beam current, accelerated beam current and beam energy as a function of laser phase for 2 pC bunch charge and 18 MV/m peak field strength (40 W rf power).*

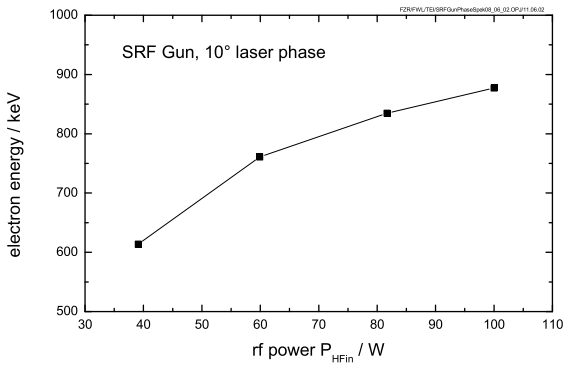

Fig. 3: *Beam energy as a function of applied rf power.*

[1] E. Barthels et al., Nucl. Instr. and Meth. A445 (2000) 408.

The beam energy in dependence on the rf power is presented in Fig. 3. In this measurements the laser phase was 10°, i.e. the electron energy had nearly it's maximum value. From the vertical spot size of the electron beam on the view screen behind the spectrometer magnet the energy width could be determined.

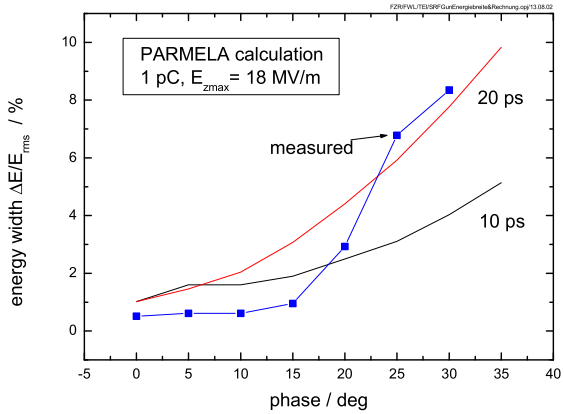

Fig. 4: *Measured energy spread as a function of laser phase and PARMELA simulation with 10 ps and 20 ps laser pulse length for 1.5 pC bunch charge and 18 MV/m peak field strength.*

The result of ΔE/E as a function of the laser phase at 40 W rf power and 2 pC bunch charge are shown in Fig. 4. Additionally, the figure shows two curves for different laser pulse lengths obtained from PARMELA calculations. The measured energy width could be caused by a laser pulse with an effective length of 20 ps which includes the jitter in the phase synchronization.

Cs_2Te Photo Cathodes for the Superconducting RF Photoelectron Gun

D. Janssen, P. Michel, P. Evtushenko, T. Quast, J. Teichert

The Rossendorf superconducting rf (SRF) photoelectron gun [1] uses caesium telluride photo cathodes. The advantages of this material are a high quantum efficiency, long life-time and ruggedness against bad vacuum. Cs_2Te is a semiconductor with a band width of about ...eV. Therefore it requires UV laser light for electron production. The laser has a 26 MHz Nd:YLF oscillator (1053 nm) with additive pulse mode looking, diode-pumped amplifiers, and twofold frequency doubling. It produces pulses at 263 nm with 5 ps length and 40 nJ maximum energy. The Cs_2Te photo layer is on the top surface of a gold-coated copper cylinder with 10 mm diameter and 15 mm length. This cylinder itself is part of a complicated cathode assembly, about 220 mm long, which can be moved inside vacuum from the preparation chamber into the resonator cavity, and can be mounted there by means of a thread.

The deposition of the Cs_2Te layers on the gold-coated cathode surface was done in the cathode preparation chamber by subsequent Te and Cs evaporation. The chamber had an ion pump and a titanium sublimation pump. The vacuum pressure was 10^{-10} mbar. In the chamber there were four evaporators for tellurium and caesium (caesium chromate), a quartz oscillator to measure evaporation rate and layer thickness and a cathode heating. The evaporator in use could be moved in front of the cathode by a manipulator. Tungsten coils around the evaporators heated them and their temperatures could be measured. An aperture in front of the cathode defined the size and position of the Cs_2Te spot. It was also used as an electron collector. For that purpose a high voltage could be applied.

The aim was to produce an about 20 nm thick spot of Cs_2Te with 5 mm diameter central to the cathode surface. Before deposition the cathode was heated to a temperature of 120°C. The deposition was started with the tellurium. The temperature of the evaporator was successively increased until Te evaporation happened. The evaporation was stopped if the desired thickness of 10 nm was reached. After that the Cs evaporation was performed in the same way. During Cs deposition the layer was illuminated with the laser beam and the photo current was monitored. The Cs evaporation was performed until the photo current saturated. We found that in the following few minutes the photo current dropped down to about 60 % of it's former value.

The main problem during the evaporation process was the rapid increase of the vacuum pressure up to about 10^{-7} mbar. To prevent a further degradation, it was necessary to increase the evaporator temperatures very slowly. We think that the bad vacuum was the reason for the low quantum efficiency of less than 1% of the produced photo cathodes. Furthermore, the reproducibility of the evaporation process and the mechanical position accuracy were unsatisfactory.

The quantum efficiency of the prepared photo cathodes were measured in the preparation chamber and inside the photo gun where the insulated cathode allow to apply a high voltage or the rf field of the cavity could be used. Fig. 1 shows the result of a quantum efficiency measurement in the preparation chamber with a slightly defocused laser spot.

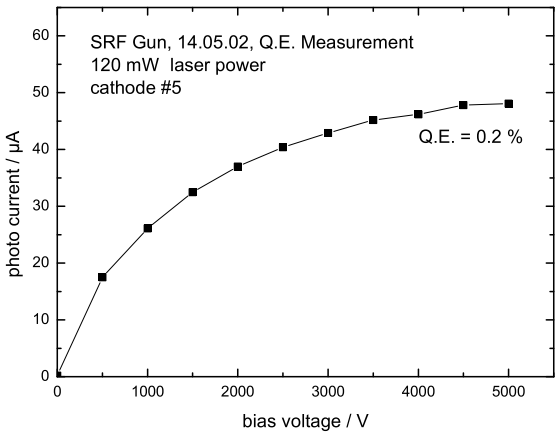

Fig. 1: *Photo current versus bias voltage of the aperture measured in the preparation chamber.*

During the use of the photo cathode in the SRF gun we observed that the photo current fluctuated with the laser spot position on the cathode. This inhomogeneity is also visible in the photograph of the cathode after use in Fig. 2.

More systematic studies of the photo emission homogeneity were performed by scanning the focused laser beam across the cathode. These measurements were done in the preparation chamber and with the cathode in the cavity with dc bias or rf field. Thereby a virtual cathode was used to get the laser beam position on the cathode. (After the movable mirror a part of laser beam was directed onto a florescence screen with a coordinate mesh.) Fig. 3 presents homogeneity measurements carried out in the preparation chamber. The circular distribution agrees with the Cs_2Te spot diameter of 5 mm but a region with high quantum efficiency was found on one side. The photo current distributions of the cathode measured in the gun cavity with dc bias and applied rf field are shown in Fig. 4. The different fields influences the distributions but in both cases a high quantum efficiency at the lower left part of the cathode is visible.

Fig. 2: *Photograph of a gold-coated cathode with deposited Cs_2Te layer.*

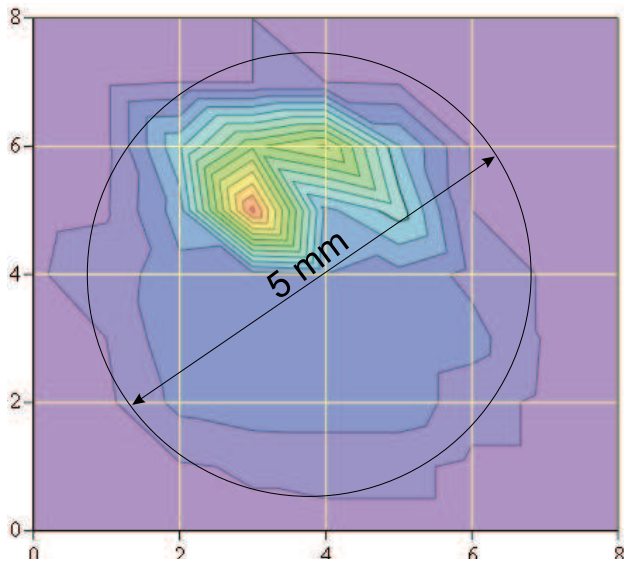

Fig. 3: *Photo current distribution measured in the preparation chamber.*

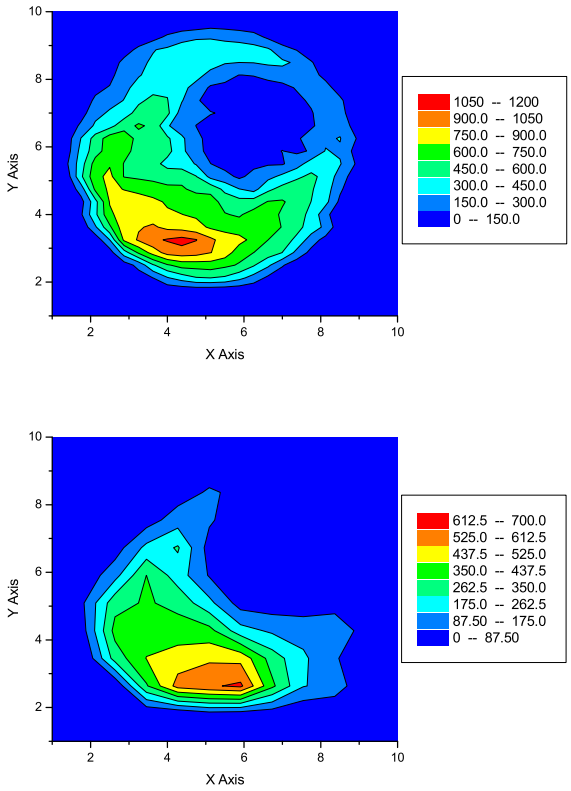

Fig. 4: *Photo current distribution of the cathode measured inside the gun cavity with applied dc bias (above) and rf field (below).*

[1] E. Barthels et al., Nucl. Instr. and Meth. A445 (2000) 408.

Superconducting RF gun drive laser diagnostic system

P. Evtushenko, T. Quast

During the experiments with the Rossendorf superconducting RF gun [1] we have found that a diagnostic of the drive laser parameters is a very important issue for the gun operation. The drive laser diagnostic system is shown in the Fig. 1.

Position and size of the laser spot on the photocathode have a strong influence on the electron beam transport in the gun cavity. Hence it is necessary to online monitor and control both parameters. Position of the laser spot on the cathode was adjusted with a remote controlled mirror holder driven by piezo motors. A quartz plate was inserted behind the mirror to reflect a part of the laser light to a reference screen with a mesh. The reference screen is placed at the same distance from the adjustable mirror as the photocathode, hence the laser spot on the reference screen has the same size and is moved by the same distance like the spot on the cathode. The position on the reference screen was monitored by a video camera.

The bunch charge was changed by controlling the laser micropulse power. Therefore a $\lambda/2$ plate at the entrance of the amplifier could be remotely rotated. To monitor the laser power during the gun operation a reflection from a quartz wedge was given on a UV diode. The diode was calibrated with the help of thermopile type powermeter.

The drive laser obviously must be synchronized to the RF system of the gun. Since it was not possible to stabilize the SRF cavity frequency to a stable master oscillator the cavity frequency was defined as a reference frequency. So the laser was synchronized to the cavity frequency. The laser oscillator works with repetition rate 26 MHz. To ensure a high accuracy the phase detection was performed at 1.3 GHz, comparing the master oscillator with the 50^{th} harmonic of the laser repetition frequency.

The phase detector with an PID controller adjust the oscillator cavity length via a piezo element. The phase detector signal represents the phase jitter of the laser with respect to the reference. In our experiments the jitter was 12 ps peak-peak. The laser jitter with respect to a stable reference is about of 2 ps.

The drive laser for the SRF gun in Rossendorf, was developed at the Max-Born-Institute in Berlin in the group of Ingo Will [2].

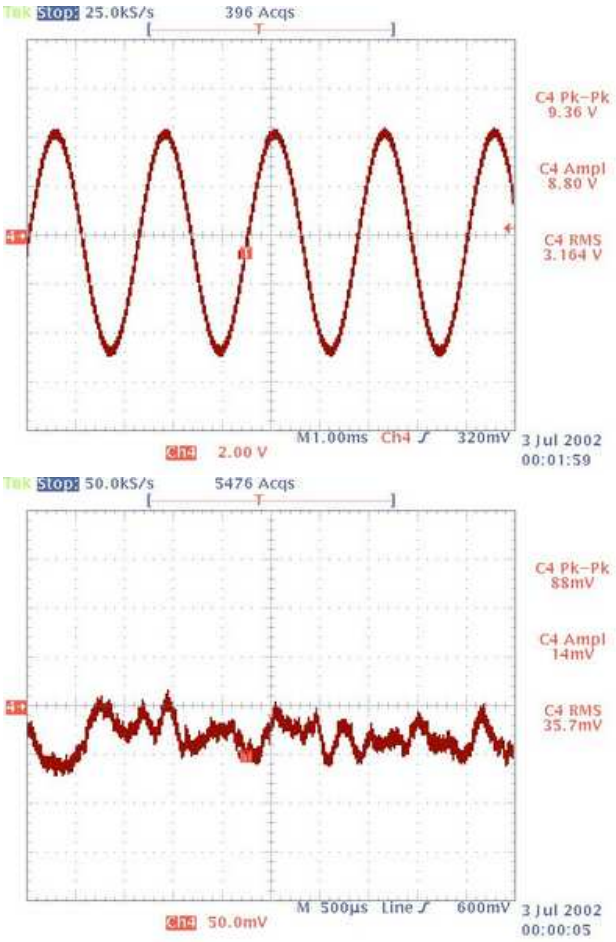

Fig. 2: *The phase detector signal: laser is not synchronized (upper), laser is synchronized to the cavity frequency (lower).*

[1] this report, p. 47 ff.
[2] will@mbi-berlin.de

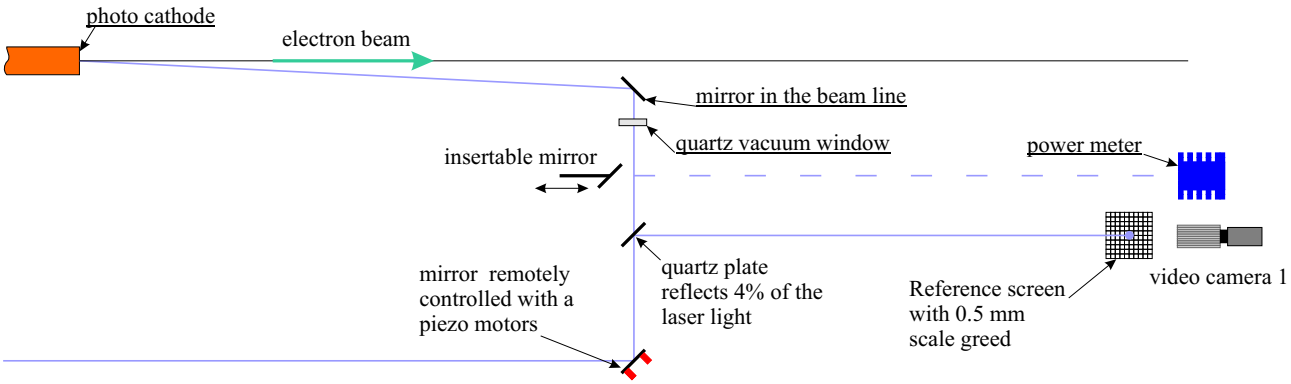

Fig. 1: *The optical diagnostic at the SRF gun.*

Cavity field calculations for the ELBE superconducting electron gun

K. Möller

In February 2002 for the first time ever at the ELBE facility an electron beam was obtained from a superconducting photoelectron RF gun (SGUN). Based on the experience gained in the prototype experiments now work is being conducted for an improved design and a final version of a superconducting electron gun. One important aspect of these activities are extensive simulation calculations. For this purpose additionally to existing codes two new computer codes have been developed. This was considered to be worthwhile since in view of the high total costs of a development of a superconducting gun it is of importance to have several independent checks of the design concept. Furthermore with source codes which are known in all detail one is highly flexible with respect to any desired modification. The first code (SGUN_FIELD) calculates the cavity fields (electric and magnetic) and the resonance frequency for a given cavity contour and a given field mode. In the second code (SGUN_MOTION) the motion of electron bunches in the cavity is calculated [1].

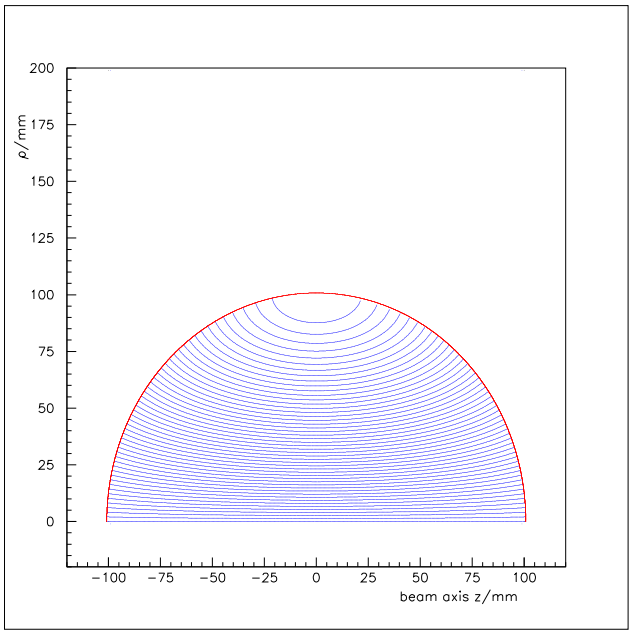

Fig. 1 *1.3 GHz fundamental mode in a spheric cavity cell.*

The SGUN_FIELD code is based on the MAXWELLian equations which are solved in cylinder coordinates imposing the usual boundary condition of vanishing tangential electric field components on the cavity surface. By defining a mesh within the cavity the partial differential equations are converted into a system of homogeneous algebraic equations. These equations are solved by an iteration method. Finally one ends up with the values of the electric field vector in the mesh points. The magnetic field is obtained by once again applying the MAXWELLian equations. Quite a lot of effort has been made to check the numerics of the SGUN_FIELD code. To this end among numerous tests the code was also applied to a spheric cavity (Fig. 1). In this case the solution can be derived in analytical form. Inserting the analytical solution into the numerical equations it turned out that the analytical solution solves these equations with high accuracy. In Figs. 2,3 results are shown for 1/2-cell cavity TM_{010}-mode fields.

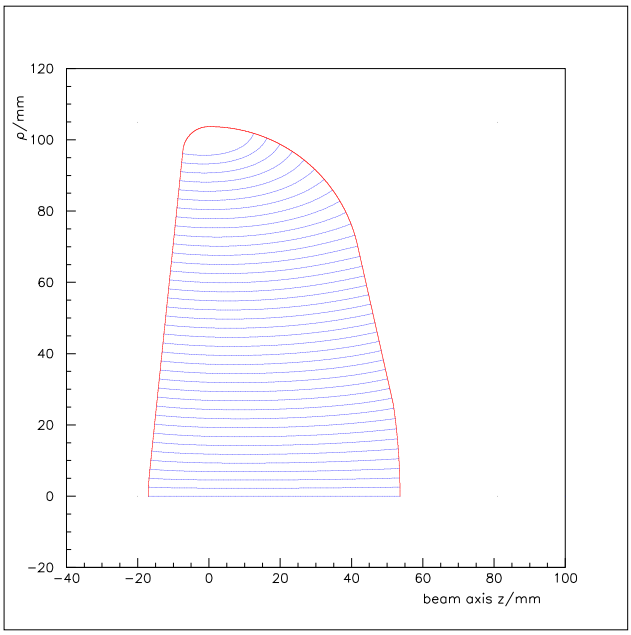

Fig. 2 *Electric field in the 1/2-cell SGUN prototype cavity.*

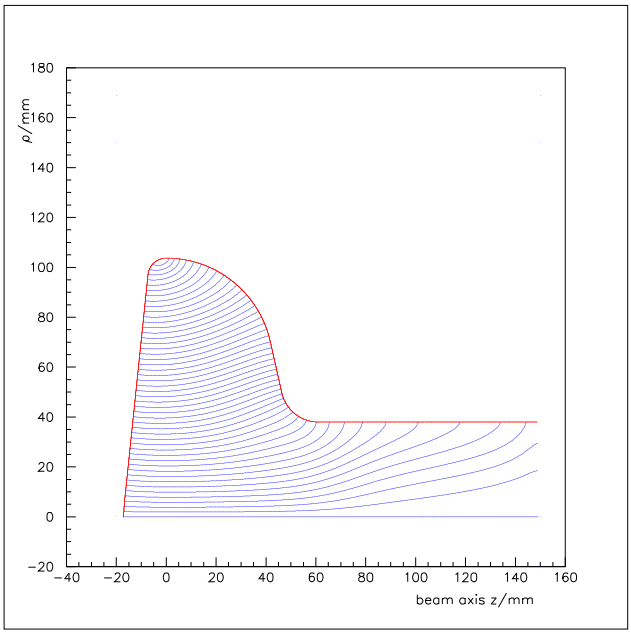

Fig. 3 *1/2-cell SGUN cavity with part of the attached beam line.*

[1] this report, p. 57

Simulation calculations of electron motion in the ELBE superconducting electron gun

K. Möller

The motion of electron bunches in cavity fields, obtained e.g. from SGUN_FIELD [1], is calculated by means of the newly developed code SGUN_MOTION. The kind of results yielded by SGUN_MOTION can be seen by looking at the examples shown in Figs. 1,2. Here the electron motion was calculated for the 1/2-cell cavity which was used at the ELBE superconducting gun prototype experiments. In Figs. 1,2 the coordinate system has been chosen such (cf. [1]) that the cavity beam axis ranges from z_{left} = -17.03 mm to z_{right} = +53.63 mm with the maximum of the cavity contour at z = 0. At the cathode in the cavity (z = z_{left}) a bunch of cylindrical shape is generated by a 3-dimensional random number generator. The electrons of the bunch undergo interactions due to the electric and magnetic cavity fields as well as to the interelectron forces as soon as they emerge from the surface of the cathode. In the figures (upper lines) the time evolution of the bunches is shown with the current positions on the beam axis of the cavity displayed as snapshots in time intervalls of 40 ps. As shown in the figures simultaneously with looking at the spatial behaviour of the bunches also a set of derived quantities is calculated and displayed such as the kinetic energy, the velocity and the transverse normalized rms emittance. Also calculated (but not shown here) are the transverse and the longitudinal particle momenta, the transverse velocity, the longitudinal emittance, the transverse and longitudinal phase space distributions and the current rf-phase. The main parameters of the example presented here are given in figure caption of Fig. 1. Fig. 2 represents the same calculation as Fig. 1 but with the interaction between the electrons switched off. From the comparison of Fig. 1 and Fig. 2 one can infer that the existence of the interelectron forces (space charge) leads to an increase of the bunch radius by about a factor 3 whereas in the absence of space charge (Fig. 2) the bunch radius even slightly decreases. This latter fact is due to the off-axis radial cavity field which results in a focusing effect. Furthermore on can conclude that the observed normalized emittance growth almost completely originates from space charge effects. It should be mentioned that in the given test example the initial velocity distribution of the electrons was set equal to zero (resulting in zero normalized emittance at start). In first test calculations the SGUN_MOTION code has revealed good performance up to 1nC bunch charge. A good agreement was obtained between the results for 1100 and 11000 bunch particles respectively. After further checks and comparison of the results with other electron transport codes the SGUN_MOTION code will be used for detailed systematic calculations to contribute to the search for an optimum design of a superconducting RF photogun.

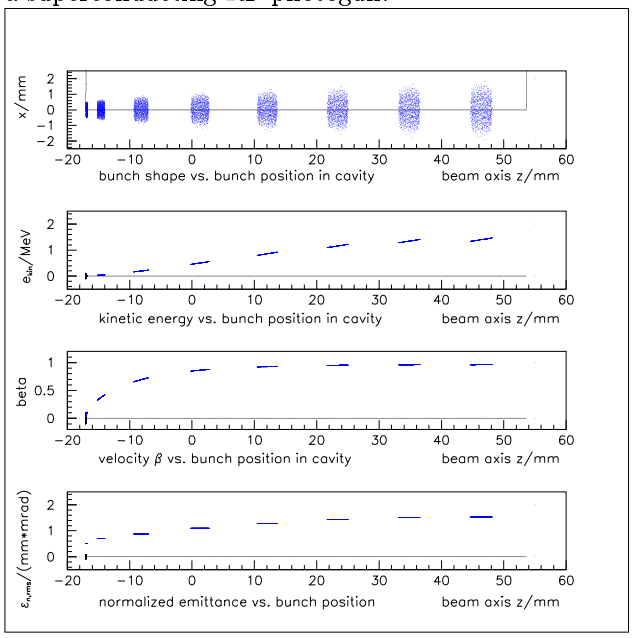

Fig. 1 *Electron bunch motion in the 1/2-cell SGUN cavity with space charge interaction switched "on". The main parameters are: average field gradient: 20 MV/m, RF phase at bunch start:* 45.8^0*, bunch length: 10 ps, bunch charge: 20 pC.*

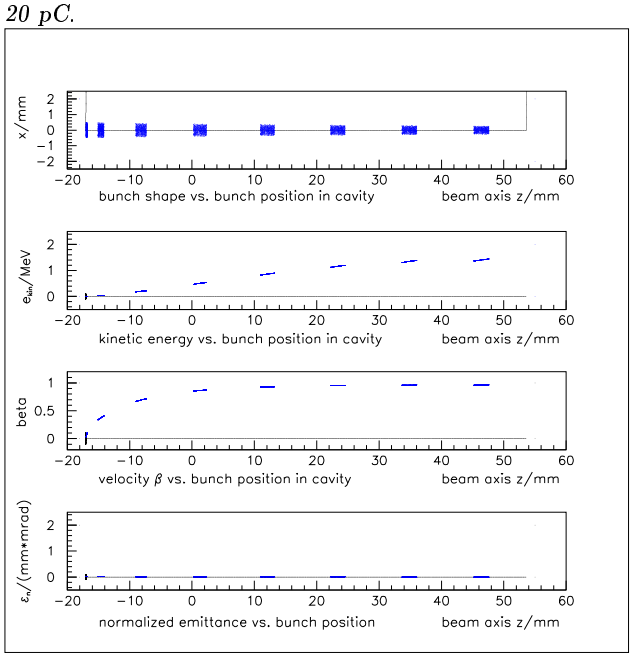

Fig. 2 *Electron bunch motion in the 1/2-cell SGUN cavity with space charge interaction switched "off". The parameters are the same as in Fig 1.*

[1] this report, p. 56

Feasibility study of an industrial 1.3 GHz 100 kW table top accelerator

Ch. Schneider

At the Forschungszentrum Rossendorf (FZR) the build-up of the superconducting (sc) 1.3 GHz accelerator ELBE is still in progress. Furthermore, a new sc photo injector (SRF gun) [1] is under development, which should accelerate electrons up to 10 MeV at 1.3 GHz frequency. Since the applications of electron accelerators also for industrial purposes are steadily increasing one can speculate about transferring the above named state of the arte technology to industrial electron accelerators. At the FZR a feasibility study of such a table top electron accelerator (TTEA) has been performed to investigate its technical limits and marketability.

The use of electron accelerators is more and more interesting for applications where the destructive potential of the electrons are used like sterilisation of medical waste and medical products, food irradiation or decontamination of sewage. For these processes a high power is required to achieve a high product throughput in a plant. The aim is therefore to use beam powers of around 100 kW or more. The energy of such electron accelerators should be kept below the threshold of the photo nuclear reaction (γ,n). For that reason the design values are 10 MeV electron energy and at least a mean beam current of 10 mA.

There are two machines on the market, which could serve for comparison because they are leader in beam power and efficiency. One is the IMPELA [2], a normal conducting linear accelerator driven in pulsed technique at 1.3 GHz with special designed cavities for cooling purpose. This machine has a beam power of 50 kW at 10 MeV beam energy. The market leader is the Rhodotron [3], equipped with a large half-wavelength coaxial cavity operated at 107.5 MHz. The beam is re-circulated through the cavity several times. The version TT300 of the Rhodotron provides a power of 150 kW at 10 MeV.

The central device in the concept of the TTEA is a sc cavity with implemented photo cathode, like the SRF gun, see Fig. 1. The cavity is made of 6 standard TESLA cells and a special 1/2 niobium cell. In the rear of the 1/2 cell is an opening for the photo cathode with following coaxial filter. The photo layer of the cathode is made of Cs_2Te therefore an UV-Laser with 0.26 μm wavelength is necessary for electron emission. For 10 mA beam current and cathode quantum efficiencies between 2 and 10% a design laser power of 6 W is required. The cavity and the cathode support are housed in a cryostat. A helium plant performs the liquid helium supply and the shield cooling of the cryostat. A small helium liquefier in the category of about 10 l/h is sufficient here. The beam is guided through a 90° bended beamline, scanned by a raster system and extracted through a window, comparable to similar irradiation plants. The RF is produced by e.g. a 130 kW klystron and coupled to the cavity by a high power coupler.

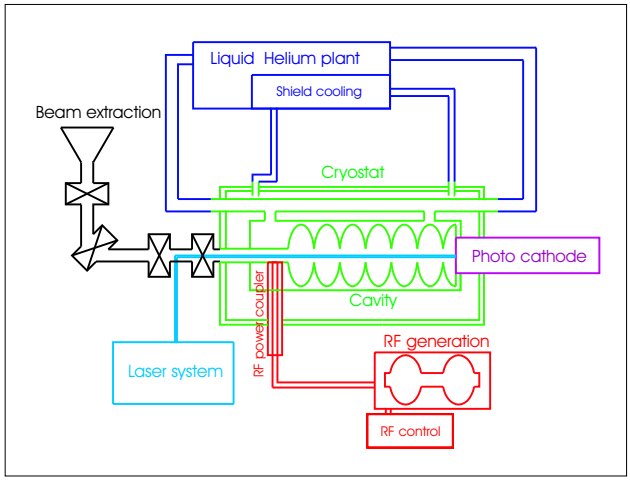

Fig. 1: *Major components of the 1.3 GHz sc table top electron accelerator driven by a photo gun.*

First results of operating the sc photo gun (SRF) at a Helium bath temperature of 4 K are described in [1]. For the evaluation of the technical feasibility of the entire concept the different components can be separated in three groups. Components that are technically approved and in similar implementations available on the market, need only adaptation and commissioning. These are the liquid Helium plant, the cryostat, the beam extraction system, the RF generation and RF control. The second group belongs to up till now not realized components but from likewise designs, literature or expertises their proper performance could be expected. These are the laser system, the RF power coupling, the 6 and 1/2 cells cavity and the quantum efficiency of the Cs_2Te cathode between 2 and 10%. The last group are components or functionalities that are not approved until now. These are the operation of the cavity cathode system at 1.8 K and the quality loss of the niobium cavity due to surface contamination from the cathode material at long time laser power operation.

From the viewpoint of efficiency the super conducting technology has its main advantages for high gradients and cw beams due to the low RF loss in the sc cavity walls. Since the production of cold helium is a very inefficient process the overall efficiency must be taken into account. In Tab. 1 the main contributions to the total efficiency for the TTEA are specified. The efficiency of the cavity with the cryogenics included is around 50% at 100 kW beam power. The total efficiency of beam power to mains power amounts to around 20%. Since the RF power loss in the cavity walls depends not on the beam current, a high beam

power is also achievable with normal conducting cavities operated in pulsed mode with very high beam current. The IMPELA accelerator e.g. is operated with a duty factor of 5% for a mean beam power of 50 kW. Taking into account efficiencies for klystron and its power supply the same as for the TTEA one ends up with a total efficiency for the IMPELA with around 15% at 50 kW beam power [2]. The concept of the Rhodotron has two major advantages. One is using a low gradient due to accelerating the beam several times through the cavity and therefore producing low RF loss in the cavity walls. The second is using a low RF frequency of 107.5 MHz generated very efficiently by a tetrode amplifier. The total efficiency of the Rhodotron amounts to around 40% at 100 kW [3].

Mains power subsystems	Power or efficiency
Mains power Helium plant	**106 kW**
Beam power (100kW) + RF loss of the cavity and power coupler	**100,3 kW**
Sum	**206,3 kW**
Efficiency of beam power (100kW)	**48,5 %**
Mains power klystron power supply	**400 kW**
+ Mains power helium plant	**506 kW**
Total efficiency: mains power to beam power	**19,8 %**

Fig. 2: *Total efficiency of the table-top accelerator.*

The marketability of irradiation plants are dominated to around 40% by the capital costs of the accelerator [4]. The operating costs of such plants are very comparable but may slightly differ due to e.g. the time period of the maintenance intervals and mains power costs. Comparing the capital costs between the different concepts some additional items for the TTEA must be considered, these are the helium plant, the Laser system and the cryostat. These further costs amount totally to around 1.5 million €. The extra systems Helium plant and laser worsen also the ease of maintenance because they enhance the complexity of the complete machine.
From the feasibility study the following conclusions can be drawn. The TTEA seems to be technical practicable except for some outstanding tests of the SRF gun concept for long term operation at high beam current and of course difficulties which could arise from actually not realized components like the laser system or the high power coupler. There are industrial accelerators on the market with comparable or slightly better parameters but simpler in design and therefore easier to maintain in an industrial surrounding. The main advantages of the SRF concept, which are excellent beam parameters like emittance, bunch length or energy spread are from minor importance for industrial applications.

[1] this report, p. 47
[2] G. H. Hare. IMPELA Electron Accelerators for industrial radiation processing.
Radiation Physics and Chemistry, Vol. 35, S. 619-626, 1990
[3] D. Defrise. Technical status of the first industrial unit of the 10 MeV, 100 kW Rhodotron.
Radiation Physics and Chemistry, Vol. 46, S. 473-476, 1995
[4] P. R. Minbiole. Economics of electron beam accelerator facilities: concept vs actual.
Radiation Physics and Chemistry, Vol. 46, S. 421-428, 1995